THE UNIVERSITY OF CALGARY

Development and Testing of a Real-Time DGPS/INS Integrated System

by

Jing Sun

A THESIS

SUBMITTED TO THE FACULTY OF GRADUATE STUDIES

IN PARTIAL FULFILLMENT OF THE REQUIREMENTS FOR THE

DEGREE OF MASTER OF SCIENCE

DEPARTMENT OF GEOMATICS ENGINEERING

CALGARY, ALBERTA

May, 1998

ABSTRACT

A real-time DGPS/INS integrated system has been designed, implemented and tested using a LTN-90-100 IMU, two Ashtech Z-XII receivers and two 486/66 computers as the major hardware components of the system. The principles of single differential GPS positioning, strapdown INS navigation and the methodology of GPS/INS integration are discussed as essential background material for the research. The research itself addresses the problems of hardware and software integration for the specific DGPS/INS system implementation chosen, justifies the choices made, and discusses in detail the GPS correction creation and transmission issues. Tests have been designed and conducted to verify the system design and assess the system performance. Results show that the achieved accuracy is metre-level in position, cm-level in velocity, 10 arcsec-level in pitch and roll and 0.08 degree in azimuth with respect to a DGPS/INS system using GPS carrier phase data.

ACKNOWLEDGMENTS

I wish to express my deep appreciation, first and foremost, to my supervisor, Dr. Klaus Peter Schwarz, for his continuous support, inspiration and guidance throughout the course of my graduate studies.

Special thanks are extended to Mr. Chritoph Amlacher for his help in the field tests. Mr. Huangqi Sun is acknowledged for the valued time and knowledge he shared in discussing topics related to this thesis. I also owe thanks to Ahmed H. Mohamed, Mostafa Mohamed, Jan Skaloud, Yecai Li, Alex Bruton, and Craig Glennie for valuable discussions and assistance during my study. My friend Marcia Inch is also thanked for correcting the English of the thesis.

Thanks are also extended to my home university, Harbin Engineering University, China, for providing me excellent education for my BSc. and MSc. degrees, partial financial support and opportunity to pursue education in Canada through educational leave.

Finally, thanks go to my husband Bo for his support, encouragement and great help in the field tests.

TABLE OF CONTENTS

LIST OF TABLES

LIST OF FIGURES

NOTATION

i) Conventions

(a) Matrices are uppercase bold

(b) Vectors are lower case bold

(c) Transformation Matrices between two coordinate systems are specified by a subscript and a superscript, e.g. $\mathbf{P}_b^e$ indicates a transformation from the body frame (b) to the earth-fixed frame (e). The angular rate vector $\boldsymbol{\omega}_{ib}^b$ indicates the rotation of the body frame with respect to the inertial frame expressed in the body frame.

(d) The operators are defined as:

(-) Kalman filter predicted value

(+) Kalman filter updated value

$\dot{x}$ derivation with respect to time

$\mathbf{A}^T$ matrix transpose

$\mathbf{A}^{-1}$ matrix inverse

f( )	is a function of
$\hat{x}$	estimated value
δ	error
Δ	single difference between receivers

ii) Symbols

b	accelerometer bias
c	speed of light
d	gyro drift
f	specific force
F	dynamics matrix
h	geodetic height
I	identity matrix
K	Kalman filter gain matrix
P	Kalman filter process noise covariance matrix
P	pseudorange
Q	spectral density matrix

$\mathbf{R}$	Kalman filter measurement noise covariance matrix
$\mathbf{x}$	system state vector
v	velocity
dT	receiver clock error
dt	satellite clock error or prediction interval
Φ	carrier phase
$\dot{\Phi}$	phase rate
Φ	transition matrix
α	reciprocal of correlation length of gyro drift
β	reciprocal correlation length of accelerometer bias
τ	velocity error correlation time (Gauss-Markov process)
ς	receiver clock drift correlation time (Gauss-Markov process)
γ	normal gravity
ρ	geometrical distance between receiver and satellite
$\dot{\rho}$	range rate
φ	roll
θ	pitch
ψ	yaw, geocentric latitude
ω	angular rate

ω_e mean rotation rate of the Earth

ϕ geodetic latitude

λ geodetic longitude

ε misalignment

iii)Acronyms

C/A	Coarse/Acquisition
DGPS	Differential GPS
DRMS	Distance Root Mean Square
UERE	User Equivalent Range Error
GMST	Greenwich Mean Sidereal Time
GPS	Global Positioning System
IERS	International Earth Rotation Service
IMU	Inertial Measurement Unit
INS	Inertial Navigation System
ITRF	International Terrestrial Reference Frame
SINS	Strapdown Inertial Navigation System
PDOP	Position Dilution of Precision
PPS	Pulse Per Second

PRN	Pseudo Random Noise
RMS	Root Mean Square
SA	Selective Availability
WGS-84	World Geodetic System 1984
ZUPT	Zero Velocity Update

CHAPTER 1

INTRODUCTION

1.1 Background and Objective

The transition from stable platform mechanizations of inertial systems to strapdown mechanization started at the end of 1960s. Direct causes for the transition were the rapid advancement of computer technology and the improvement in rate sensor technology which is particularly well adapted for use in strapdown systems. The perceived benefits of strapdown inertial systems are reductions in weight, complexity, and cost, as well as increased reliability, thus opening a wider range of applications. In particular, the evolution of Ring Laser Gyros (RLG) provided compact instruments which had good scale factor linearity, low sensitivity to host vehicle acceleration, and a dynamic range which is adequate for military and commercial aircraft applications (Greenspan, 1995).

Even though a strapdown system has advantages over a gimbaled system, it has the same problem as the gimbaled system, namely the deterioration of the navigation performance

with time. Researchers have found an efficient way to bound INS navigation errors by updating the INS velocity and position with external measurements which have consistent accuracy with time. These external measurements can be barometric altitude, Doppler logger velocity, and positions from other navigation systems, such as Loran-C, Omega, GPS, etc. Among them, GPS measurements are the most versatile and stable updates in many applications.

GPS, as a high accuracy navigation system is used for the determination of position, velocity, acceleration, and time transfer. GPS provides consistently accurate navigation parameters which are largely independent of time, location and weather. Real-time differential GPS (DGPS) eliminates most of the atmospheric, ephemeris and clock errors and a 5-metre accuracy can be easily achieved in most situations (Kee, 1991 and McLellan et al., 1994). Real-time DGPS methodologies include Regional Area DGPS (RADGPS) (Gao et al., 1997), conventional single-reference DGPS, multi-reference DGPS, multi-reference Wide Area DGPS (WADGPS), and World Wide DGPS (WWDGPS) (McLellan et al., 1994). In this research, a local area single-reference DGPS is used. Differential corrections are transmitted by a Radio Data Link System. Research shows that GPS can also provide attitude parameters using a multi-antenna configuration (Cohen et al., 1992, Schwarz et al., 1992, El-Mowafy, 1994, Cannon et al., 1994). However, the achievable accuracy is a function of the baseline length (Lu, 1995).

Stand-alone GPS has the problem of signal blockage and attenuation in mountainous areas, dense forests, and areas with high-rise buildings. Another problem with GPS is its low data rate, typically lower than 10 Hz, which can not meet the requirement of some applications (Crane et al., 1995).

The problems of GPS as a stand-alone navigation system can in most cases be overcome by a GPS/INS integrated system. In the integration scheme, the INS as the master navigation system outputs high rate navigation parameters, typically 50 Hz or higher, while the GPS offers external position and velocity information for updating INS position and velocity to prevent error drifts. As updates are needed only every few seconds, modern GPS receivers with 1 Hz data rate are very well suited for this task. INS will still provide high accuracy navigation parameters in the short term during GPS signal blockage and can be used to repair GPS cycle slips when carrier phase measurements are used for the positioning calculations, see for instance El-Sheimy (1996).

GPS/INS integration schemes have been investigated by e.g. Cox (1978), Hartman (1988), Schwarz et al. (1984), Upadhyay et al. (1982). The integration can be classified as the hardware and the software integration. The latter is further divided as feedback and feedforward integration.

The software integration can be implemented either in an aided or an embedded approach (Schwarz et al., 1994c). The aided approach will be discussed in chapter 4 and used for the real-time integrated system. In this approach, decentralized filters are designed due to its computational efficiency. GPS position and velocity from the GPS navigation filter, called the local filter, are fused into the integration filter, called the master filter. In the embedded approach, the raw measurements are used instead.

The standard GPS and INS integration approach is to process the residuals by a Kalman filter to estimate and compensate various errors in both systems (Greenspan, 1995). Kalman filter theory and algorithms are well documented in Gelb (1974). Kalman filter implementation issues are studied in Karatsinides (1994), Kwan et al. (1993), and Tang et al. (1993).

The use of an integrated GPS/INS for direct georeferencing of remotely sensed data has become an operational procedure in the last few years. In general, the integration is done in post-mission mode and can therefore make use of the precise GPS carrier phase data. For many remote sensing and mapping applications, this mode is preferable because there is no need for real-time use of the data and high positioning accuracy can be achieved in this way. The key issue in GPS precise positioning using carrier phase measurements is the ambiguity resolution. Many efforts have been made to fix the integer ambiguities (Chen, 1993, Euler, 1992, Hatch, 1991, and Teunissen et al., 1994).

In this research, only GPS C/A code pseudorange and raw Doppler observations are used in real-time DGPS positioning calculations. This is because there are some emerging applications, such as forest fire control and real-time mapping with digital cameras, that would greatly profit from real-time georeferencing. In such applications, less accurate positioning is needed, so carrier phase GPS is replaced by pseudorange GPS. Another reason for using a real-time DGPS/INS is attitude control. In remote sensing, most remote sensors are physically mounted on the vehicles. Sensors endure the same dynamics as the vehicles. Under high dynamics, images are blurred by the motion. Even though post-mission compensation can improve the image quality, isolating the sensors from the vehicle motion is still preferable. Such a requirement can be met by mounting remote sensors on a stabilized platform. Thus, a real-time attitude reference is needed.

The objective of this research is the development of a real-time DGPS/INS integrated system prototype which offers high rate navigation data based on the hardware and some software resources available in the department. The recorded GPS and INS raw measurements can be used for a post-mission georeferencing analysis. A potential application of such a system is as an attitude reference for a stabilized remote sensing platform.

1.2 Thesis Outline

In Chapter 2, coordinate frames which are used in strapdown inertial navigation calculations are defined, INS initial alignment is discussed and strapdown INS mechanization in the e-frame is described.

In Chapter 3, issues of real-time DGPS positioning are discussed and the mathematical formulas for pseudorange and Doppler corrections are given. The principle of single differenced GPS positioning is addressed and its suitability for this application is pointed out.

Chapter 4 focuses on GPS/INS integration issues. Kalman filtering is reviewed and the filter tuning issues are addressed. The INS error model and measurement model are set up and GPS/INS integration methodology is discussed.

In Chapter 5, system design and implementation is discussed which includes hardware, software, data acquisition, and the synchronization of the GPS and INS data streams.

In Chapter 6, static and kinematic tests are described and test results are presented and analyzed.

Chapter 7 concludes the research work and gives some recommendations for the further development of the system.

CHAPTER 2

STRAPDOWN INERTIAL NAVIGATION SYSTEM

In a strapdown inertial navigation system, the box containing the inertial sensors is directly attached to the vehicle. The sensors are therefore not mounted on a stable platform as in the case of a gimbaled system where the navigation calculations are carried out by mechanizing a specific coordinate frame physically. For a strapdown system, a mathematical platform is established using the raw measurements from the gyros and accelerometers in the computer; thus, the navigation calculations are based on this mathematical platform. As the navigation computations are usually not carried out in the frame in which the measurements are obtained and the measurements cannot be integrated to get the solution directly, a more complex computational procedure is necessary than in the case of a gimbaled system. It involves the use of several coordinate frames which will be defined in section 2.1. It also requires the orientation of the mathematical platform, the so-called alignment, which will be treated in section 2.2. Finally, it requires the mathematical transformation of the raw sensor data from the

quickly varying body frame, defined by vehicle motion, to a stable coordinate frame in which the integrations can take place. Thus the strapdown mechanization in Earth-fixed frame will be discussed in section 2.3.

2.1 Coordinate Frames

In this section, coordinate frames used in the strapdown navigation computations are defined.

a. Inertial Frame (i-frame)

The mean right ascension system with geocentric origin is used as a sufficient approximation of an inertial frame of reference. It is shown in Figure 2-1 (Wong, 1988). The definition of the Inertial frame is given as follows:

Origin: at the mass center of the Earth;

x-axis: pointing towards the mean vernal equinox;

y-axis: completing a right-handed system;

z-axis: coincident with the mean rotation axis of the Earth.

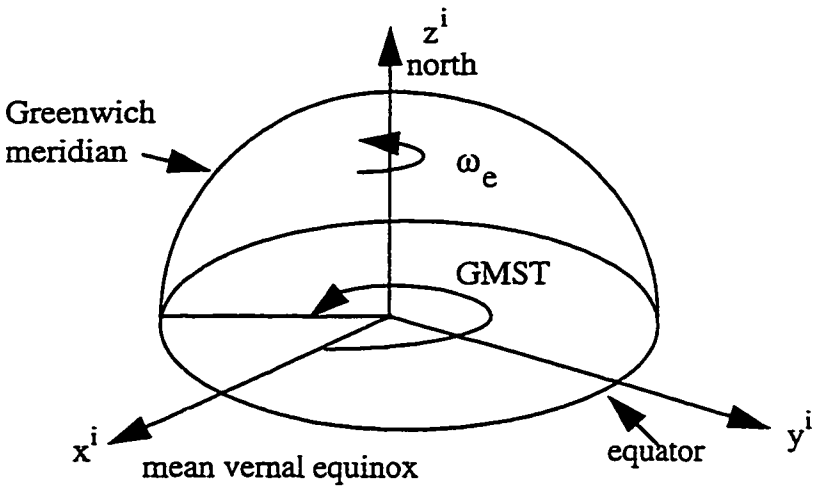

Figure 2-1 Inertial Frame

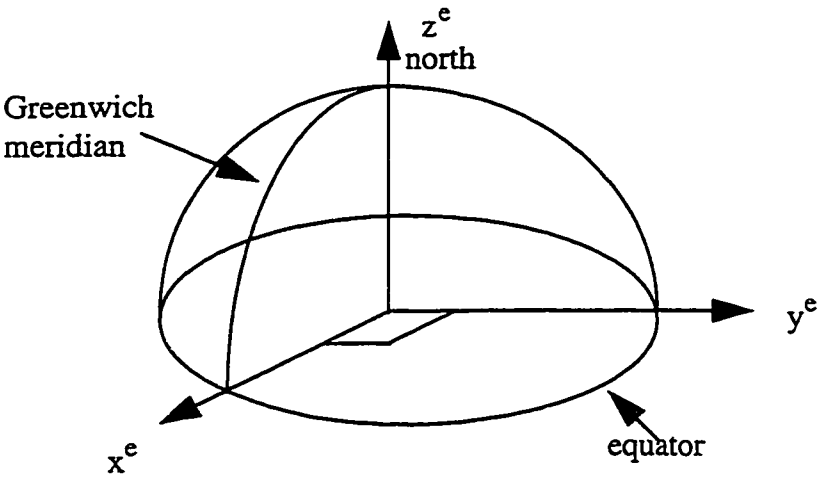

Figure 2-2 Earth-Fixed Frame

b. Conventional Terrestrial Frame (Earth-fixed frame, or e-frame)

The Conventional Terrestrial Frame is an Earth-fixed frame as illustrated in Figure 2-2 (Wong, 1988). It is defined as follows:

Origin: at the mass center of the Earth;

x-axis: pointing towards the mean Greenwich meridian in the equatorial plane;

y-axis: completing a right-handed system;

z-axis: mean rotation axis of the Earth.

In this definition, the i-frame and e-frame differ by a constant angular rotation which equals the mean rotation of the Earth ω_e about a common z-axis. The small variations in orientation and speed between the actual rotation axis of the Earth and the mean rotation axis can be neglected for all practical purposes.

c. Local-Level Frame (l-frame)

The local-level frame is the most frequently-used coordinate frame in navigational computations. It is defined with respect to a reference ellipsoid. The definition is described as:

Origin: at the origin of the sensor frame;

x-axis: pointing to the ellipsoidal east;

y-axis: pointing to the ellipsoidal north;

z-axis: pointing up along the ellipsoidal normal.

It is therefore a right-handed frame.

The relationship between e-frame and l-frame can be described by the transformation matrix $\mathbf{R}_l^e$ in Equation 2-1. Figure 2-3 (Wong, 1988) shows the l-frame.

$$\mathbf{R}_l^e = \begin{pmatrix} -\sin\lambda & -\sin\phi\cos\lambda & \cos\phi\cos\lambda \\ \cos\lambda & -\sin\phi\sin\lambda & \cos\phi\sin\lambda \\ 0 & \cos\phi & \sin\phi \end{pmatrix} \qquad (2\text{-}1)$$

The difference between Local-Level frame and Local-Geodetic frame is that the former one is a right-handed system, while the later one is a left-handed system. The difference between the Local-Level frame and the Local-Astronomic frame lies in the definition of z-axis in addition to the handedness of the frames. The z-axis of the l-frame is orthogonal to an ellipsoid, that of the Local-Astronomic frame is orthogonal to an equipotential surface (Schwarz and Wei, 1997).

d. Body Frame (b-frame)

The Body frame is an orthogonal frame which is attached to the vehicle. Its axes coincide with the input axes of the sensor block; thus, the raw data output of the Inertial Measurement Unit (IMU) are the components of the rotation rate and the acceleration experienced by the sensor block along the body axes. They can be used to determine the vehicle attitude with respect to the Local-Level frame. The b-frame of the LTN-90-100 IMU is shown in Figure 2-4.

Its definition is :

Origin: at the center of the IMU;

y-axis: pointing towards the head of the vehicle;

x-axis: completing a right-handed system;

z-axis: pointing up.

The l-frame can be rotated to the b-frame by three consecutive rotations about the axes of a right-handed system. The first rotation is made about the z-axis and the rotation angle is called yaw (ψ), its angular rate is $-\dot{\psi}$. The second rotation is done about the rotated x-axis and is called the pitch (θ), its rotation rate is $-\dot{\theta}$. The last rotation about the rotated

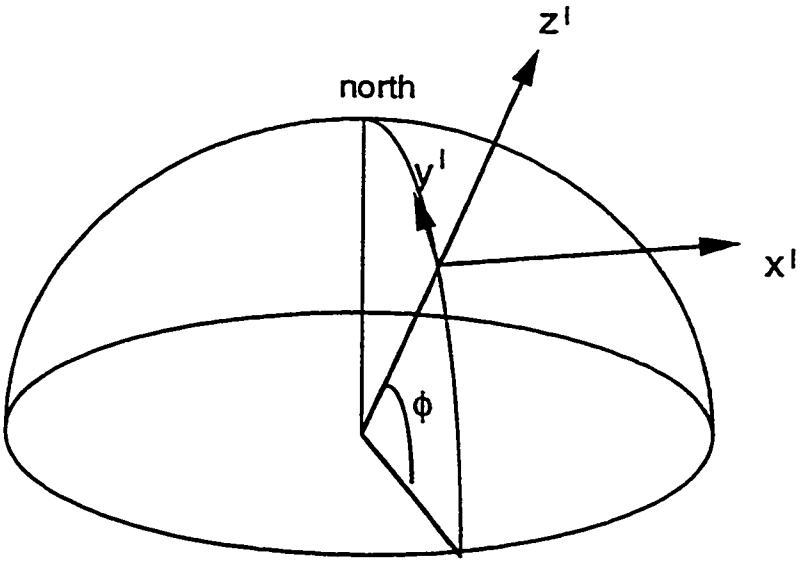

Figure 2-3 Local-Level Frame

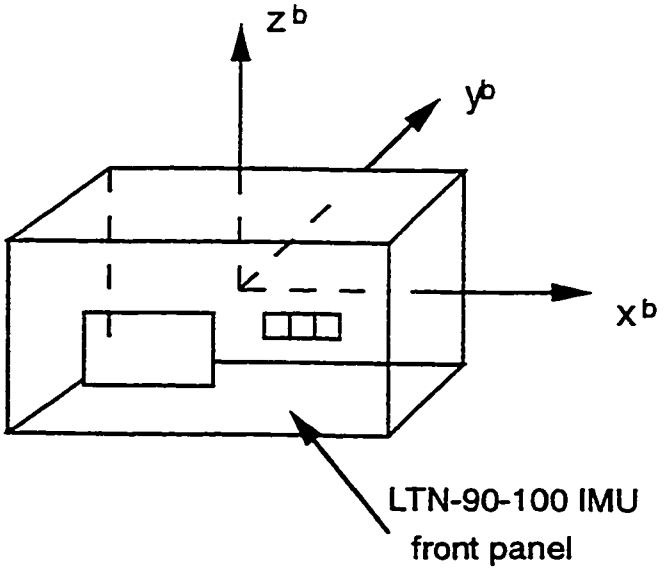

Figure 2-4 Body Frame

y-axis completes the total rotation of the two frames. The rotated angle is defined as roll (φ) and its rotation rate is $-\dot{\varphi}$. The relationship between the l-frame and the b-frame can be described by the transformation matrix $\mathbf{R}_b^l$.

$$\mathbf{R}_b^l = \begin{pmatrix} \cos\psi\cos\varphi - \sin\psi\sin\theta\sin\varphi & -\sin\psi\cos\theta & \cos\psi\sin\varphi + \sin\psi\sin\theta\cos\varphi \\ \sin\psi\cos\varphi + \cos\psi\sin\theta\sin\varphi & \cos\psi\cos\theta & \sin\psi\sin\varphi - \cos\psi\sin\theta\cos\varphi \\ -\cos\theta\sin\varphi & \sin\theta & \cos\theta\cos\varphi \end{pmatrix} \tag{2-2}$$

2.2 Initial Alignment

The INS navigation solution is based on the integration of the measurements obtained from the inertial sensors. Thus, system performance is affected by the quality of the initial values, such as the initial position, velocity and the initial attitude.

The purpose of the initial alignment is to determine the initial attitude of the vehicle, i.e. the initial transformation matrix from the b-frame to the l-frame in the Strapdown Inertial Navigation System (SINS). The initial position must be given and the initial velocity of the vehicle is enforced by starting with a static period where the vehicle does not move. During this period , the $\mathbf{R}_b^l$ matrix which defines the initial attitude is determined.

The initial alignment procedure of a SINS consists of two steps, the coarse alignment and the fine alignment.

a. Coarse Alignment

The coarse alignment aims at obtaining an approximate initial attitude value in a short period of time, e.g. 2 minutes; then, the fine alignment can be carried out with the approximate initial attitude value. The attitude obtained in this step is good to 40 arcsec in pitch and roll and about 1 degree in azimuth when using the LTN-90-100 IMU (Wong, 1988).

Assuming that the vehicle is stationary during the alignment, only the Earth's rotation and the gravity are sensed by the inertial sensors. The rotation rates sensed by the gyros are ω_{ie}^{b} which can be transformed to the l-frame by:

$$\omega_{ie}^{l} = \mathbf{R}_{b}^{l}\, \omega_{ie}^{b} = \begin{pmatrix} \omega_e \sin\psi \cos\phi \\ \omega_e \cos\psi \cos\phi \\ \omega_e \sin\phi \end{pmatrix} \qquad (2\text{-}3)$$

Using the equation, the yaw is determined by :

$$\psi = \tan^{-1}\left(\frac{<\omega_{ie}^{l}>_{x}}{<\omega_{ie}^{l}>_{y}}\right) \tag{2-4}$$

Where $<\omega_{ie}^{l}>_{x}$ and $<\omega_{ie}^{l}>_{y}$ are the x and y components of ω_{ie}^{l} .

The attitude matrix $\mathbf{R}_{b}^{l}$ in Equation 2-3 is done by an iterative process. In each step, ω_{ie}^{l} is averaged and the velocity is calculated using the mechanization equations. Then, the yaw is calculated using Equation 2-4 with an averaged ω_{ie}^{l}, the pitch and roll are updated, and the velocity is reset to zero. The errors in pitch and roll are:

$$\delta\theta = -\sin^{-1}\left(\frac{<\mathbf{v}^{b}>_{y}}{T\gamma}\right) \tag{2-5}$$

and

$$\delta\varphi = \sin^{-1}\left(\frac{<\mathbf{v}^{b}>_{x}}{T\gamma}\right) \tag{2-6}$$

where

T is the attitude update interval;

γ is normal gravity.

and $< \mathbf{v}^b >_x, < \mathbf{v}^b >_y$ are the x and y components of $\mathbf{v}^b$.

T has been chosen as 4 seconds. Normal gravity is computed using Equation 2-7.

$$\gamma = \sqrt{(\gamma_x^e)^2 + (\gamma_y^e)^2 + (\gamma_z^e)^2} \tag{2-7}$$

$\gamma_x^e, \gamma_y^e, \gamma_z^e$ are the x, y and z components of $\gamma^e \cdot \gamma^e$ is given by Equation 2-8.

$$\gamma^e = \frac{a_1}{r}\begin{bmatrix} \{c_1 + c_2 t^2 + c_3 t^4 + c_4 t^6\} x^e \\ \{c_1 + c_2 t^2 + c_3 t^4 + c_4 t^6\} y^e \\ \{d_1 + d_2 t^2 + d_3 t^4 + d_4 t^6\} z^e \end{bmatrix} + \begin{bmatrix} \omega_e^2 x^e \\ \omega_e^2 y^e \\ 0 \end{bmatrix} \tag{2-8}$$

where

$$t = \tan\psi \tag{2-9}$$

$$r = \sqrt{(x^e)^2 + (y^e)^2 + (z^e)^2} \tag{2-10}$$

and

x^e, y^e, z^e are the geocentric coordinates;

ψ is the geocentric latitude;

r is the magnitude of the geocentric position vector.

For the detailed expressions of the parameters a_1, c_i and d_i, see Wei and Schwarz (1990a).

b. Fine Alignment

The attitude determination is improved during the fine alignment. A Kalman filter is used to estimate the system errors and the sensor error corrections. The velocity output is considered as the velocity error and is used to update the estimated system errors. This means that zero motion of the IMU is assigned during alignment and that this condition is used to determine the system errors. The measured velocity is often called a zero velocity update (ZUPT) in the literature. The update interval has been selected as 10 seconds (Wong, 1988). The Kalman filter and the error model will be discussed in Chapter 4. As the coordinate update does not bring substantial improvement to the estimated misalignment errors due to the accurate velocity updates, only at the end of the fine alignment, are the known coordinates of the initial point used to update the estimated misalignment errors (Wong, 1988).

2.3 Strapdown Mechanization in the Earth-Fixed Frame

Strapdown inertial navigation equations can be expressed in an arbitrary frame, such as the Inertial frame, the Earth-fixed frame or the Local-level frame. The choice of a specific frame is application dependent. For GPS/INS integration, the e-frame is often used because of its computational efficiency and convenience. The SINS mechanization in the e-frame is described in Figure 2-5 (Wei and Schwarz, 1990a, Zhang, 1995a).

The measurements from the gyros and the accelerometers are the angular velocities and the specific forces about and along the three body axes with respect to the i-frame. After compensation of the sensor errors, the angular velocities are integrated to update the transformation matrix from the b-frame to the e-frame, i.e. $\mathbf{R}_b^e$, using the quaternion approach; the linear accelerations along the body axes obtained from the specific force measurements are transformed to the e-frame and integrated to obtain the velocity and position in the e-frame. In the last step, the navigation parameters in the e-frame are transformed to the l-frame to derive geodetic navigational parameters. For a detailed description of the mechanization, see Wei and Schwarz (1990a). In the following, the essential formulas used in the coding are listed for reference.

$$\theta = (\theta_x, \theta_y, \theta_z)^T = (\omega_x \Delta t, \omega_y \Delta t, \omega_z \Delta t)^T \qquad (2\text{-}11)$$

where $\omega_x, \omega_y, \omega_z$ are the body angular rates sensed by the gyros; Δt is the sampling interval; $\theta_x, \theta_y, \theta_z$ are the incremental angular changes due to the angular rates; $\theta = \sqrt{\theta_x^2 + \theta_y^2 + \theta_z^2}$ is the rotation angle. The rotation of the body frame with respect to the computational frame (e-frame in this case) is described by the quaternion **q**.

$$\mathbf{q} = \begin{pmatrix} q_1 \\ q_2 \\ q_3 \\ q_4 \end{pmatrix} = \begin{pmatrix} \frac{\theta_x}{\theta}\sin\frac{\theta}{2} \\ \frac{\theta_y}{\theta}\sin\frac{\theta}{2} \\ \frac{\theta_z}{\theta}\sin\frac{\theta}{2} \\ \cos\frac{\theta}{2} \end{pmatrix} \tag{2-12}$$

The quaternion is solved by

$$\mathbf{q}_{k+1} = \mathbf{q}_k + \frac{1}{2}[2(\cos\frac{\theta}{2} - 1)\mathbf{I} + \frac{2}{\theta}\sin\frac{\theta}{2}\mathbf{S}(\theta)]\mathbf{q}_k \tag{2-13}$$

where

$$\mathbf{S}(\theta) = \begin{pmatrix} 0 & \theta_z & -\theta_y & \theta_x \\ -\theta_z & 0 & \theta_x & \theta_y \\ \theta_y & -\theta_x & 0 & \theta_z \\ -\theta_x & -\theta_y & -\theta_z & 0 \end{pmatrix} \tag{2-14}$$

The relationship between the transformation matrix and the quaternion is expressed as:

$$R_b^e = \begin{pmatrix} R_{11} & R_{12} & R_{13} \\ R_{21} & R_{22} & R_{23} \\ R_{31} & R_{32} & R_{33} \end{pmatrix} = \begin{pmatrix} (q_1^2 - q_2^2 - q_3^2 + q_4^2) & 2(q_1q_2 - q_3q_4) & 2(q_1q_3 + q_2q_4) \\ 2(q_1q_2 + q_3q_4) & (q_2^2 - q_1^2 - q_3^2 + q_4^2) & 2(q_2q_3 - q_1q_4) \\ 2(q_1q_3 - q_2q_4) & 2(q_2q_3 + q_1q_4) & (q_3^2 - q_1^2 - q_2^2 + q_4^2) \end{pmatrix} \tag{2-15}$$

The initial quaternion can be obtained from

$$\begin{pmatrix} q_4 \\ q_1 \\ q_2 \\ q_3 \end{pmatrix} = \begin{pmatrix} 0.5(1 + R_{11} + R_{22} + R_{33})^{1/2} \\ 0.25(R_{32} - R_{23}) / q_4 \\ 0.25(R_{13} - R_{31}) / q_4 \\ 0.25(R_{21} - R_{12}) / q_4 \end{pmatrix} \tag{2-16}$$

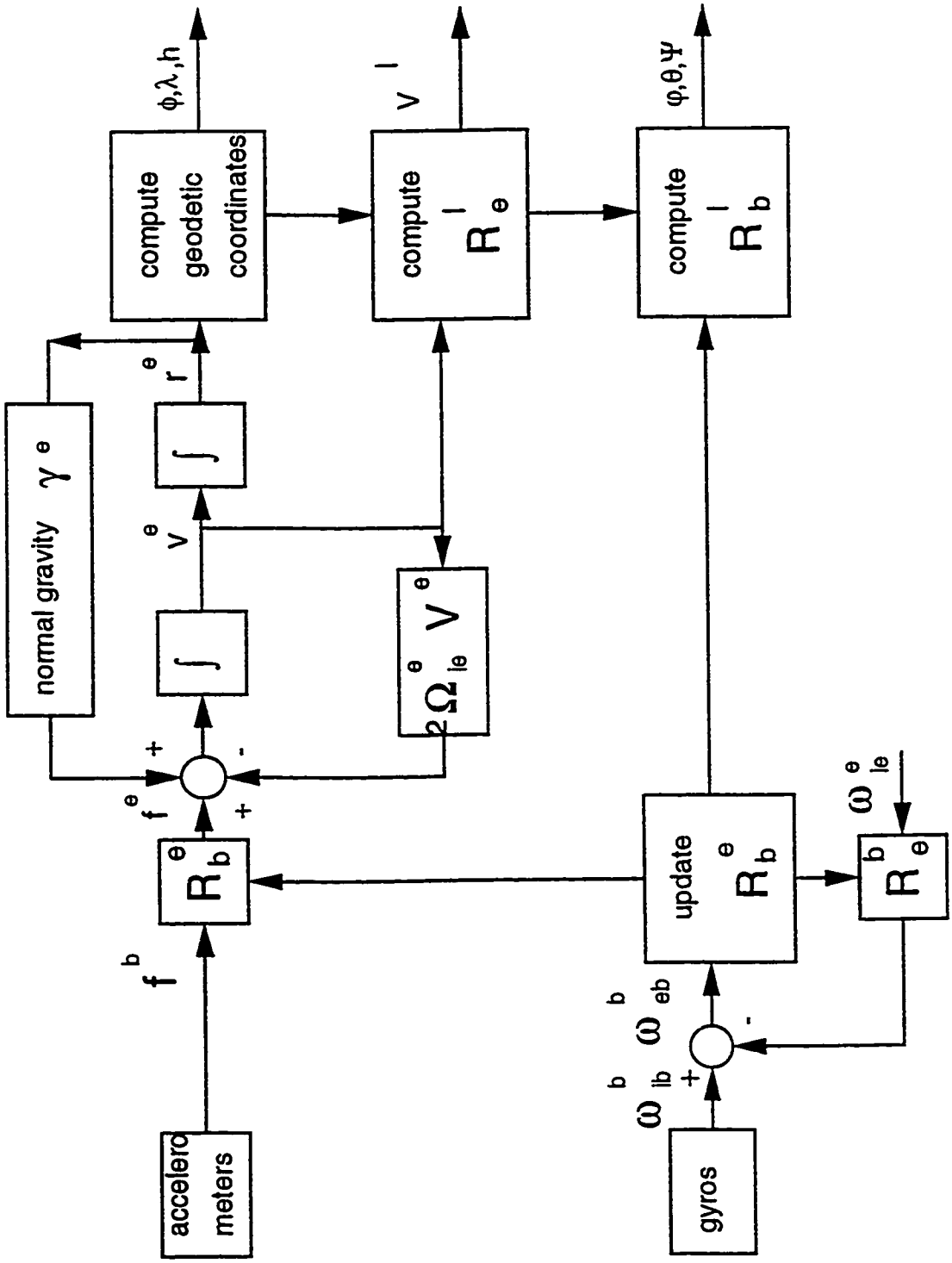

Figure 2-5 SINS Mechanization in the e-frame

CHAPTER 3

REAL-TIME DGPS POSITIONING

GPS derived position and velocity will be fused with INS derived position and velocity to prevent the deterioration of INS performance with time, in order to develop an operational integrated GPS/INS system.

GPS single point positioning accuracy is affected by satellite clock errors, atmospheric propagation errors, orbital errors, multipath and receiver-related errors. To control the accuracy of GPS available to non-authorized users, Selective Availability (SA) is implemented by DoD through satellite clock dithering and broadcast orbit accuracy degradation. With SA on, the positioning accuracy is about 100 m (2drms) in horizontal and 156 m (2σ) in height (Lachapelle et al., 1995). Using a differential technique, the error sources can be either eliminated or significantly reduced. The achievable positioning accuracy is 2 m or less with 95th percentile in horizontal and less than 2 m STD in height with C/A code pseudorange measurements (Tang, 1996), and the velocity

accuracy is less than 2 cm/s with raw Doppler measurements (Cannon et al., 1997) using AshTech Z-XII receivers.

In single-reference differential GPS positioning (DGPS), one receiver is set up at a reference position whose coordinates are known, and the receiver is called the master station. Another receiver roves with the vehicle whose position is to be determined; it is called the rover station.

In a real-time DGPS positioning system, the corrections to the raw measurements are sent to the rover station by a Radio Data Link System. Differential calculations are carried out to eliminate or reduce errors at the rover station. This results in an accuracy of 1 to a few meters in positioning with C/A code pseudorange and Doppler measurements. At the master station, GPS raw measurements are recorded, and the corrections are calculated and sent to the radio transceiver through one of the computer's serial communication ports. The modulated radio signal from the transceiver is transmitted to another radio transceiver at the rover station. After the signal has been demodulated, it is received by the rover station computer through a serial communication port. The transmission issues will be discussed in detail in Chapter 5.

In this chapter, real-time single difference GPS positioning using C/A code pseudorange and raw Doppler observations will be discussed.

3.1 Corrections to Pseudorange and Doppler Measurements

The single difference GPS pseudorange and Doppler observation equations are given in Equations 3-1 and 3-2, respectively.

$$\Delta p = \Delta\rho + c\Delta d_T + \Delta d_{ion} + \Delta d_{trop} + \Delta d\rho + \varepsilon_{\Delta p} \tag{3-1}$$

$$\Delta\dot{\Phi} = \Delta\dot{\rho} + c\Delta\dot{d}_T - \Delta\dot{d}_{ion} + \Delta\dot{d}_{trop} + \Delta\dot{d\rho} + \varepsilon_{\Delta\dot{\Phi}} \tag{3-2}$$

Where

p : pseudorange observation;

$\dot{\Phi}$: pseudorange Doppler observation;

ρ , $\dot{\rho}$: range and range rate;

c : the speed of light;

d_T , $\dot{d}_T$: receiver clock bias and drift;

d_{ion} , $\dot{d}_{ion}$: ionospheric delay and delay drift;

d_{trop} , $\dot{d}_{trop}$: troposhperic delay and delay drift;

$d\rho$, $\dot{d\rho}$: orbital error and error drift;

$\varepsilon_{\Delta\rho}, \varepsilon_{\Delta\dot{\Phi}}$: receiver pseudorange and Doppler measurement noise and multipath;

Δ : the difference between receivers.

At the master station, satellite coordinates and velocities are calculated with the broadcast ephemeris message. With the master station coordinates and velocity (zero in most cases) known, the calculated range and range rate between the master station and a satellite are given by Equations 3-3 and 3-4, respectively. The pseudorange and Doppler observations contain the errors discussed above. Corrections to these errors can be derived by subtracting the calculated range and range rate from the pseudorange and Doppler observations, see Equations 3-5, and 3-6.

$$\rho_c = \sqrt{(x_s^e - x_m^e)^2 + (y_s^e - y_m^e)^2 + (z_s^e - z_m^e)^2} \tag{3-3}$$

$$\dot{\rho}_c = [(x_s^e - x_m^e)\dot{x}_s^e + (y_s^e - y_m^e)\dot{y}_s^e + (z_s^e - z_m^e)\dot{z}_s^e] / \rho_c \tag{3-4}$$

where

$\rho_c, \dot{\rho}_c$: calculated range and range rate;

x_s^e, y_s^e, z_s^e : satellite coordinates in the e-frame;

x_m^e, y_m^e, z_m^e : master station coordinates in the e-frame;

$\dot{x}_s^e, \dot{y}_s^e, \dot{z}_s^e$: satellite velocities in the e-frame.

$$\delta\rho = p - \rho_c \tag{3-5}$$

$$\delta\dot{\rho} = \dot{p} - \dot{\rho}_c \tag{3-6}$$

Where

$\delta\rho$: pseudorange correction;

$\delta\dot{\rho}$: range rate correction.

At the rover, corrections are subtracted from the pseudorange and Doppler observations with the same satellite PRN as at the master station, thus realizing single difference GPS calculations expressed in Equations 3-1 and 3-2.

The calculation and the transmission of the corrections may take a few seconds (Zhang, 1995b, Lan, 1996). This time is called the time latency. To avoid the time latency at the rover station, the actual corrections applied to the pseudorange are predicted from the previous available corrections. It has been shown that the behavior of the pseudorange corrections is linear over a short time period such as 20 seconds (Tang, 1996). The predicted pseudorange corrections can be derived with Equation 3-7.

$$\delta\rho(t) = \delta\rho(t_p) + \delta\dot{\rho}(t_p)(t - t_p) \tag{3-7}$$

Where

$\delta\rho(t)$: predicted pseudorange correction at current epoch;

$\delta\rho(t_p)$: pseudorange correction at previous epoch;

$\delta\dot{\rho}(t_p)$: range rate correction at previous epoch.

3.2 Single Difference GPS Positioning

The velocity and position errors of the rover station are estimated by a Kalman filter. Kalman filtering will be discussed in Chapter 4. Three position error components, three velocity error components and the receiver clock bias and drift are modeled in the system state vector shown in Equation 3-8. The velocity errors and the receiver clock drift are modeled as first-order Gauss-Markov processes (Zhang, 1995b).

$$\mathbf{x} = (\delta x_r^e \delta y_r^e \delta z_r^e \delta \dot{x}_r^e \delta \dot{y}_r^e \delta \dot{z}_r^e \delta b_{clk} \delta \dot{b}_{clk}) \tag{3-8}$$

where

$\mathbf{x}$: the system state vector;

$\delta x_r^e, \delta y_r^e, \delta z_r^e$: rover station position errors in the e-frame;

$\delta \dot{x}_r^e, \delta \dot{y}_r^e, \delta \dot{z}_r^e$: rover station velocity errors in the e-frame;

δb_{clk} : receiver clock bias;

$\delta \dot{b}_{clk}$: receiver clock drift.

The discrete system model and the measurement model are defined in Equations 3-9 and 3-10, respectively. The actual measurements are the misclosures of the predicted and the observed range and range rate given in Equation 3-11.

$$\mathbf{x}_k = \Phi_{k-1}\, \mathbf{x}_{k-1} + \mathbf{w}_{k-1} \tag{3-9}$$

$$\mathbf{z}_k = \mathbf{H}_k \mathbf{x}_k + \mathbf{u}_k \tag{3-10}$$

$$\mathbf{z} = \begin{pmatrix} \Delta\rho_{pre} - \Delta\rho_{obs} \\ \Delta\dot{\rho}_{pre} - \Delta\dot{\rho}_{obs} \end{pmatrix} \tag{3-11}$$

where

Φ : transition matrix;

$\mathbf{w}$: the system noise;

$\mathbf{z}$: measurement vector;

H: design matrix;

u: measurement noise;

ρ_{pre}, $\dot{\rho}_{pre}$: predicted range and range rate;

ρ_{obs}, $\dot{\rho}_{obs}$: observed range and range rate;

The transition matrix and the design matrix take the form of Equations 3-12 and 3-13, respectively (Zhang, 1995b).

$$\Phi = \begin{bmatrix} 1 & 0 & 0 & dt & 0 & 0 & 0 & 0 \\ 0 & 1 & 0 & 0 & dt & 0 & 0 & 0 \\ 0 & 0 & 1 & 0 & 0 & dt & 0 & 0 \\ 0 & 0 & 0 & e^{-dt/\tau} & 0 & 0 & 0 & 0 \\ 0 & 0 & 0 & 0 & e^{-dt/\tau} & 0 & 0 & 0 \\ 0 & 0 & 0 & 0 & 0 & e^{-dt/\tau} & 0 & 0 \\ 0 & 0 & 0 & 0 & 0 & 0 & 1 & dt \\ 0 & 0 & 0 & 0 & 0 & 0 & 0 & e^{-dt/\zeta} \end{bmatrix} \qquad (3\text{-}12)$$

$$H=\begin{bmatrix} \frac{d\rho_1}{dx} & \frac{d\rho_1}{dy} & \frac{d\rho_1}{dz} & 0 & 0 & 0 & 1 & 0 \\ \vdots & \vdots & \vdots & \vdots & \vdots & \vdots & \vdots & \vdots \\ \frac{d\rho_n}{dx} & \frac{d\rho_n}{dy} & \frac{d\rho_n}{dz} & 0 & 0 & 0 & 1 & 0 \\ \frac{d\dot{\rho}_1}{dx} & \frac{d\dot{\rho}_1}{dy} & \frac{d\dot{\rho}_1}{dz} & \frac{d\dot{\rho}_1}{d\dot{x}} & \frac{d\dot{\rho}_1}{d\dot{y}} & \frac{d\dot{\rho}_1}{d\dot{z}} & 0 & 1 \\ \vdots & \vdots & \vdots & \vdots & \vdots & \vdots & \vdots & \vdots \\ \frac{d\dot{\rho}_n}{dx} & \frac{d\dot{\rho}_n}{dy} & \frac{d\dot{\rho}_n}{dz} & \frac{d\dot{\rho}_n}{d\dot{x}} & \frac{d\dot{\rho}_n}{d\dot{y}} & \frac{d\dot{\rho}_n}{d\dot{z}} & 0 & 1 \end{bmatrix} \tag{3-13}$$

where

$$\frac{d\rho_i}{dx}=\frac{d\dot{\rho}_i}{d\dot{x}}=-\frac{x_s^i-x}{\rho_i},\quad \frac{d\rho_i}{dy}=\frac{d\dot{\rho}_i}{d\dot{y}}=-\frac{y_s^i-y}{\rho_i},\quad \frac{d\rho_i}{dz}=\frac{d\dot{\rho}_i}{d\dot{z}}=-\frac{z_s^i-z}{\rho_i}$$

$$\frac{d\dot{\rho}_i}{dx}=-\frac{\dot{x}_s^i-\dot{x}}{\rho_i}+\frac{x_s^i-x}{\rho_i^3}[(x_s^i-x)(\dot{x}_s^i-\dot{x})+(y_s^i-y)(\dot{y}_s^i-\dot{y})+(z_s^i-z)(\dot{z}_s^i-\dot{z})]$$

$$\frac{d\dot{\rho}_i}{dy}=-\frac{\dot{y}_s^i-\dot{y}}{\rho_i}+\frac{y_s^i-y}{\rho_i^3}[(x_s^i-x)(\dot{x}_s^i-\dot{x})+(y_s^i-y)(\dot{y}_s^i-\dot{y})+(z_s^i-z)(\dot{z}_s^i-\dot{z})]$$

$$\frac{d\dot{\rho}_i}{dz}=-\frac{\dot{z}_s^i-\dot{z}}{\rho_i}+\frac{z_s^i-z}{\rho_i^3}[(x_s^i-x)(\dot{x}_s^i-\dot{x})+(y_s^i-y)(\dot{y}_s^i-\dot{y})+(z_s^i-z)(\dot{z}_s^i-\dot{z})]$$

ρ_i: range between satellite i and the rover;

x_s^i, y_s^i, z_s^i: coordinates of satellite i;

dt: Kalman filter prediction interval;

n: number of satellites observed by both receivers;

ζ : receiver clock drift correlation time (Gauss-Markov process);

τ : velocity error correlation time (Gauss-Markov process).

dt is chosen as 1 second. ζ and τ depend on the receiver clock characteristics and vehicle dynamics, respectively. ζ is chosen as 3600 seconds for the AshTech Z-XII receivers (Zhang, 1995b) and τ is chosen as 10 seconds during the field tests.

The initial variance and spectral densities used in the DGPS Kalman filter are listed in Table 3-1.

Table 3-1 Initial Variances and Spectral Densities for the DGPS Kalman Filter

Parameter	Initial variance	Spectral density
Position	10000.0 m^2	10.0 m^2Hz
Velocity	0.25 $(m/s)^2$	2.0 $(m/s)^2$Hz
Receiver clock bias	10000.0 m^2	$1.0*10^{-2}$ m^2Hz
Receiver clock drift	1.0 $(m/s)^2$	$1.0*10^{-6}$ $(m/s)^2$Hz

The variances for measurement noise are 25 m^2 for pseudorange and 0.0025 $(m/s)^2$ for phase rate.

After setting up all the Kalman filter parameters, extended Kalman filtering is applied.

CHAPTER 4

GPS/INS INTEGRATION

Increased computer power and multi-sensor technology have resulted in the development of integrated navigation systems in which the master systems output high-rate navigation data, while the local sensors or systems offer external measurements to update the errors of the master systems.

With GPS in full operation, GPS integrated with INS or inertial sensors has become an important means of navigation.

In GPS/INS integration, INS becomes an error-bounded navigator when GPS data is available. The high rate inertial data is output with little error growth between GPS updates. Since the INS error state coefficients are continuously updated at every GPS measurement, the INS continues to output high-quality solutions using the calibrated values of error states such as gyro drifts and accelerator biases (Greenspan, 1995).

The synergism of integrating an inertial navigation system is well known. At the software level, there are two major approaches, embedded and aided. In the aided approach, GPS and INS are loosely coupled. The INS uses the velocity and/or position data from the GPS navigation solution to improve its predicted state vector. In the embedded approach, GPS and INS are tightly coupled at the measurement level. The INS uses pseudorange, range rate and/or carrier phase measurements from GPS to update its predicted state vector (Schwarz and Wei, 1994c).

The corresponding Kalman filters for the two approaches are called decentralized and centralized filters, respectively. The performances of the two approaches have been investigated in Schwarz and Wei (1994c).

The aided integration scheme has been used in the real-time integrated system developed in this research because, conceptually, it is easier to understand, the computational burden is reduced, software implementation is easier, and the performance is almost the same as that of the embedded integration.

Because the quality of the integration depends on the accuracy with which the state vector models the time varying errors of the integrated system and the Kalman filter and its statistical characterization of the error process, both will be discussed in the following. In section 4.1, Kalman filtering will be introduced first; in sections 4.2 and 4.3, the INS

error model and measurement model will be set up; section 4.4 discusses the selection of the filter parameters; in section 4.5, the aided integration scheme will be described.

4.1 Kalman Filtering

In discrete Kalman filtering, the system is described by a linear dynamic model:

$$\mathbf{x}_k = \Phi_{k-1}\,\mathbf{x}_{k-1} + \mathbf{w}_{k-1} \tag{4-1}$$

and the measurement by a linear model:

$$\mathbf{z}_k = \mathbf{H}_k\mathbf{x}_k + \mathbf{u}_k \tag{4-2}$$

where

Φ is the transition matrix;

$\mathbf{w}$ is the system noise;

$\mathbf{z}$ is the measurement vector;

$\mathbf{H}$ is the design matrix;

$\mathbf{u}$ is the measurement noise.

Three assumptions are made to define the Kalman filter:

1. The system noise and the measurement noise are uncorrelated and zero mean random processes, i.e.:

$$E[\mathbf{w}_k \mathbf{u}_j^T] = 0 \text{ for all j and k} \tag{4-3}$$

$$\mathbf{w}_k \sim N(\mathbf{0}, \mathbf{Q}_k); \qquad \mathbf{u}_k \sim N(\mathbf{0}, \mathbf{R}_k)$$

and the covariance matrices are:

$$E[\mathbf{w}_k \mathbf{w}_j^T] = \begin{cases} \mathbf{Q}_k, k = j \\ \mathbf{0}, k \neq j \end{cases} \quad ; \quad E[\mathbf{u}_k \mathbf{u}_j^T] = \begin{cases} \mathbf{R}_k, k = j \\ \mathbf{0}, k \neq j \end{cases} \tag{4-4}$$

2. The initial system state vector $\mathbf{x}_0$ is uncorrelated to both system noise and measurement noise.

$$E[\mathbf{x}_0 \mathbf{w}_k^T] = 0 \quad ; \quad E[\mathbf{x}_0 \mathbf{u}_k^T] = 0 \tag{4-5}$$

3. The initial mean value of the system state and the covariance matrix of the initial system noise are known, i.e.

$$\bar{\mathbf{x}}_0 = E[\mathbf{x}_0] \quad ; \qquad \mathbf{P}_0 = E[(\mathbf{x}_0 - \bar{\mathbf{x}}_0)(\mathbf{x}_0 - \bar{\mathbf{x}}_0)^T] \tag{4-6}$$

There are two steps in Kalman filtering. The first step is the prediction by the system model, i.e.:

$$\hat{\mathbf{x}}_k(-) = \Phi_{k-1}\, \hat{x}_{k-1}(+)\,; \qquad \mathbf{P}_k(-) = \Phi_{k-1}\, \mathbf{P}_{k-1}(+)\, \Phi_{k-1}^T + \mathbf{Q}_{k-1} \tag{4-7}$$

and the second step is the measurement update of the system model:

Kalman gain matrix: $\mathbf{K}_k = \mathbf{P}_k(-)\mathbf{H}_k^T[\mathbf{H}_k\mathbf{P}_k(-)\mathbf{H}_k^T + \mathbf{R}_k]^{-1}$ (4-8)

Error covariance update: $\mathbf{P}_k(+) = [\mathbf{I} - \mathbf{K}_k\mathbf{H}_k]\mathbf{P}_k(-)$ (4-9)

State prediction update: $\hat{\mathbf{x}}_k(+) = \hat{\mathbf{x}}_k(-) + \mathbf{K}_k[\mathbf{z}_k - \mathbf{H}_k\, \hat{\mathbf{x}}_k(-)]$ (4-10)

4.2 INS Error Model

Theoretically, any error state of both the GPS and the INS system can be included in the integrated Kalman filter. Because GPS system errors are modeled in the GPS Kalman

filter in Chapter 3, only INS related error states will be modeled in the master filter. The error state vector therefore consists of 5 three-dimensional vectors to model errors in position, velocity, and misalignment as well as gyro drift and accelerometer bias (Lapucha, 1990, Wong, 1988, Zhang, 1995a), altogether the 15 states shown in Equation 4-11.

$$\mathbf{x} = (\varepsilon_x^e \varepsilon_y^e \varepsilon_z^e \delta x^e \delta y^e \delta z^e \delta v_x^e \delta v_y^e \delta v_z^e d_x^b d_y^b d_z^b b_x^b b_y^b b_z^b) \tag{4-11}$$

Where

$\varepsilon_x^e, \varepsilon_y^e, \varepsilon_z^e$: three misalignment errors in the e-frame;

$\delta x^e, \delta y^e, \delta z^e$: three position errors in the e-frame;

$\delta v_x^e, \delta v_y^e, \delta v_z^e$: three velocity errors in the e-frame;

d_x^b, d_y^b, d_z^b: three gyro drifts in the b-frame;

b_x^b, b_y^b, b_z^b: three accelerometer biases in the b-frame.

The three gyro drifts and the three accelerometer biases are modeled as first-order Gauss-Markov processes, i.e.:

$$\dot{d} = -\alpha d + w_d \tag{4-12}$$

$$\dot{b} = -\beta b + w_b \tag{4-13}$$

where α and β are the reciprocals of the correlation lengths of the two Gauss-Markov processes, respectively. Both of the correlation lengths have been chosen to be 40 hours.

The error system is described by a linear dynamic model:

$$\dot{\mathbf{x}} = \mathbf{F}\mathbf{x} + \mathbf{w} \tag{4-14}$$

where

$\mathbf{x}$ is the system state vector;

$\mathbf{F}$ is the dynamics matrix;

$\mathbf{w}$ is the system noise.

When the system is modeled in the e-frame, $\mathbf{F}$ is given by Equation 4-15 (Wei and Schwarz, 1990a).

$\mathbf{F}=$

$$\begin{bmatrix}
0 & \omega_e & 0 & 0 & 0 & 0 & 0 & 0 & 0 & R_{11} & R_{12} & R_{13} & 0 & 0 & 0 \\
-\omega_e & 0 & 0 & 0 & 0 & 0 & 0 & 0 & 0 & R_{21} & R_{22} & R_{23} & 0 & 0 & 0 \\
0 & 0 & 0 & 0 & 0 & 0 & 0 & 0 & 0 & R_{31} & R_{32} & R_{33} & 0 & 0 & 0 \\
0 & 0 & 0 & 0 & 0 & 0 & 1 & 0 & 0 & 0 & 0 & 0 & 0 & 0 & 0 \\
0 & 0 & 0 & 0 & 0 & 0 & 0 & 1 & 0 & 0 & 0 & 0 & 0 & 0 & 0 \\
0 & 0 & 0 & 0 & 0 & 0 & 0 & 0 & 1 & 0 & 0 & 0 & 0 & 0 & 0 \\
0 & f_z & -f_y & N_{11} & N_{12} & N_{13} & 0 & 2\omega_e & 0 & 0 & 0 & 0 & R_{11} & R_{12} & R_{13} \\
-f_z & 0 & f_x & N_{21} & N_{22} & N_{23} & -2\omega_e & 0 & 0 & 0 & 0 & 0 & R_{21} & R_{22} & R_{23} \\
f_y & -f_x & 0 & N_{31} & N_{32} & N_{33} & 0 & 0 & 0 & 0 & 0 & 0 & R_{31} & R_{32} & R_{33} \\
0 & 0 & 0 & 0 & 0 & 0 & 0 & 0 & 0 & -\alpha & 0 & 0 & 0 & 0 & 0 \\
0 & 0 & 0 & 0 & 0 & 0 & 0 & 0 & 0 & 0 & -\alpha & 0 & 0 & 0 & 0 \\
0 & 0 & 0 & 0 & 0 & 0 & 0 & 0 & 0 & 0 & 0 & -\alpha & 0 & 0 & 0 \\
0 & 0 & 0 & 0 & 0 & 0 & 0 & 0 & 0 & 0 & 0 & 0 & -\beta & 0 & 0 \\
0 & 0 & 0 & 0 & 0 & 0 & 0 & 0 & 0 & 0 & 0 & 0 & 0 & -\beta & 0 \\
0 & 0 & 0 & 0 & 0 & 0 & 0 & 0 & 0 & 0 & 0 & 0 & 0 & 0 & -\beta
\end{bmatrix} \tag{4-15}$$

where

ω_e is the Earth rotation rate;

f_x, f_y, f_z are the specific force components expressed in the e-frame;

R_{ij} are elements of the transformation matrix R_b^e;

N_{ij} are elements of the normal gravity coefficient matrix N^e.

The above error system model must be discretized before the discrete Kalman filter is applied.

The transition matrix Φ in Equation 4-1 can be calculated by Equation 4-16.

$$\Phi = e^{\mathbf{F}\Delta t} \tag{4-16}$$

Where Δt is the discretization interval. Φ is approximated after the first term of the Taylor series expansion of $e^{\mathbf{F}\Delta t}$, i.e.:

$$\Phi = \mathbf{I} + \mathbf{F}\Delta t \tag{4-17}$$

4.3 Measurement Model

In the aided integration scheme, INS uses GPS position and/or velocity to update the error state vector. The measurements used in such an integration scheme are the misclosures of position and/or velocity between the INS predicted position and/or velocity, and the GPS position and/or velocity after lever arm effects have been compensated for.

The lever arm effect is due to the spatial offset between the INS mass center and the GPS receiver antenna phase center. The lever arm effects on position and velocity in the e-frame are computed by Equations 4-18 and 4-19 (Zhang,1995a), respectively.

$$\delta \mathbf{r}^e = \mathbf{R}_b^e \mathbf{r}_{GPS-INS}^b \tag{4-18}$$

$$\delta \mathbf{v}^e = \dot{\mathbf{R}}_b^e \, \mathbf{r}_{GPS-INS}^b \tag{4-19}$$

The $\mathbf{r}_{GPS-INS}^b$ is the offset vector between the GPS receiver antenna phase center and the INS mass center in the b-frame. The offset is measured before each test and input into the system as a known parameter. ω_{lb}^b is the angular velocity of the b-frame with respective to the l-frame expressed in the b-frame. $\delta \mathbf{r}^e$ and $\delta \mathbf{v}^e$ are the lever arm effects on position and velocity, respectively.

The position and velocity misclosures are $\mathbf{z}(\mathbf{r})$ and $\mathbf{z}(\mathbf{v})$ which will be computed by Equations 4-20 and 4-21, respectively.

$$\mathbf{z}(\mathbf{r}) = \mathbf{r}_{INS}^e + \delta \mathbf{r}^e - \mathbf{r}_{GPS}^e \tag{4-20}$$

$$\mathbf{z}(\mathbf{v}) = \mathbf{v}_{INS}^e + \delta \mathbf{v}^e - \mathbf{v}_{GPS}^e \tag{4-21}$$

where

$\mathbf{r}_{INS}^e, \mathbf{v}_{INS}^e$: INS-derived position and velocity vectors in the e-frame;

$\mathbf{r}_{GPS}^e, \mathbf{v}_{GPS}^e$: GPS-derived position and velocity vectors in the e-frame.

4.4 Selection of the Kalman Filter Parameters

After identifying the error states of the filter and defining the system and measurement models, selecting the filter parameters becomes the major task which includes the determination of the matrices $\mathbf{P}_o$, $\mathbf{Q}$ and $\mathbf{R}$ and the initial error state vector $\mathbf{x}_o$.

For a well calibrated system, the errors of the navigation quantities at the end of the coarse alignment are random from one alignment to another, thus the initial error state vector is set to zero (Wong, 1988), i.e.:

$$\mathbf{x}_o = \mathbf{0}$$

The initial variances of the misalignments are dependent on the accuracy of the coarse alignment. They have been chosen as 1600 $(arc\,\text{sec})^2$ in the east and north directions and 1 $(\text{deg.})^2$ in the vertical direction.

During the initial alignment, the vehicle is stationary and the velocities are reset to zero at the end of the alignment. The variance has been selected as $1.0 * 10^{-6} (m/s)^2$.

The initial coordinates are from real-time DGPS. The initial variance of coordinates are determined by the positioning accuracy of DGPS. It has been determined as $4m^2$.

The initial variances of the residual gyro drifts and accelerometer biases depend on the accuracy of the system calibration (Wong, 1988). They have been estimated as $1.0*10^{-4}(\text{deg.}/h)^2$ and $1.0*10^{-7}(m/s^2)^2$, respectively.

The spectral density matrix **Q** represents the inadequacy of the error states. They are determined from sensor accuracies and system calibration. For a detailed discussion of the derivation of **Q**, see Wong, 1988. Table 4-1 lists the spectral densities for the integration filter.

Table 4-1 Kalman Filter Spectral Densities

Parameter	Spectral density
Misalignments	$1.0 arc\sec^2 Hz$
Position	0
Velocity	$1.0*10^{-4}(m/s)^2 Hz$
Gyro drifts	$1.4*10^{-11}(\text{deg.}/h)^2 Hz$
Accel. biases	$1.4*10^{-11}(m/s^2)^2 Hz$

The last parameter of the integration filter is the measurement noise variance matrix **R**. The external measurements are the DGPS-derived velocity and position. The variances chosen should reflect the accuracy of the measurements. Thus the variances are

$1\ (cm/s)^2$ for the velocity measurements and $1\ m^2$ for the position measurements.

The vector $\mathbf{x}_o$ and the matrices $\mathbf{P}_o$, $\mathbf{Q}$ and $\mathbf{R}$ derived above will be applied to the real-time integrated system. Test results will be analyzed in chapter 6.

4.5 Aided GPS/INS Integration

In the real-time integrated GPS/INS developed in this research, only one local filter is designed for GPS navigation estimation. The solutions from the local filter are periodically fused into the integration filter.

The integration filter can be implemented either in a feedforward manner or a feedback manner. In the feedback configuration, the navigation errors estimated by the integration filter are fed back to the inertial navigation computation to correct the navigation errors; and the estimates of the inertial sensor error corrections are fed back to add to the inertial sensor errors. The aided feedback integration configuration is shown in Figure 4-1.

In Figure 4-1, GPS pseudorange and Doppler measurements at the rover station and the corrections transmitted from the master station are processed by the local Kalman filter. The position and velocity solutions from the local filter are fused into the integration filter. Before the integration, the GPS solutions are checked to prohibit the bad solutions

going into the integration filter. This ensures the quality of the final navigation results. The GPS validity check includes satellite number check and the GPS navigation parameter check. If the satellite number is less than 4, the GPS navigation parameters are not used for update in the aided integration scheme (Wei and Schwarz, 1990b).The GPS navigation parameter check is realized by checking the position and velocity misclosures. If any component of the velocity misclosures is larger than the velocity misclosure threshold, there will be no velocity update. If any component of the position misclosures is larger than the position misclosure threshold and at the same time, if any one of the velocity misclosures is larger than its threshold, there will be no position update. Otherwise, if the velocity misclosures are all within the limit, there is still a position update. The thresholds are 1 m/s for velocity and 2 m for position.

If the GPS solution is valid, integration will take place. The estimated navigation errors will be subtracted from the INS mechanization results. The estimated sensor error corrections are added to the sensor errors for the next epoch sensor error calibration.

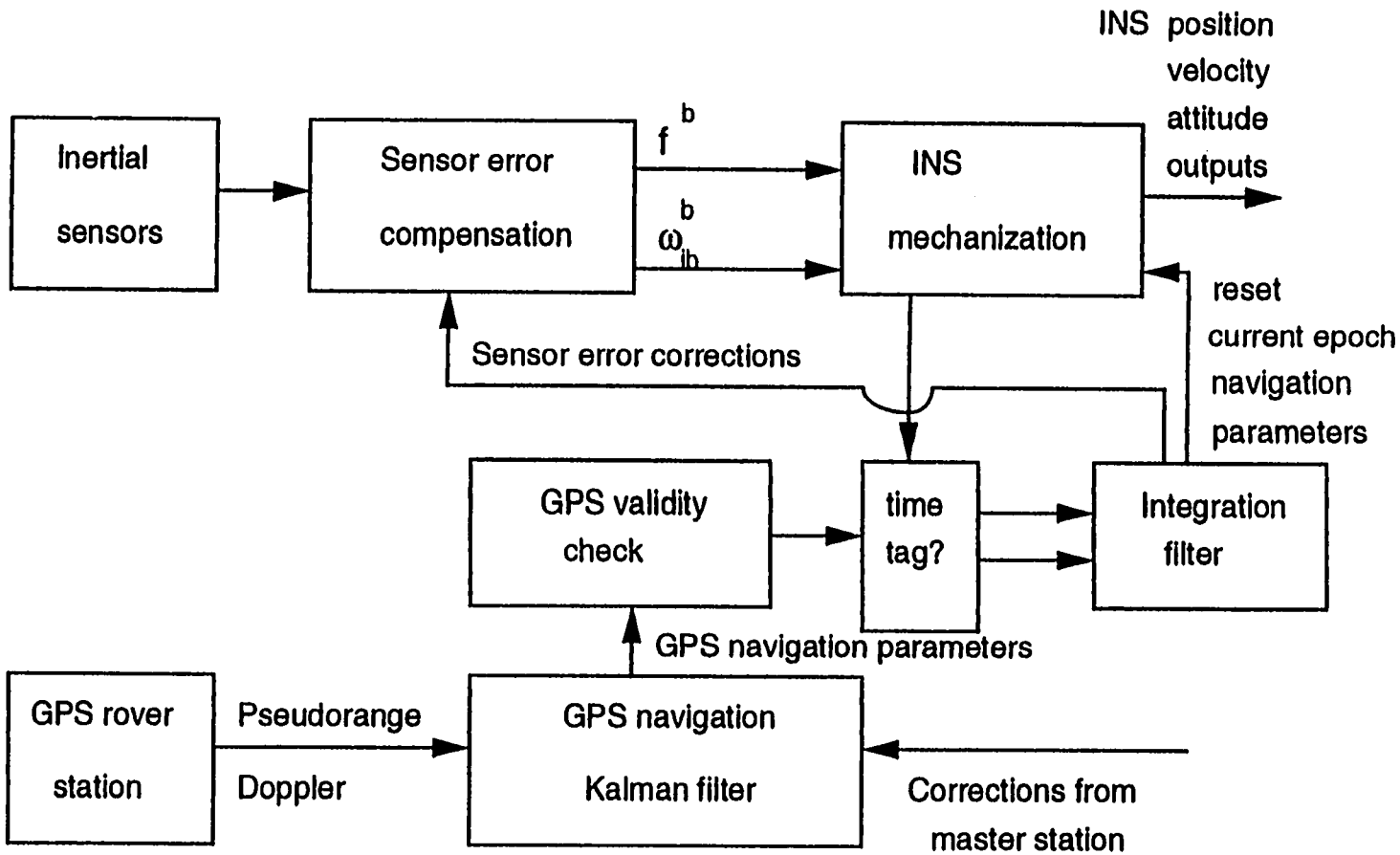

Figure 4-1 Block Diagram of Aided Feedback DGPS/INS Integration

CHAPTER 5

SYSTEM IMPLEMENTATION

In this chapter, system implementation will be discussed which includes the hardware components, data acquisition, and the software design.

5.1 Hardware

Inertial Measurement Unit (IMU)

One of the key hardware components of the real-time system is the Inertial Measurement Unit. An LTN-90-100 IMU is used as the SINS. The LTN-90-100 is a high accuracy inertial reference unit. The specifications given by the manufacturer are listed in Table 5-1.

Table 5-1 LTN-90-100 IMU Specifications

Accelerometers	
Scale factor repeatability	50 ppm(1 yr)(1σ)
Scale factor Kii	10 $\mu g / g^2$ max.
Scale factor temperature predictability	10 ppm (-20 to 70° C)
Net bias accuracy	50 μg (1 yr) (-20 to 70° C)(1σ)
Bias short term stability	5.0 μg (1σ)
Alignment stability	5 s (1σ)
Operating temperature range	-54 to +95° C
Shock	100 g, 11 ms
Maximum acceleration	25 g
Gyros	
Random drift	0.0025°/h
Bias repeatability (all causes)	0.01°/h (1σ)
S.F. stability (overall environment)	5 ppm (1σ)
Maximum rate	±400°/s

The IMU sensor assembly consists of a precision mounting block with three Litton A-4 linear accelerometers in one triad module, one high voltage power supply, and three LG-8028B laser gyros.

The IMU interface is in the industry ARINC 429 standard. It outputs navigation parameters and the raw measurements.

SS1000 ARINC Board

To reduce the host computer burden, a special purpose board was designed which is inserted in the computer bus slot. The SS1000 ARINC board loads the data from the IMU and writes the data to its local dual port memory.

GPS receivers

GPS receivers used throughout the tests are AshTech Z-XII receivers which are dual frequency, 12-channel receivers. The receiver outputs C/A code pseudorange, carrier phase and phase rate on L1, and P-code pseudorange, carrier phase, and phase rate on L2. In the real-time system, 0.5 Hz C/A code pseudorange and Doppler measurements are used for GPS positioning computation. In addition to raw measurement data, the receiver also outputs navigation data and Pulse Per Second (PPS) signals which are used for the INS and GPS data synchronization.

Computers

Two 486/66 PC computers are used. One is a Desktop which is used at the master station to collect GPS data and calculate and transmit the corrections to the rover station. The other one is a Lunchbox computer which is used at the rover station to collect the GPS data, the corrections from the master station, and the INS data and perform real-time navigation computations.

Radio Data Link System

Corrections are transmitted from master station to rover station by a commercial Radio Data Link System. The system consists of two antennas, two radio transceivers, a Base Station Data Link Control (BDLC), and a Mobile Radio Modem (MRM). At the master station, correction data is sent to the radio transceiver through a RS232 serial communication port with a Baud rate of 9600. The radio transceiver transmits the data modulated by BDLC at an UHF frequency with a power of 25 watts. At the rover station, the transmitted radio signals are received and demodulated by a radio data receiving system which includes a radio transceiver and the MRM. The computer logs the data through a RS232 port with the Baud rate of 9600. The real-time data link is illustrated by Figure 5-1.

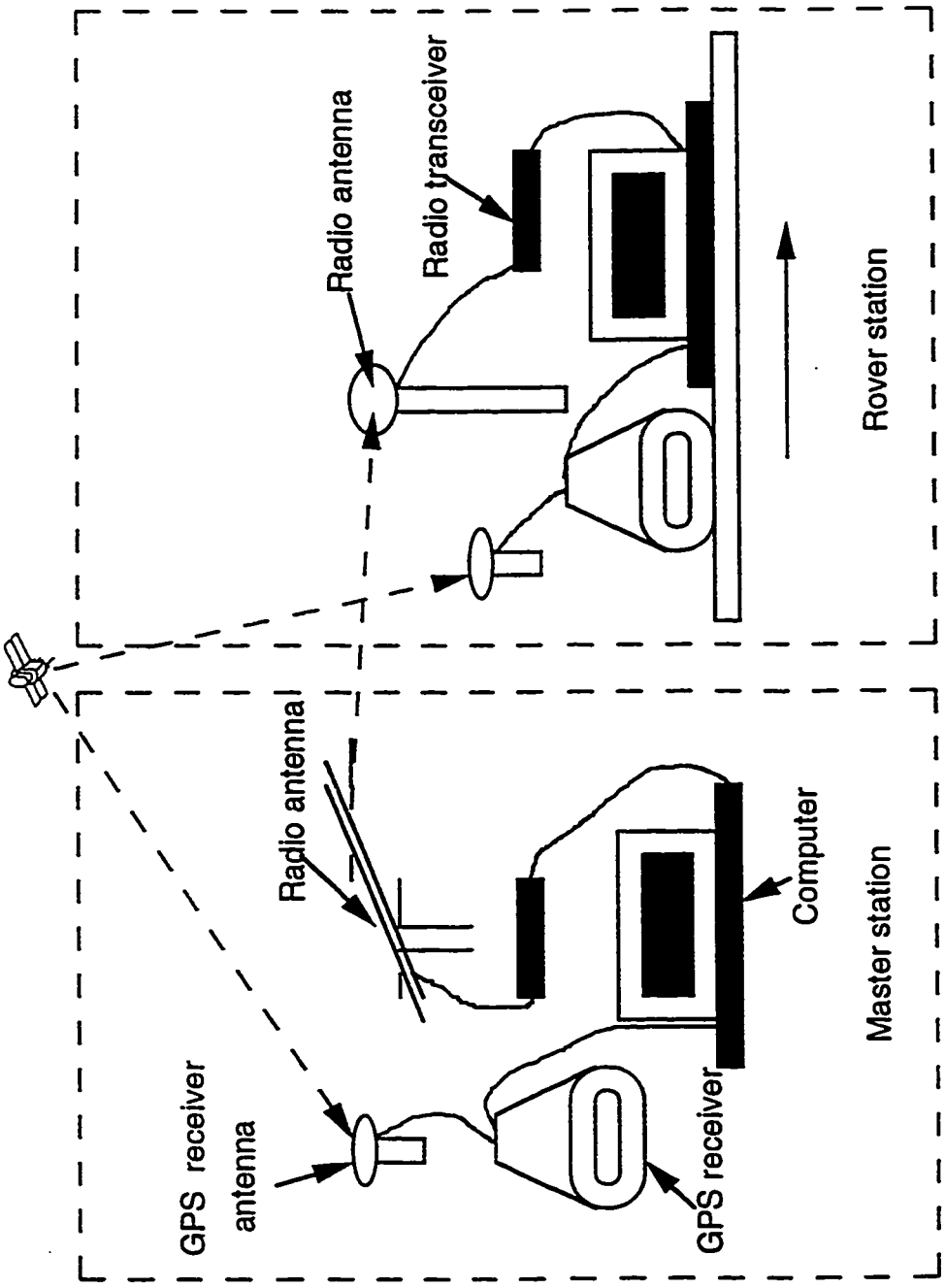

Figure 5-1 Real-Time Data Link

5.2 GPS/INS Data Acquisition

INS Data Acquisition at the Rover Station

The INS data is acquired by the SS1000 ARINC board. A resident program is running on the board. It selects the incoming data according to the user's requirement and puts the data into the dual port memory. It generates an interrupt to the host computer after it receives the last label indicated by the host computer command in the initialization. By responding to the interrupt, the host computer puts the computer time to the INS record as a time tag and copies the record from the dual port memory on the board together with the time tag into its local memory, which is a ring buffer.

GPS Data Acquisition at the Rover Station

GPS data is collected through a RS232 port. Each byte of the data generates an interrupt which is served by the corresponding interrupt handler. The interrupt handler stores the data into another ring buffer.

Correction Data Acquisition at the Rover Station

Correction data from the master station is received in the same way as the GPS data. Another RS232 port interrupt handler puts the data into a ring buffer.

The main program checks each of the three ring buffers to see whether a full record has been received. If that is the case, it unpacks the data to a meaningful structure, stores the data to hard disk, and does the navigation computations.

The data acquisition configuration at the rover station is given by Figure 5-2.

GPS Data Acquisition at the Master Station

At the master station, GPS data is received in the same way as at the rover station. Once a full GPS data record has been received, the corrections are calculated and sent to the radio transceiver. The raw measurements and navigation data from the receiver are stored. The data acquisition configuration at the master station is shown in Figure 5-3.

5.3 Synchronization of the GPS and INS Data Streams

One of the most important tasks in an integrated system is the time synchronization of the different data streams.

The PPS signal from the GPS receiver is used for time synchronization. The PPS signal is received by the computer through a LPT port. When the interrupt handler responds to the LPT interrupt, the computer time is taken, which is the PPS time tag in the computer time frame. The GPS time corresponding to the PPS signal record is obtained from the corresponding GPS navigation record, i.e. the PBEN record for AshTech Z-XII receiver. The offset between the GPS time frame and the computer time frame is, therefore, obtained. Applying this offset to the INS time tag in the computer time frame will result in the INS time tag in the GPS time frame which can be expressed by Equation 5-1.

$$t_{ins}^{gps} = t_{ins}^{c} + (t_{pps}^{gps} - t_{pps}^{c}), \tag{5-1}$$

where

t_{ins}^{gps} : INS time tag in GPS time frame;

t_{ins}^{c} : INS time tag in computer time frame;

t_{pps}^{gps} : PPS time tag in GPS time frame;

t_{pps}^{c} : PPS time tag in computer time frame.

If there are no delays in serving PPS interrupt, the time tagging accuracy should be within the PPS accuracy, i.e. 1 ms. Unfortunately, delays are unavoidable. Delays and other error

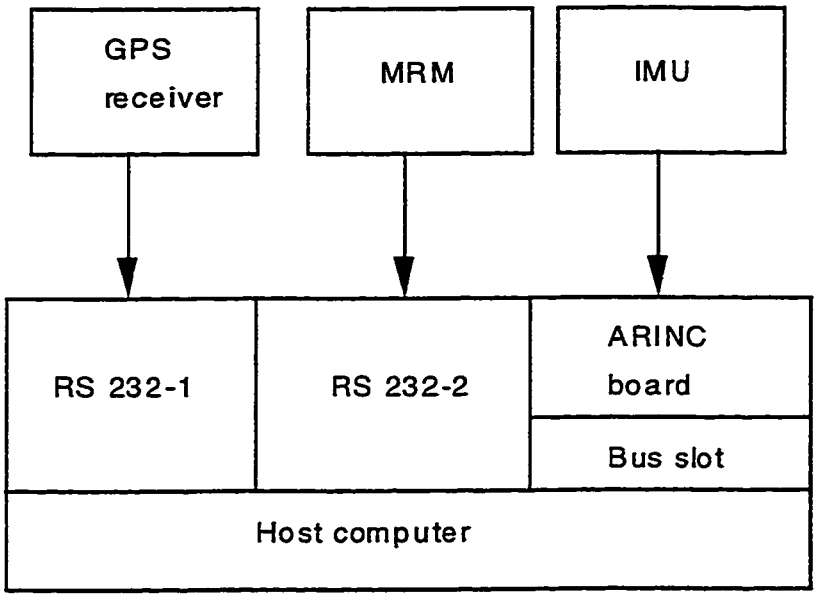

Figure 5-2 Rover Station Data Acquisition Configuration

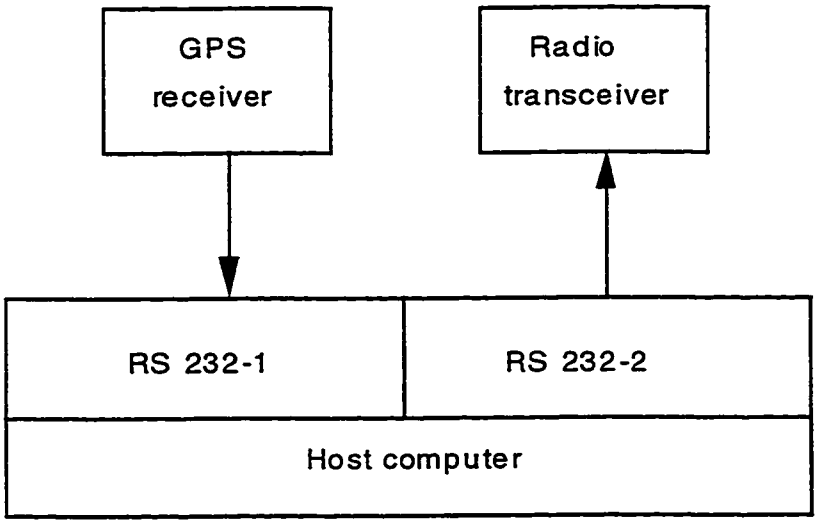

Figure 5-3 Master Station Data Acquisition Configuration

sources cause time synchronization errors. There are four types of errors, i.e. internal delays in the INS and the GPS receivers, data transmission delay, time tagging error, and computer clock reading errors. The effects of the time synchronization error are proportional to the speed of the vehicle, for instance, one millisec synchronization error causes 1.6 cm position error for a vehicle moving at 60 km/h. Thus, the requirements for synchronization accuracy will change for different applications. The estimated synchronization error is from 1 ms to 2 ms. For a detailed discussion of these errors and delays, see El-Sheimy (1996).

5.4 Software Design

After the discussion of SINS, GPS positioning and GPS/INS integration methodology in Chapters 2, 3 and 4, respectively and the selection of hardware components, software development becomes the major task. The software developed was based on an available real-time DGPS software package and the SINS mechanization functions and the Kalman filter routines have been taken from a post-mission GPS/INS software package. There are two software packages working at the master station and rover station, respectively. The software is coded in C and running under MSDOS 6.0.

The software at the master station carries out the following functions:

1. initialization,

2. logs GPS raw measurements,

3. computes the calculated range and range rate (Equations 3-3 and 3-4),

4. forms pseudorange and Doppler corrections (Equations 3-5 and 3-6),

5. sends the corrections to the radio transceiver,

6. stores GPS raw measurement and navigation data to hard disk,

7. displays the navigation results from the receiver and the correction information.

The software at the rover station performs the following functions:

1. initialization,

2. collects INS and GPS raw measurements and corrections from the master station,

3. SINS initial alignment and navigation computations (Equations 2-3 to 2-10 and 2-11 to 2-16),

4. zero velocity updates,

5. GPS navigation solution computation (Equations 3-8 to 3-13 and 4-7 to 4-10),

6. GPS/INS integration (Equations 4-11 to 4-21 and 4-7 to 4-10),

7. storage of GPS and INS raw measurements and corrections to hard disk,

8. display and storage of navigation results from both DGPS and INS.

The initialization at the master station receives the master station coordinates and the output data file names from the user through the keyboard and initializes the communication ports.

During initialization at the rover station, initial parameters are read from an ASCII file which contains Kalman filter parameters, datum, alignment length, ZUPT length, constant gyro drifts and accelerometer biases from calibration and output data file names. The initialization of the communication ports also takes place at this time.

The stored GPS raw measurement contains the C/A code pseudorange, Doppler and carrier phase on L1 and carrier phase on L2. It is stored for post-mission processing analysis.

The main program flow chart at the master station is given in Figure 5-4. The GPS/INS integration main program flow chart is shown in Figures 5-5a and 5-5b .

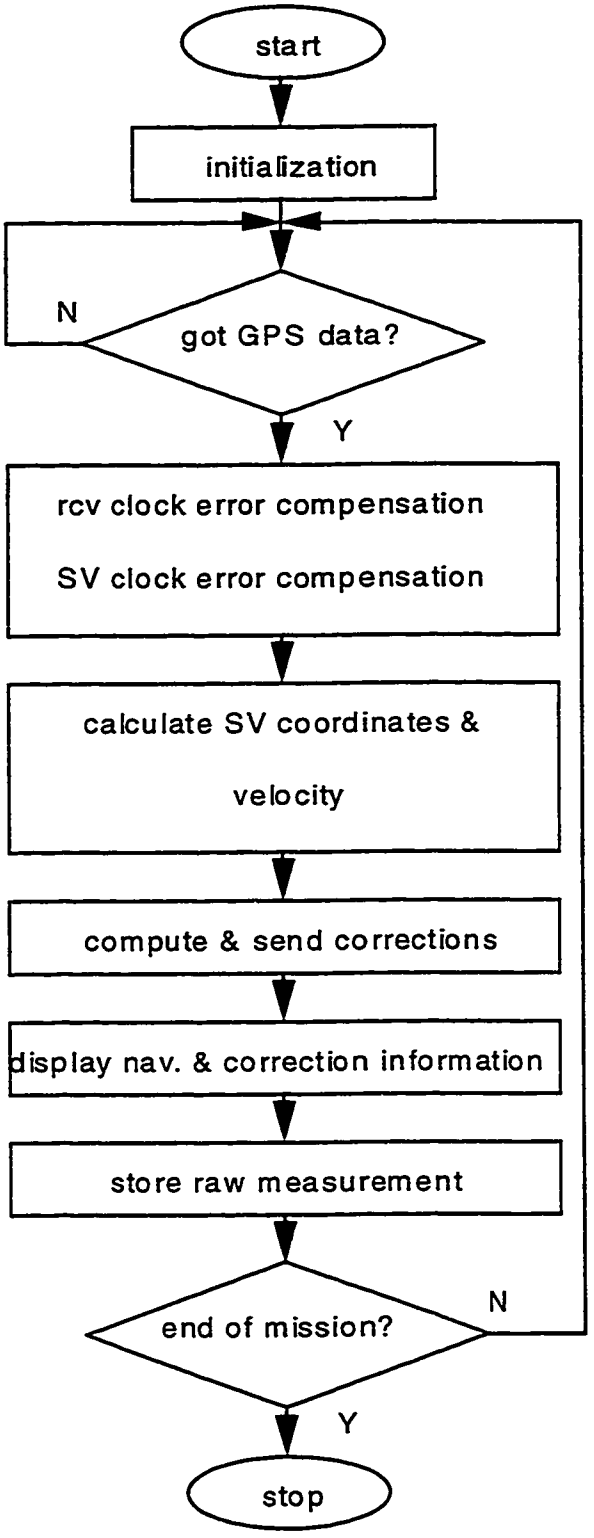

Figure 5-4 Master Station Main Program Flow Chart

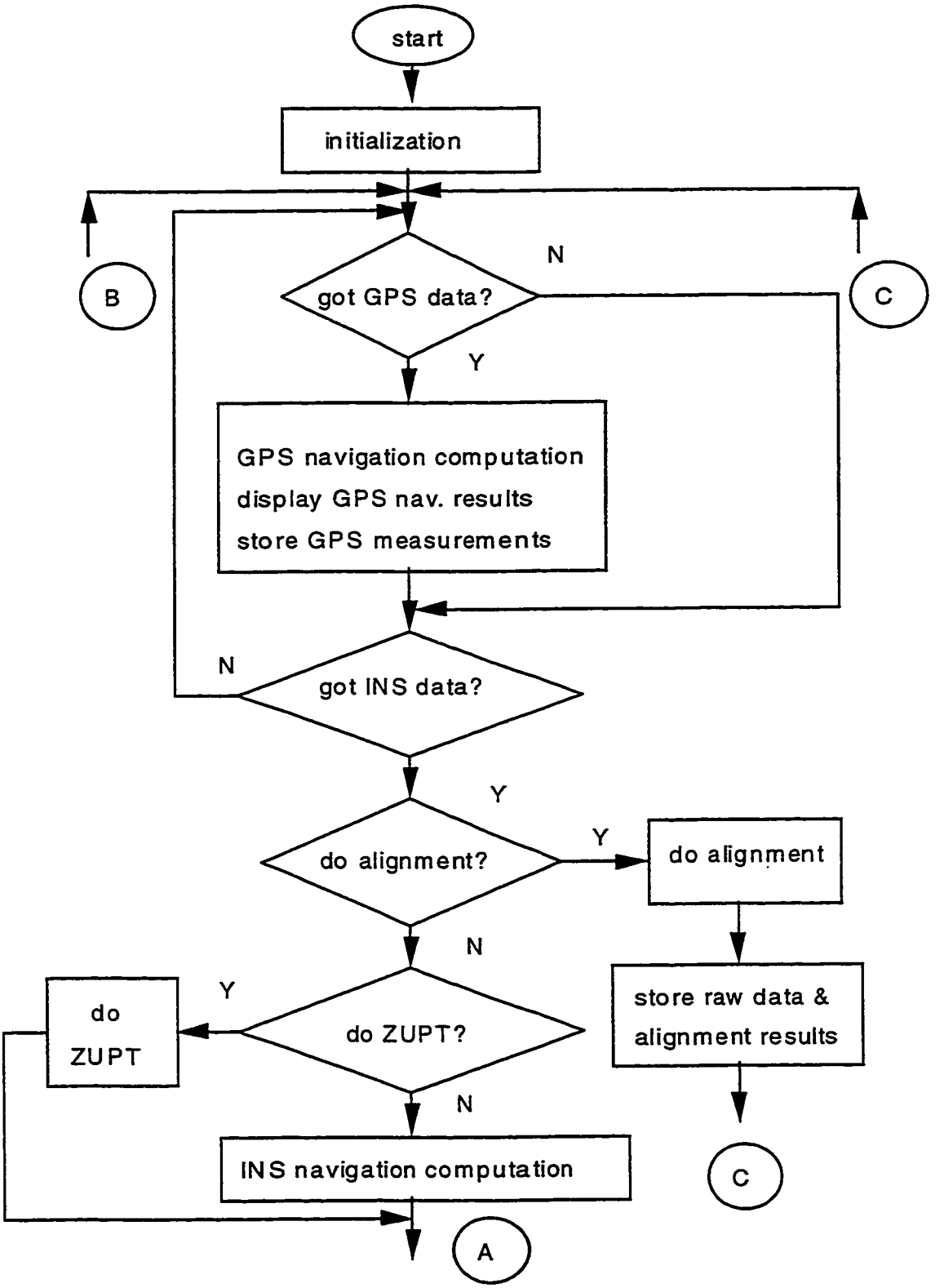

Figure 5-5a GPS/INS Integration Main Program Flow Chart

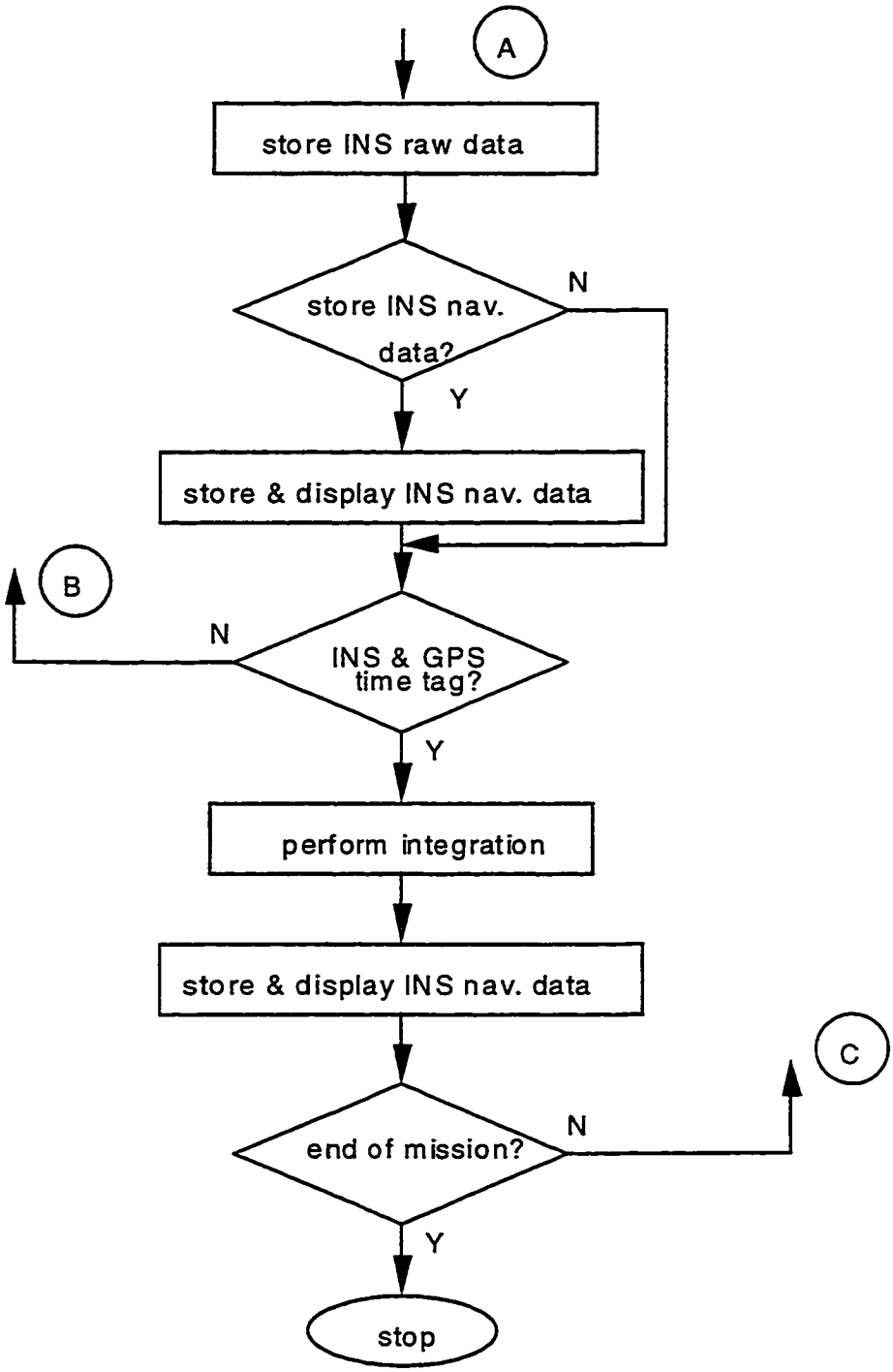

Figure 5-5b GPS/INS Integration Main Program Flow Chart

CHAPTER 6

TESTING AND RESULTS

Testing a system consists of four distinct steps. Testing the hardware function; testing the software function; testing the system function, i.e. the integration of the hardware and the software; and testing the system specifications. The purpose of testing is to verify the hardware and software design; to enhance the system functions; to tune the Kalman filters; and to evaluate the system performance.

In this chapter, static and kinematic tests have been conducted to verify the system design and the system functions. System performance has been assessed through the test results.

In section 6.1, the test setup is described. The reference values which are used to evaluate the system performances are given in section 6.2. In section 6.3, static test results are discussed. The results of two kinematic tests are analyzed in section 6.4. Section 6.5 discusses the system performance.

6.1 Test Description

a. Master Station

The master station was set up on the roof of the Engineering Building at the University of Calgary. There are several pillars on the roof whose coordinates in WGS-84 were surveyed by transferring the International Earth Rotation Service (IERS) Terrestrial Reference Frame (ITRF) 92 three-dimensional coordinates of a Canadian Active Control System using static DGPS carrier-phase survey (Henriksen et al., 1996). The absolute accuracy of the pillar coordinates is about 10 centimetres. The sketch of the pillars is shown in Figure 6-1.

Throughout the tests, the master station GPS receiver antenna was installed on pillar N2. The master station radio antenna was also mounted on the roof which provides good conditions for radio signal transmission (Zhang, 1995b). The drawback of this location is that it is a relatively high multipath environment.

b. Rover Station

Static test

During the static test, the rover receiver antenna was installed on pillar N3. The LTN-90-100 IMU was sitting close to the pillar. The offset between the GPS receiver antenna phase center and the origin of the body frame of the IMU in an arbitrary frame was derived using DGPS carrier-phase positioning and theodolite-measured angles. It was then transformed to the body frame using the heading information from the IMU. The offset was -1.53, -1.25 and 0.63 metres in x, y and z directions in the body frame, respectively. The accuracy of the offset is about 2 centimetres.

Kinematic test

During the kinematic tests, the rover station GPS receiver antenna was installed on top of the IMU. The IMU was put in a car trunk (the lid of the trunk was taken off). The offset between the GPS receiver antenna phase center and the origin of the body frame was surveyed in the same way as in the static test, it was 0.02, 0.05 and 1.03 metres in x, y and z directions in the body frame, respectively. The radio antenna was mounted on the roof of the car. The GPS receiver, radio transceiver and the computer were put inside the car. The setup is shown in Figure 6-2. The IMU, GPS receiver and radio transceiver were powered by 12V batteries.

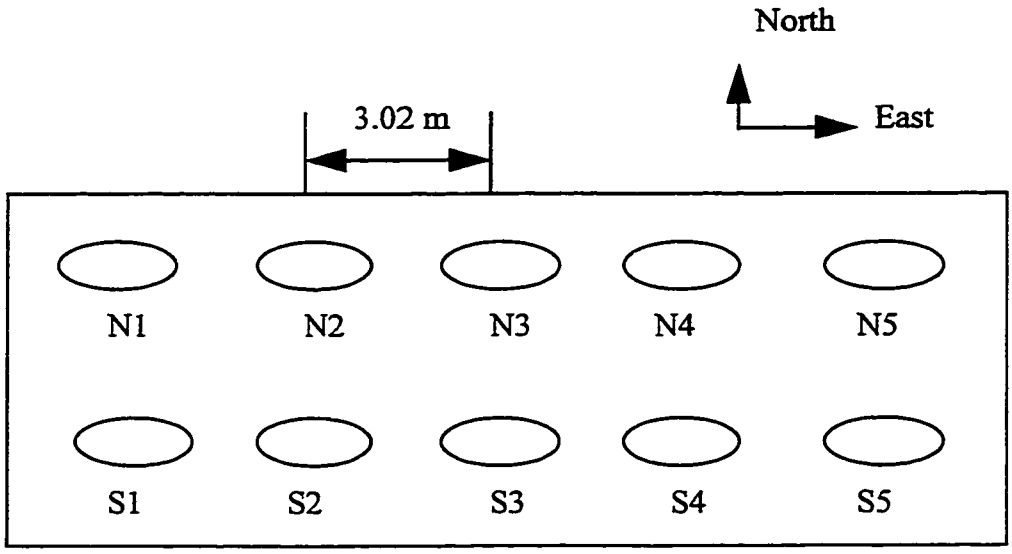

Figure 6-1 Sketch of the Pillars

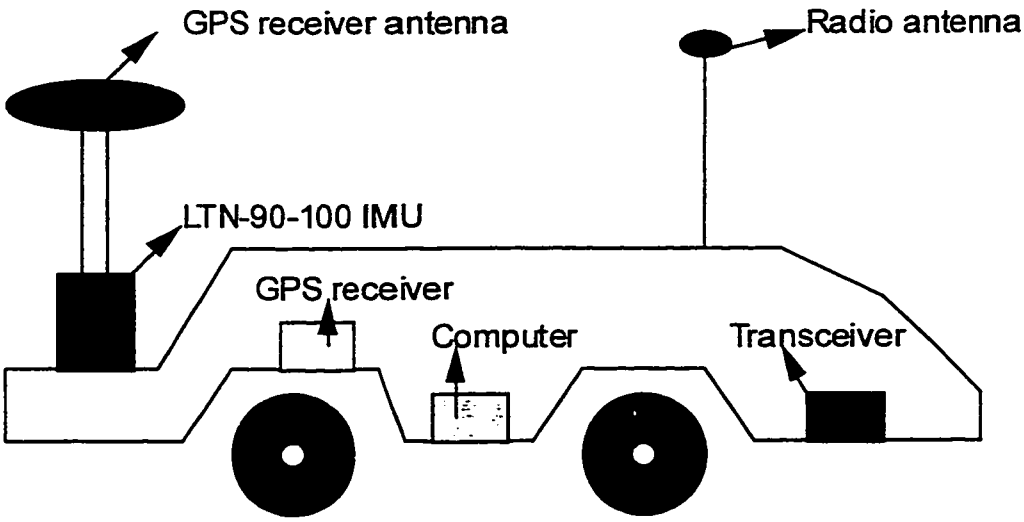

Figure 6-2 Test Setup

6.2 Reference

For the static test, the position and velocity references for the GPS antenna and the IMU are the known coordinates and zero velocities. The references for pitch and roll have been derived in the same way as in the kinematic tests which will be described in the following.

For the kinematic tests, the reference chosen for evaluating the performance of the real-time DGPS/INS integrated system is a GPS/INS post-mission processing package, which is called **Kingspad**. This package has been developed at the University of Calgary and has been tested in many applications (El-Sheimy, 1996, Skaloud, 1996 and Zhang, 1995a). In this software, double differenced GPS carrier phase and Doppler observations are used for GPS positioning calculation. The wide-laning technique has been used for the integer carrier phase ambiguity resolution. When the ambiguities are fixed, the relative positioning accuracy is at the level of 10 cm and the relative velocity accuracy at the level of a few mm/s. The derived GPS position and velocity are integrated with the INS data. These results are used as the reference for the real-time DGPS and the DGPS/INS integration, respectively.

In the following analysis, errors are defined as the differences between the reference and the real-time results. The mean and Root Mean Square (RMS) of the errors are determined where the RMS is defined as:

$$\text{RMS}=\sqrt{\frac{\sum_{i=1}^{n} y_i^2}{n}} \qquad (6\text{-}1)$$

where n is the number of data points and y_i is the data.

6.3 Results of the Static Test

Figures 6-3a and 6-3b show the stand-alone INS navigation performance (from post-mission processing). Since all parameters show the systematic patterns of a stand-alone INS, only a few of them are shown. Systematic errors show up in all navigation parameters. Figures 6-4a and 6-4b give the integrated system navigation performance. As expected, the systematic errors of the stand-alone INS are eliminated by the GPS position and velocity updates. The azimuth performance has not improved much. This was due to the fact that the azimuth error mainly depends on the vertical misalignment in the l-frame as to be shown in the following.

In the local-level frame, the roll error $\delta\varphi$ and the pitch error $\delta\theta$ depend on the east misalignment ε_e^l and north misalignment ε_n^l, the yaw error $\delta\psi$ mainly depends on the vertical misalignment ε_u^l .

$$\delta\varphi = -\varepsilon_e^l \frac{\sin\psi}{\cos\theta} + \varepsilon_n^l \frac{\cos\psi}{\cos\theta} \tag{6-2}$$

$$\delta\theta = \varepsilon_e^l \cos\psi + \varepsilon_n^l \sin\psi \tag{6-3}$$

$$\delta\psi = \varepsilon_e^l \sin\psi \tan\theta - \varepsilon_n^l \cos\psi \tan\theta + \varepsilon_u^l \tag{6-4}$$

The INS velocity errors in the l-frame due to misalignments and accelerometer biases are expressed as:

$$\dot{\delta v_e} = f_u \varepsilon_n^l - f_n \varepsilon_u^l + b_e \tag{6-5}$$

$$\dot{\delta v_n} = -f_u \varepsilon_e^l + f_e \varepsilon_u^l + b_n \tag{6-6}$$

$$\dot{\delta v_u} = f_n \varepsilon_e^l - f_e \varepsilon_n^l + b_u \tag{6-7}$$

where f_e, f_n, f_u are three specific force components in the l-frame, b_e, b_n, b_u are the accelerometer biases in the l-frame. Equations 6-5 to 6-7 show that ε_e^l and ε_n^l affect the velocity errors through f_e, f_n, and f_u. f_u contains the gravity component and is always large. Thus ε_e^l and ε_n^l are well estimated from velocity measurements. ε_u^l affects the velocity errors through f_e, f_n. As f_e and f_n are not zero only when the vehicle has accelerations in horizontal plane, therefore the vertical misalignment is only observable through velocity measurements when the vehicle experiences acceleration during maneuvers. Since there were no accelerations during the static test, the azimuth performance did not improve. This is also true for the post-mission processing, see Figure 6-5. As no other azimuth reference was available, the azimuth value at the end of the fine alignment has been used as the reference. The accuracy of the azimuth after the fine alignment is between 0.5 to 1.5 arcmin (RMS), see Liu (1992). The references for pitch and roll have been obtained from the post-mission processing software.

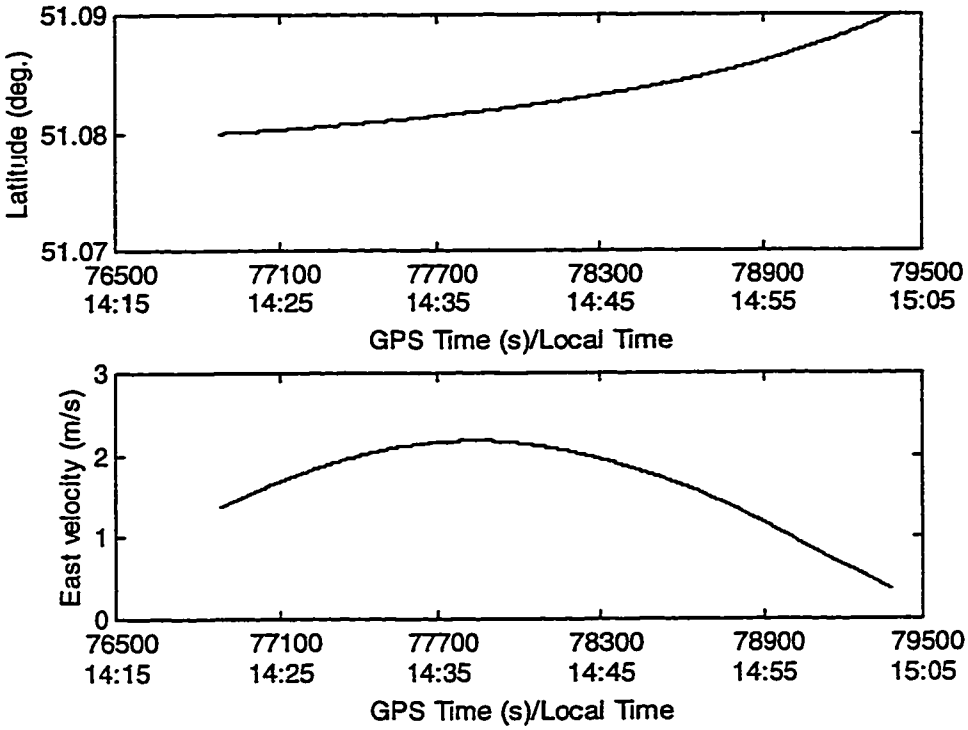

Figure 6-3a Stand-Alone INS Latitude and East Velocity

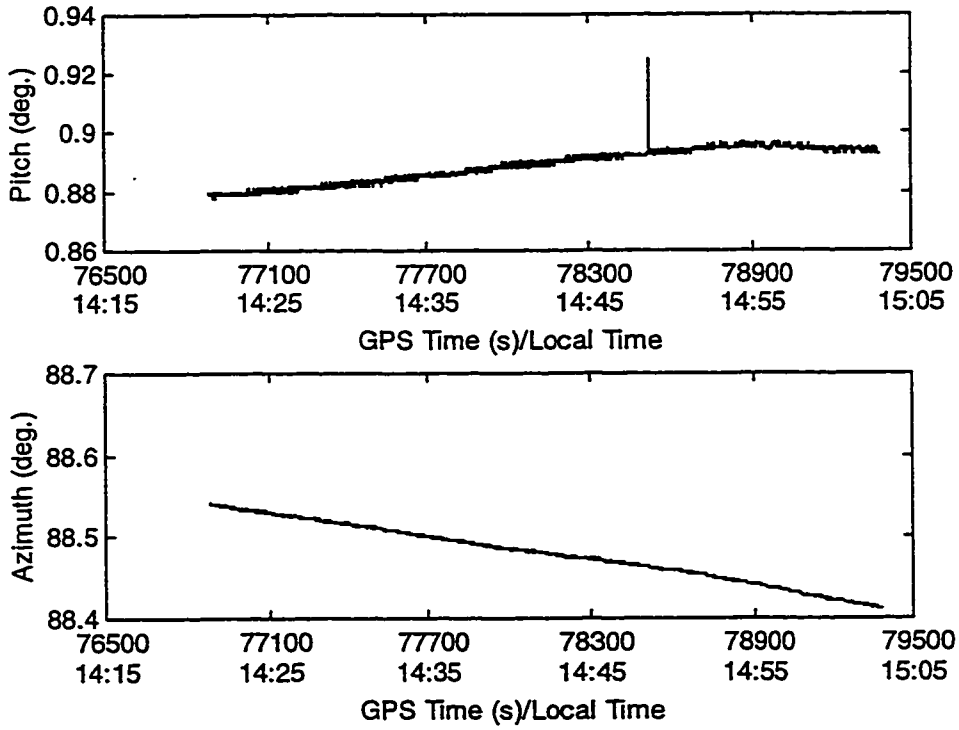

Figure 6-3b Stand-Alone INS Pitch and Azimuth

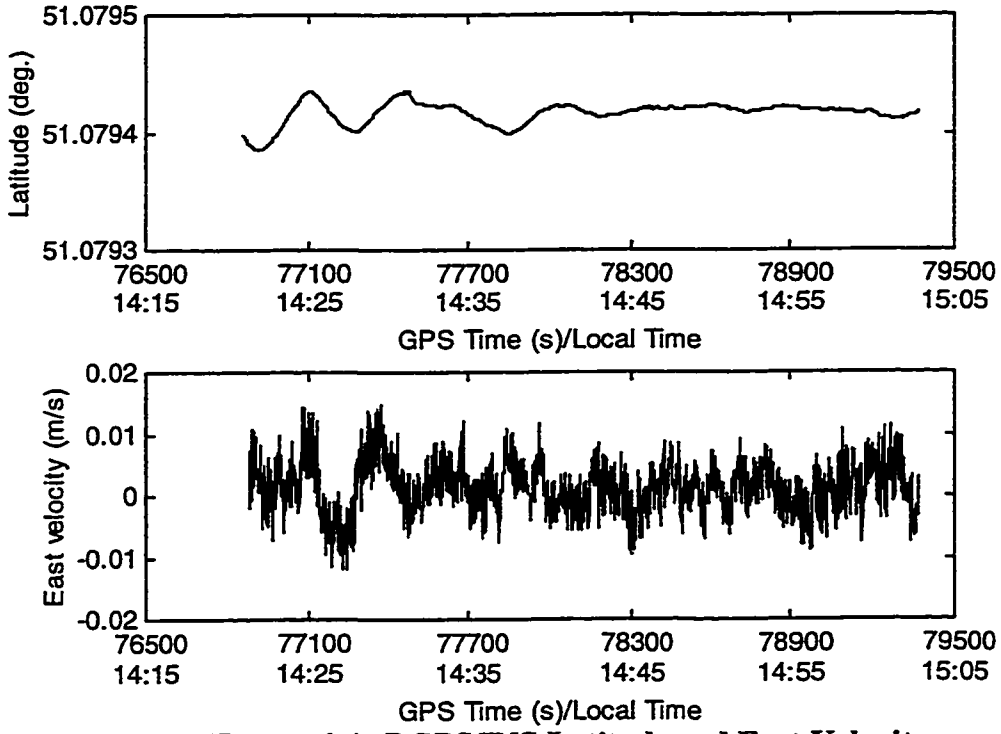

Figure 6-4a DGPS/INS Latitude and East Velocity

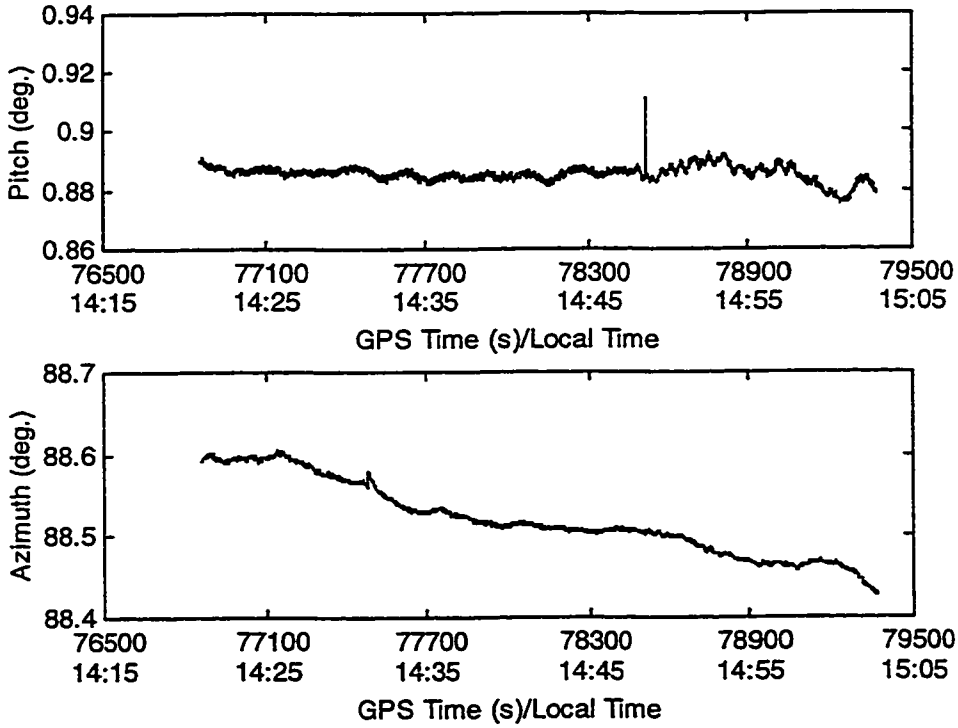

Figure 6-4b DGPS/INS Pitch and Azimuth

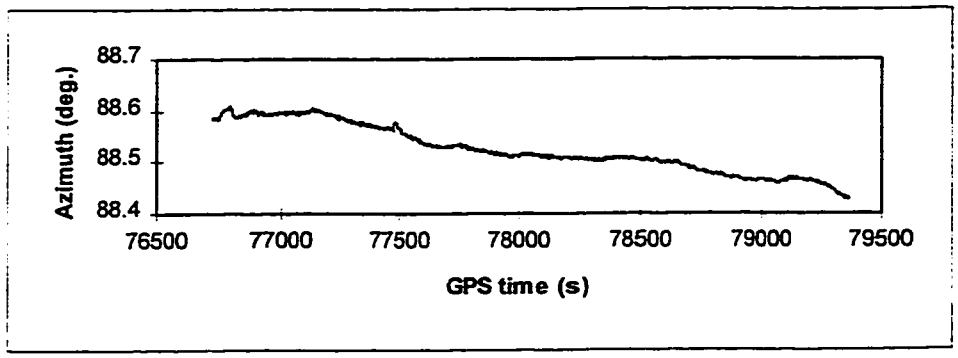

Figure 6-5 Azimuth From Post-Mission Processing

During the static test, 7 to 8 satellites were observed, and the PDOP varied in a small range, only from 1.77 to 1.95, as shown in Figure 6-6. The DGPS and DGPS/INS position and velocity errors are given in Figures 6-7a to 6-8c, the DGPS/INS attitude errors are shown in Figure 6-9. The statistical values of these errors are listed in Tables 6-1 to 6-3.

DGPS horizontal position accuracy is better than 1 metre (RMS), vertical position accuracy is about 2 metres (RMS). The low frequency variations in position and velocity errors are caused by C/A code multipath, the high frequency noise is from C/A code and Doppler measurement noise. The vertical components of the errors are larger than the horizontal ones because the PDOP has a large vertical component. GPS updates improve INS performance, i.e. time dependency in the DGPS/INS solution is now eliminated. It is also clear that DGPS positioning accuracy determines DGPS/INS positioning accuracy. The DGPS/INS horizontal position accuracy is about 1 metre (RMS), the height accuracy is about two metres (RMS). The sudden jumps in DGPS velocity and position errors are due to jumps in the differential corrections which affect the DGPS/INS solution through updates. As an example, the differential corrections for PRN 16 from GPS time

74782 s to 79382 s are shown in Figure 6-10. At GPS time 77478 s , jumps of about 7 m in range correction and 10 cm/s in phase rate correction occurred. The effects can be seen in the north and vertical velocities. They also affect the roll through misalignments which are estimated from the velocities. The positive effect of the integration can be seen in the DGPS/INS position which is not affected, because the position of the DGPS/INS is obtained by integrating the velocity. The DGPS position errors from post-mission processing are given in Figure 6-11 in which there is no jump. This indicates that the jumps in the differential corrections may result from transmission problem. Whether it is caused by hardware or software problem needs further investigation. GPS code and Doppler measurement noise has been reduced in DGPS/INS position and velocity. Multipath still affects DGPS/INS position and velocity.

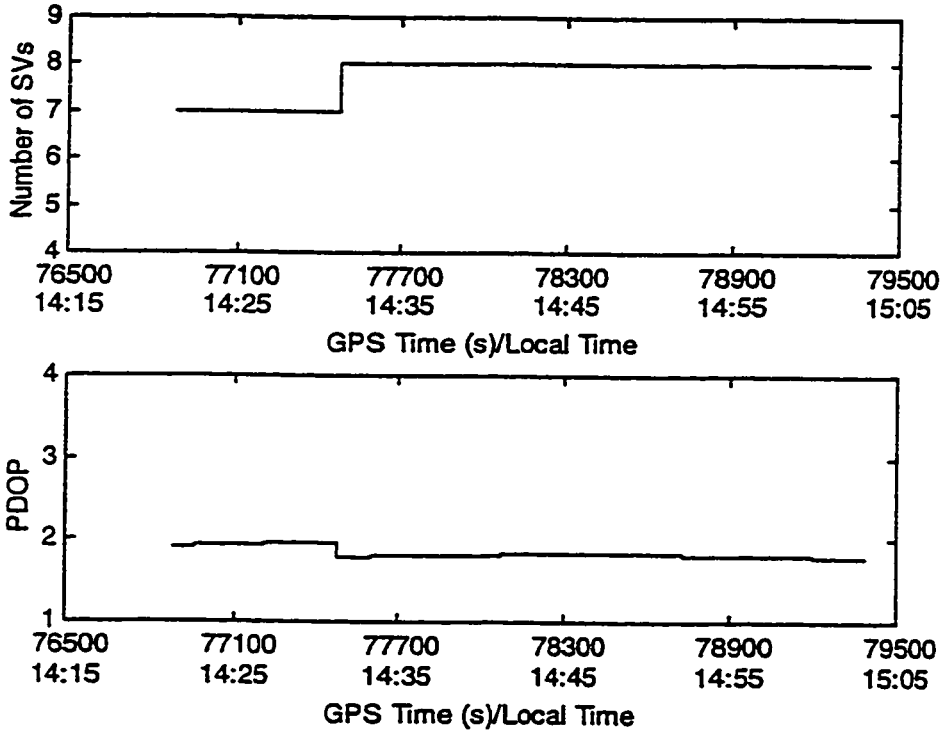

Figure 6-6 Number of Satellites Observed and PDOP During the Static Test

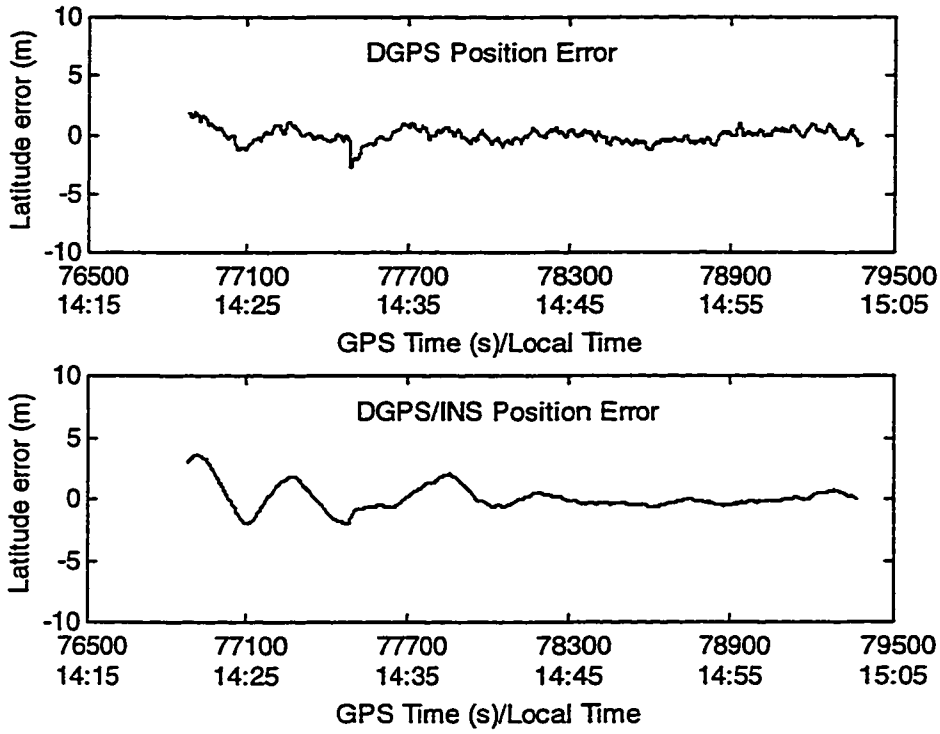

Figure 6-7a DGPS and DGPS/INS Latitude Errors of the Static Test

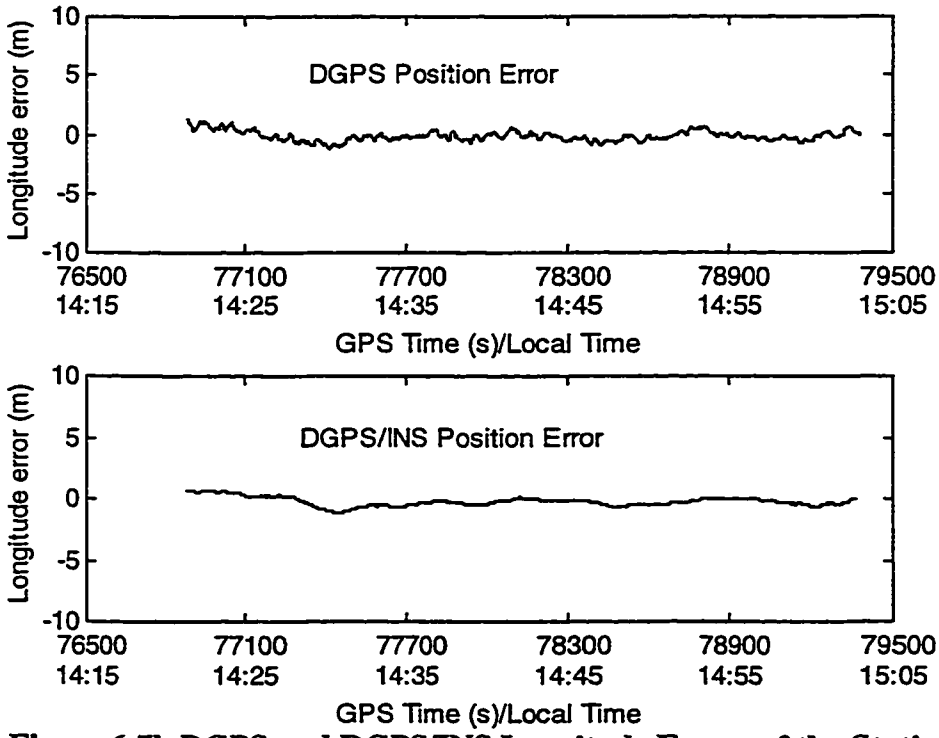

Figure 6-7b DGPS and DGPS/INS Longitude Errors of the Static Test

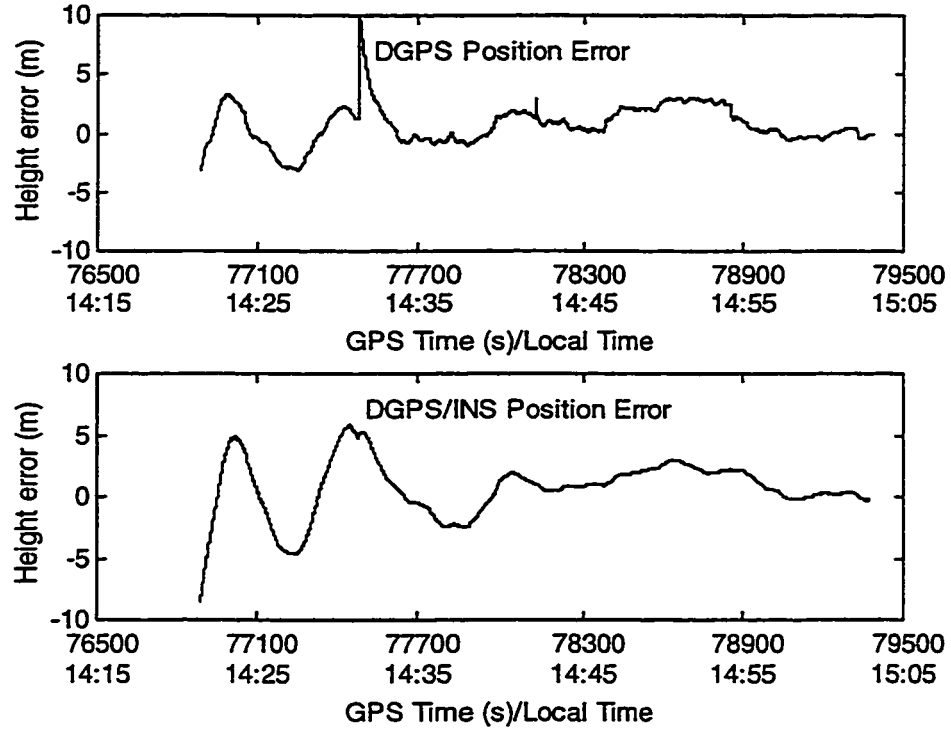

Figure 6-7c DGPS and DGPS/INS Height Errors of the Static Test

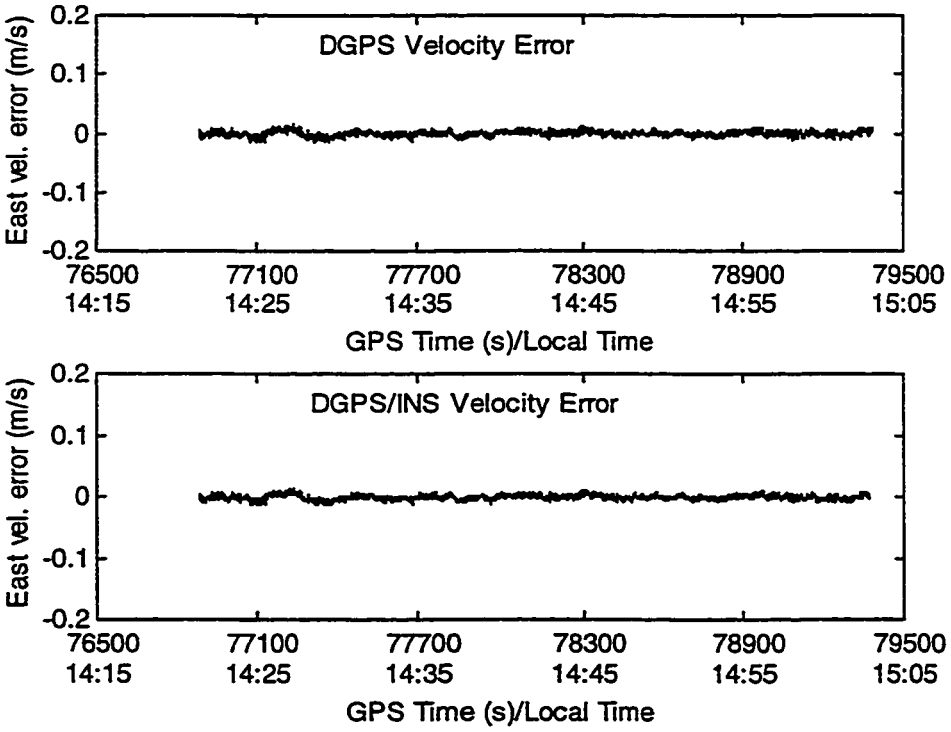

Figure 6-8a DGPS and DGPS/INS East Velocity Errors of the Static Test

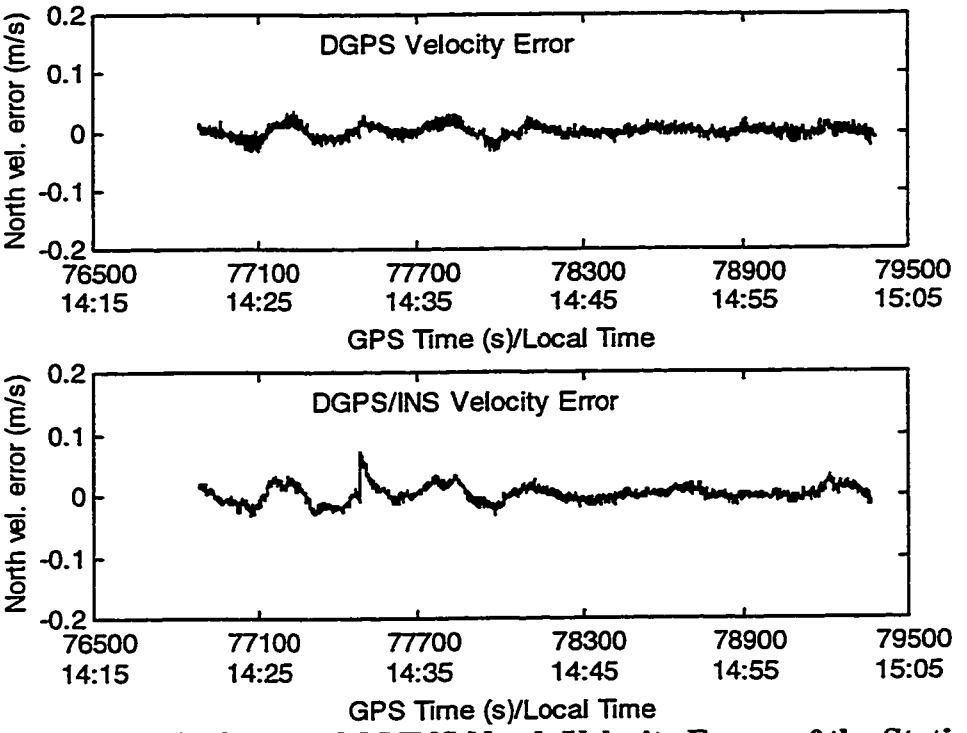

Figure 6-8b DGPS and DGPS/INS North Velocity Errors of the Static Test

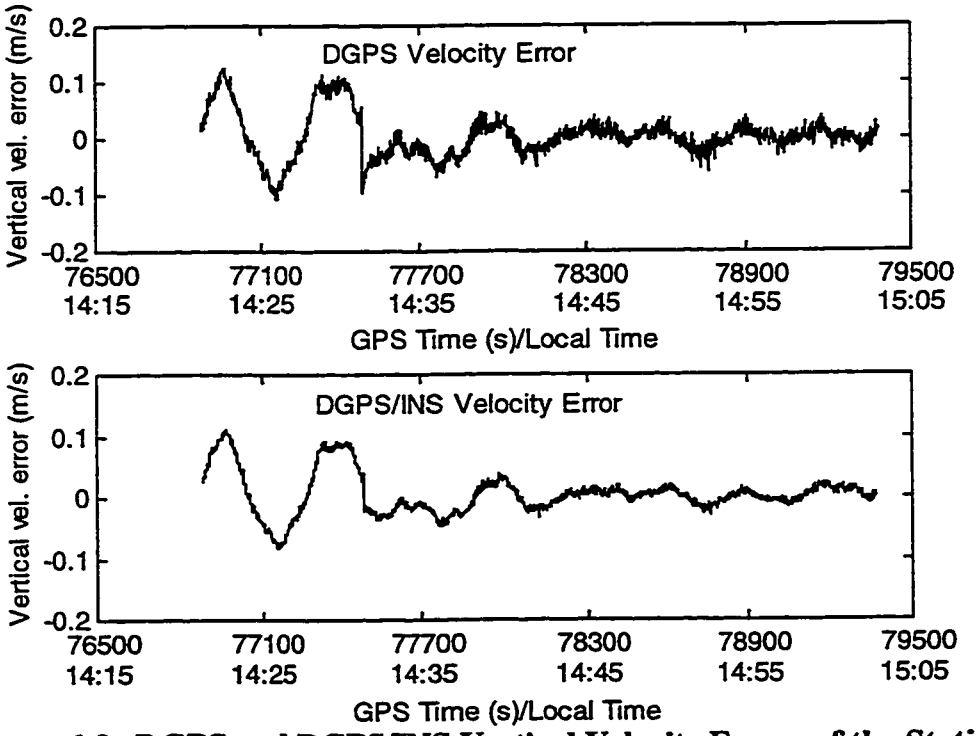

Figure 6-8c DGPS and DGPS/INS Vertical Velocity Errors of the Static Test

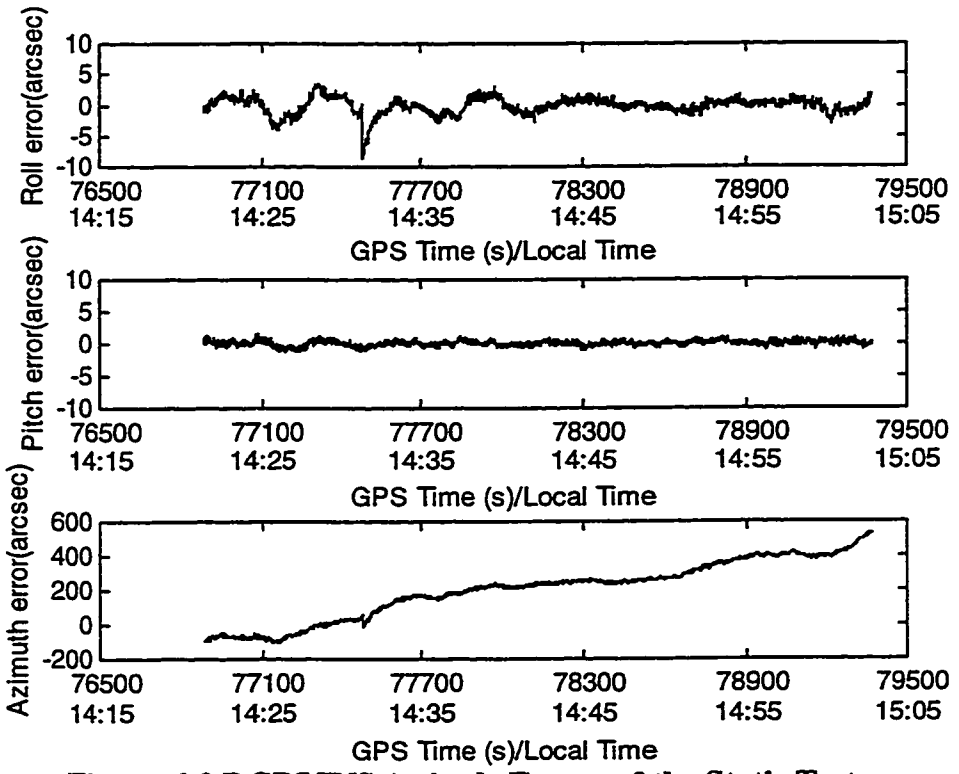

Figure 6-9 DGPS/INS Attitude Errors of the Static Test

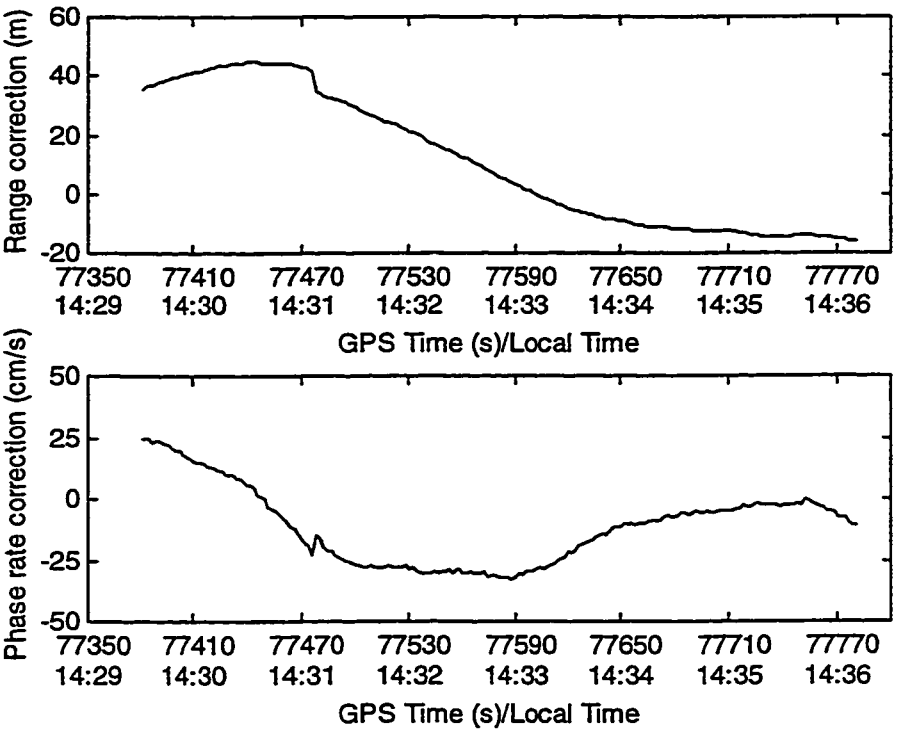

Figure 6-10 Differential Corrections For PRN 16

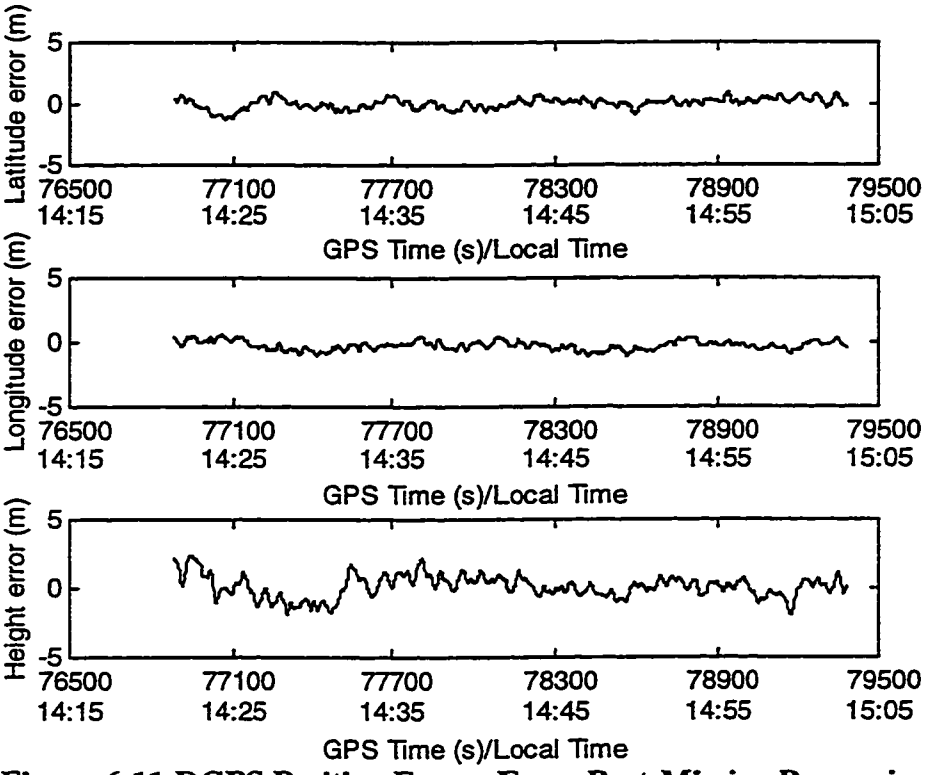

Figure 6-11 DGPS Position Errors From Post-Mission Processing

Table 6-1 DGPS and DGPS/INS Position Errors of the Static Test

	Mean (m)		RMS (m)	
	DGPS	DGPS/INS	DGPS	DGPS/INS
Latitude error	-0.09	0.08	0.63	1.03
Longitude error	-0.16	-0.24	0.46	0.45
Height error	0.76	0.72	1.86	2.42

Table 6-2 DGPS and DGPS/INS Velocity Errors of the Static Test

	Mean (cm/s)		RMS (cm/s)	
	DGPS	DGPS/INS	DGPS	DGPS/INS
East velocity error	-0.1	-0.1	0.5	0.4
North velocity error	0.1	0.2	1.0	1.4
Vertical velocity error	0.3	0.4	4.0	3.5

Table 6-3 DGPS/INS Attitude Errors of the Static Test

	Roll error	Pitch error	Azimuth error
Mean (arcsec)	-0.1	0.1	201
RMS (arcsec)	1.4	0.4	269

6.4 Kinematic Tests and Results

Kinematic tests were conducted in Calgary on Dec.12, 1997. The car was driven along major city roads which had a number of overpasses along the routes. The baseline length for each test was from 0.5 km to 2.1 km. Each test started with about 20 minutes in static mode, followed by about 40 minutes in kinematic mode. The static mode is needed for the INS real-time initial alignment and, in this specific case, is also used for the GPS ambiguity resolution when computing the reference solutions in post-mission processing.

6.4.1 Results of Kinematic Test #1

The trajectory of the test is shown in Figure 6-12. The car started at S, the parking lot #10 of the University of Calgary, then it followed the route of A, B, C, D, E, F, G ,H, C, D, E, F, G, H, B, A. There are four overpasses on the route. The one at F is about 20 metres long. The other three are about 5 metres long. The car went under the long overpass (20 m long) twice, and each time two satellites dropped. But there were still 5 to 6 satellites observed in each case. This maybe due to the coasting effect of the receiver. When the car went under the other overpasses, generally one or no satellite dropped. Velocity and attitude of the IMU (from post-mission processing) are given in Figures A-1 and A-2 in the appendix. When computing the reference solutions in post-mission processing, ambiguities were fixed.

During the test, 5 to 8 satellites were observed, and the PDOP varied between 1.65 and 2.4 as shown in Figure 6-13. The DGPS and DGPS/INS position and velocity errors are given in Figures 6-14a to 6-15c, respectively; the DGPS/INS attitude errors are given in Figure 6-16. The statistical values of the errors are listed in Tables 6-4 to 6-6.

Because the master-rover distance is short, the real-time DGPS positioning accuracy is determined mainly by receiver noise, multipath, correction transmission latency and receiver-satellite geometry which is represented by the PDOP value. The transmission latency of the system is about 2 seconds. It should be noted that the increasing PDOP value causes a bias of about 4 metres in the longitude error after GPS time 496366 s, see Figure 6-14b.

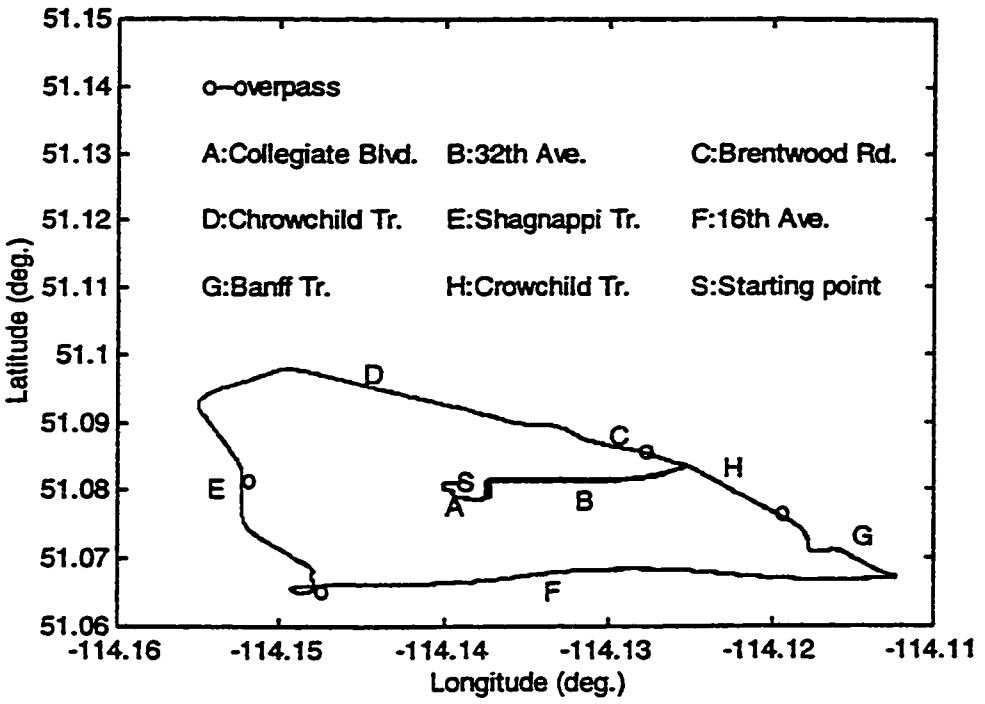

Figure 6-12 Trajectory of Kinematic Test #1

This phenomenon also shows up in the post-mission processing results which are given in Figure 6-17. Figure 6-17 gives the DGPS position errors from post-mission processing (differences between carrier phase positioning and C/A code pseudorange positioning). It may result from an incorrectly fixed ambiguity when computing the reference trajectory, as cycle slips occurred several times after GPS time 496366 s.

The last spike in the height error (about 18 m) in Figure 6-14c is due to a sudden jump in the range correction from the master station, so there is no match in the velocity error. To show that the jump is in the range correction, the differential corrections of PRN 22 from GPS time 496200 s to 496600 s are shown in Figure 6-18. A 17 m jump occurred in the range correction at GPS time 496366 s which caused the 18 m jump in DGPS height

error. The post-mission results do not show a jump of this size. Jumps in differential corrections can be avoided by predicting current corrections from previous ones and comparing them with the corresponding measured ones. If there is a large discrepancy between measured and predicted, the measured corrections should be replaced by the predicted ones. Clearly, this is only possible for a few epochs, as long as the predicted corrections are reliable.

In the current prototype of the real-time system, only current epoch GPS time and corrections to pseudorange and phase rate are transmitted from master station to rover station. This may result in different ephemeris messages being used at the master station and the rover station, respectively, when computing the coordinates of a satellite. If this results in jumps in the real-time DGPS solution, it would not appear in the post-mission solution, because only the ephemeris messages recorded at the master station have been used in post-mission processing. This problem can be solved by transmitting the issue of clock data of the ephemeris messages from the master station to the rover station to take into account the time difference between the ephemeris messages received at the two stations.

The DGPS/INS navigation errors depend on the DGPS position and velocity accuracy, synchronization errors, quality of the inertial sensors and the vehicle dynamics. The DGPS/INS position errors are smoother than the GPS position errors which can be attributed to the smoothing effect when integrating INS velocity. Spikes are found in the DGPS/INS velocity errors. Some of them coincide with spikes in the DGPS velocity errors. Some of the spikes in DGPS velocity errors are reduced or eliminated by integration, others are amplified when the direction of DGPS velocity error and the error

in the predicted INS velocity coincide. The DGPS/INS horizontal position accuracy (RMS) is about the same as that of DGPS. The DGPS/INS height accuracy is better than that of DGPS. The DGPS/INS horizontal velocity errors are larger than those of DGPS due to the spikes . In general, the errors in pitch and roll are much smaller than those in azimuth. This can be explained by Equations 6-2 to 6-7 in section 6.3. As has been pointed out, the roll error and the pitch error depend on the east and north misalignments while the yaw error mainly depends on the vertical misalignment. The east and north misalignments of the INS are better estimated than the vertical misalignment when using GPS Doppler observations to update the INS (Zhang, 1995a). Thus the errors in pitch and roll are much smaller than the azimuth error. The spikes in the DGPS/INS velocity errors at GPS time 495458 s and 496210 s cause jumps in the azimuth error in the same direction which result in a large azimuth error.

The accuracy of the real-time integrated system depends not only on its own Kalman filter parameters, i.e. **Q** and **R** matrices, but also on the Kalman filter parameters used in computing the reference solutions. Different spikes in DGPS/INS velocity errors show up when different **Q** and **R** matrices are used in computing the reference solutions.

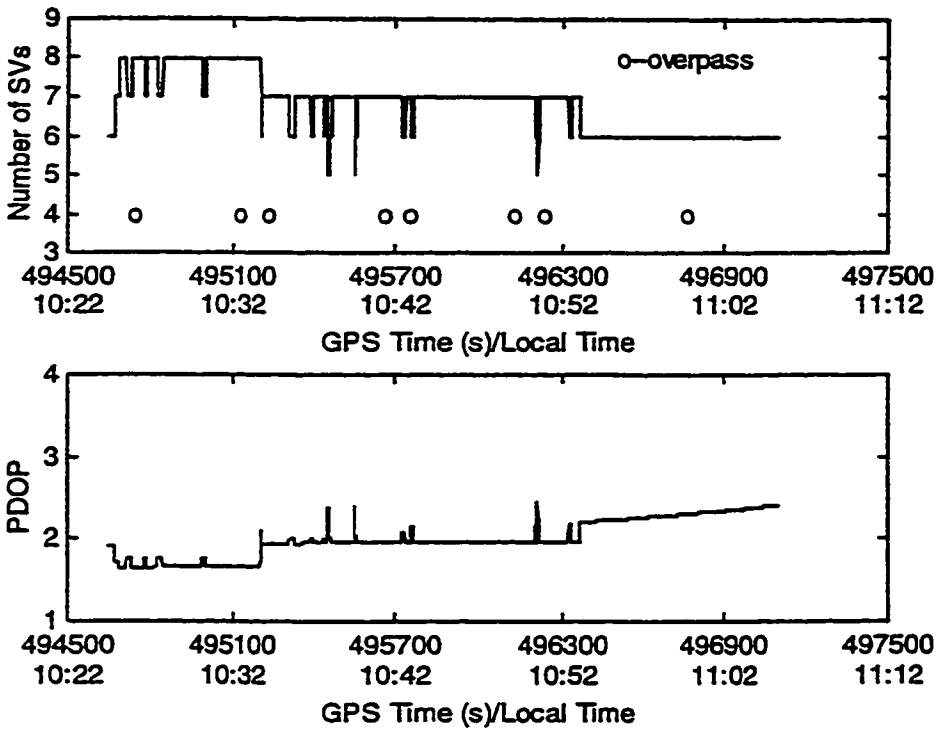

Figure 6-13 Number of Satellites Observed and PDOP During Kinematic Test #1

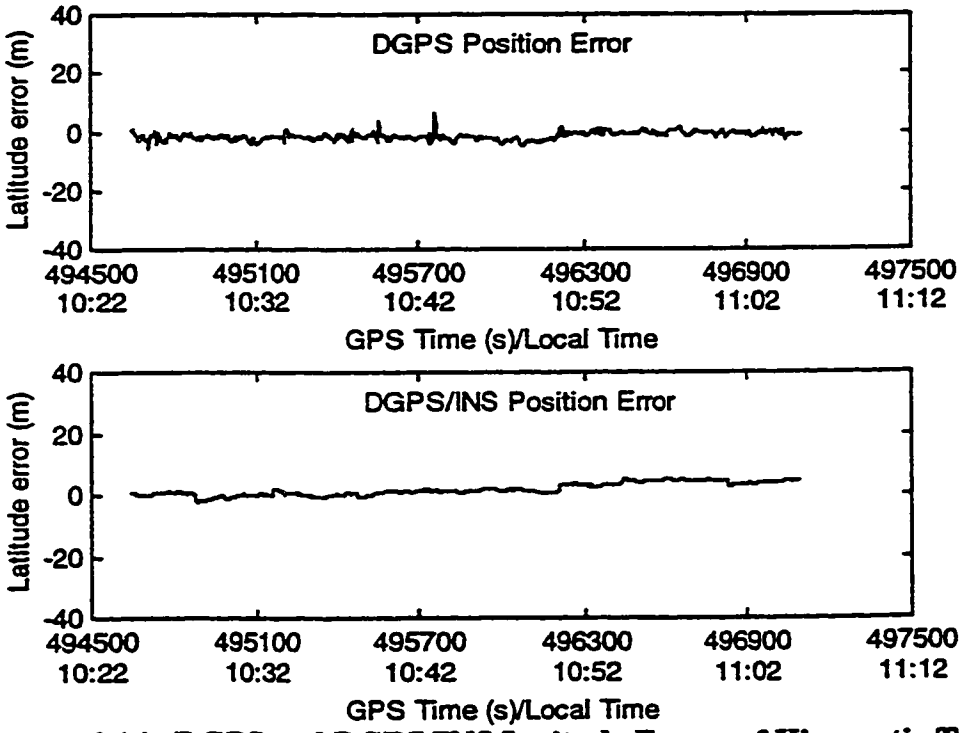

Figure 6-14a DGPS and DGPS/INS Latitude Errors of Kinematic Test #1

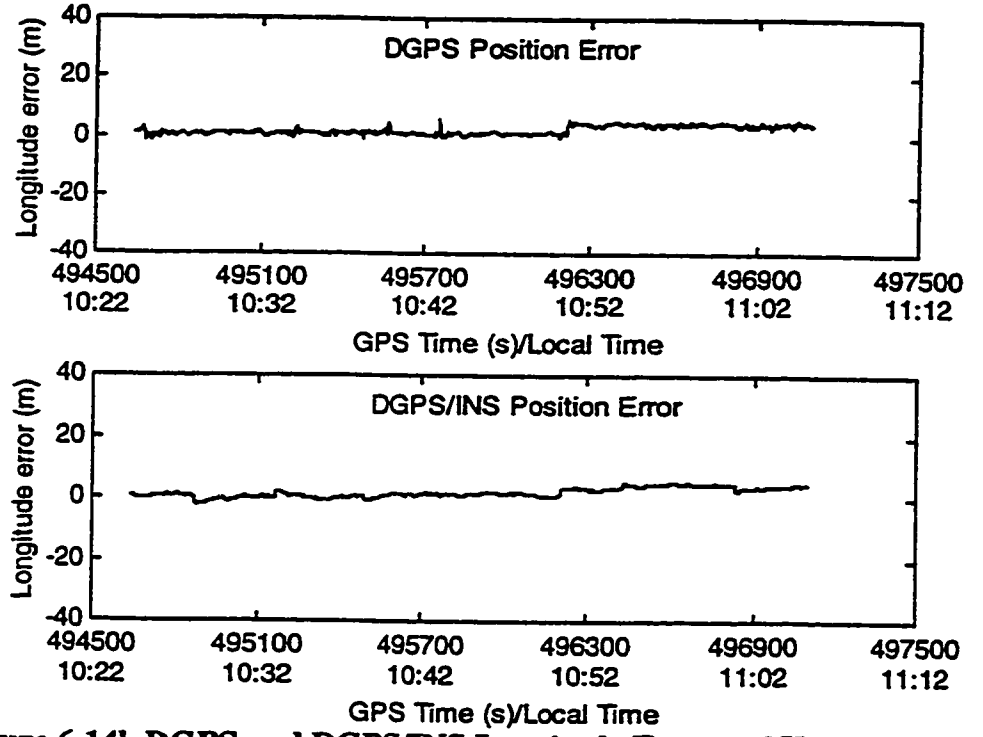

Figure 6-14b DGPS and DGPS/INS Longitude Errors of Kinematic Test #1

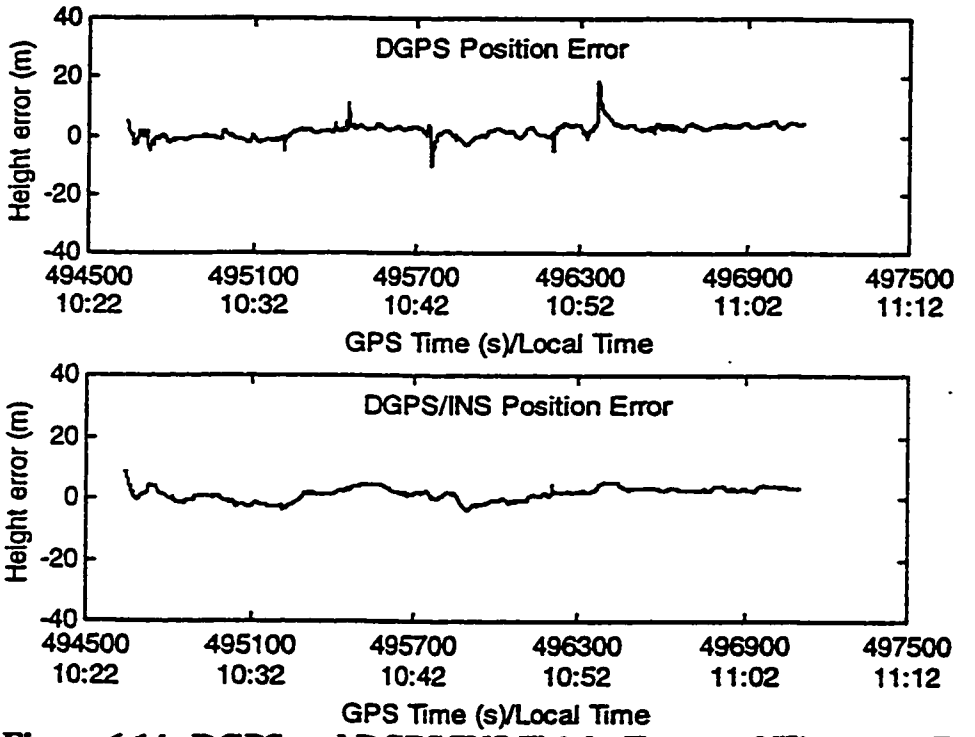

Figure 6-14c DGPS and DGPS/INS Height Errors of Kinematic Test #1

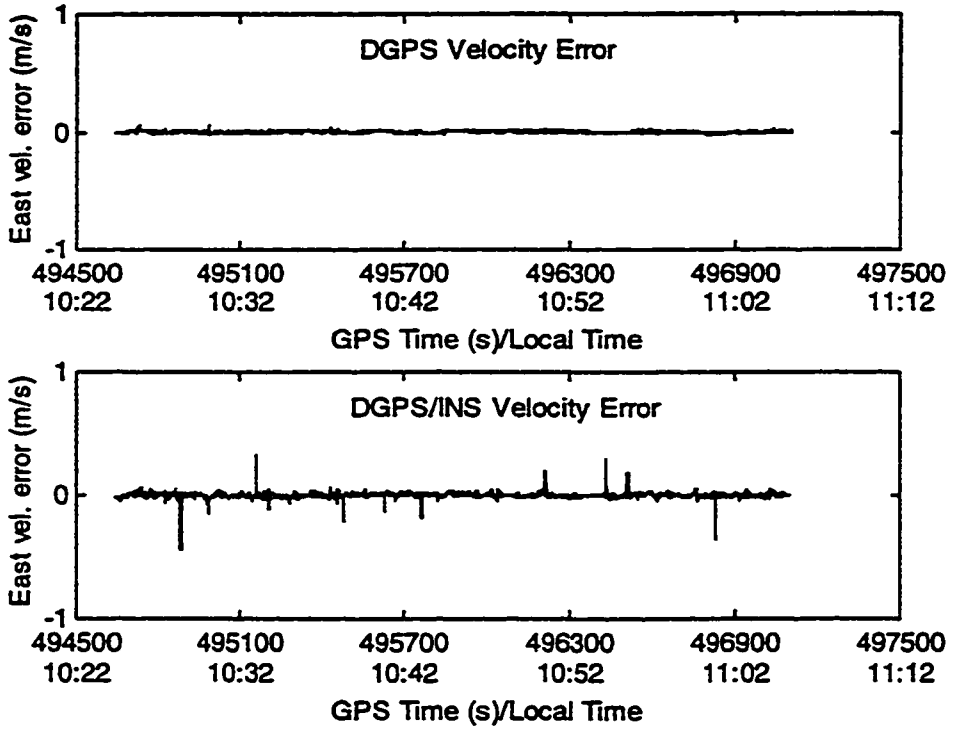

Figure 6-15a DGPS and DGPS/INS East Velocity Errors of Kinematic Test #1

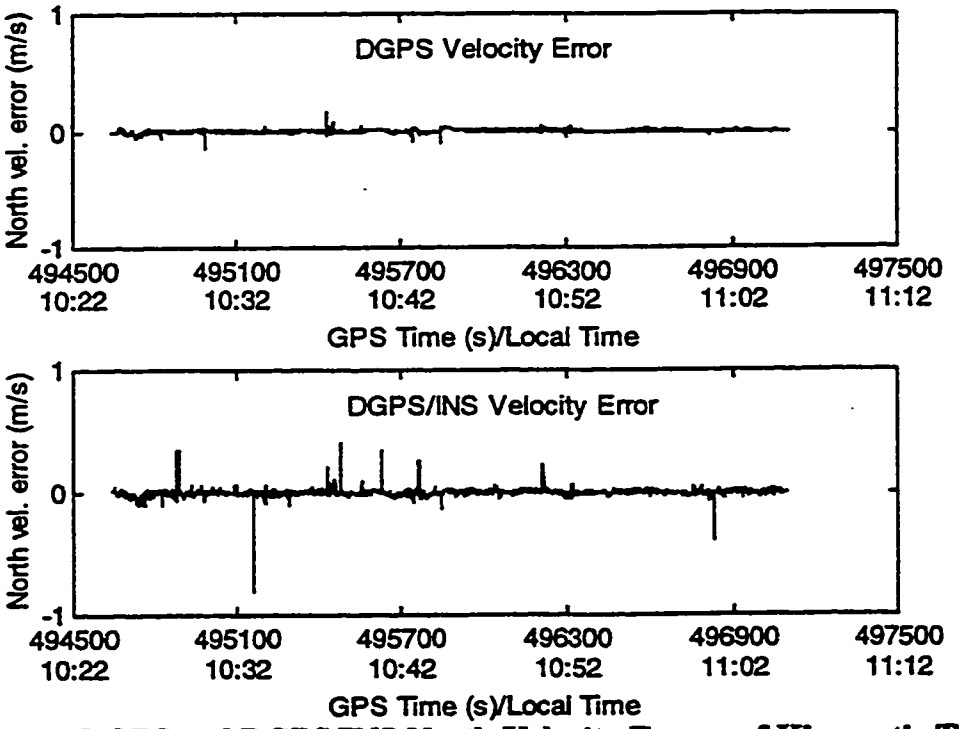

Figure 6-15b DGPS and DGPS/INS North Velocity Errors of Kinematic Test #1

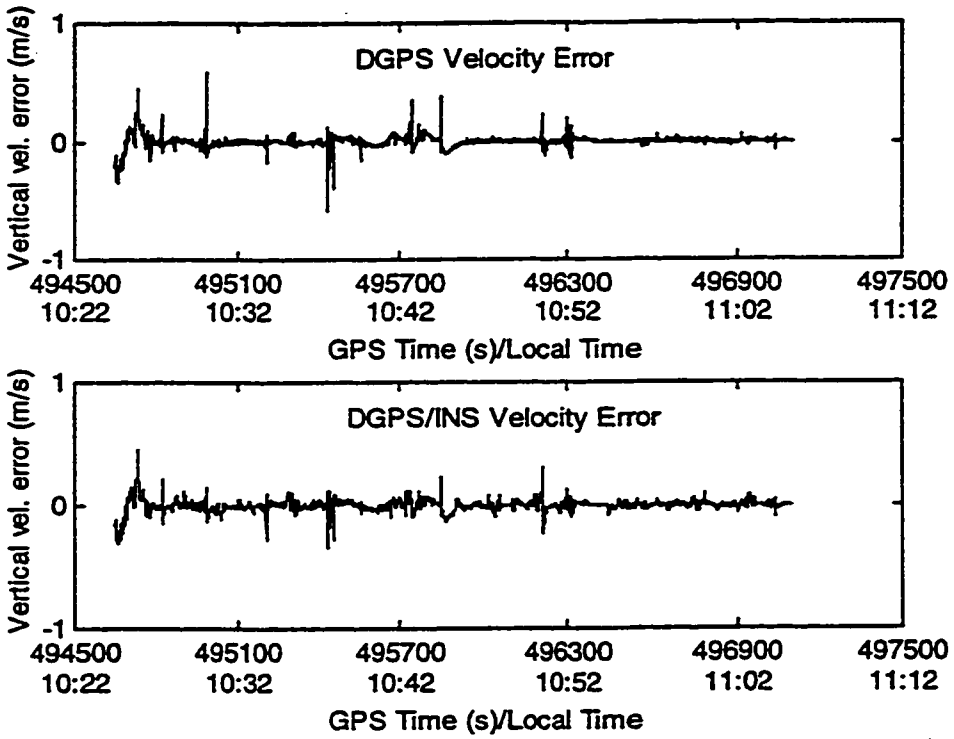

Figure 6-15c DGPS and DGPS/INS Vertical Velocity Errors of Kinematic Test #1

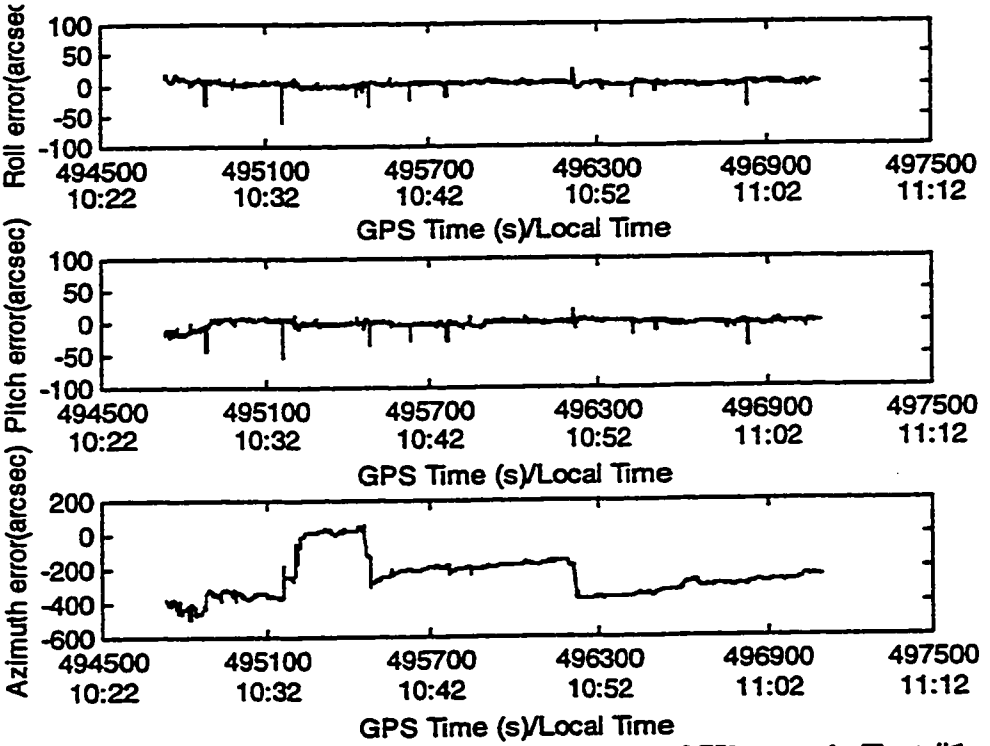

Figure 6-16 DGPS/INS Attitude Errors of Kinematic Test #1

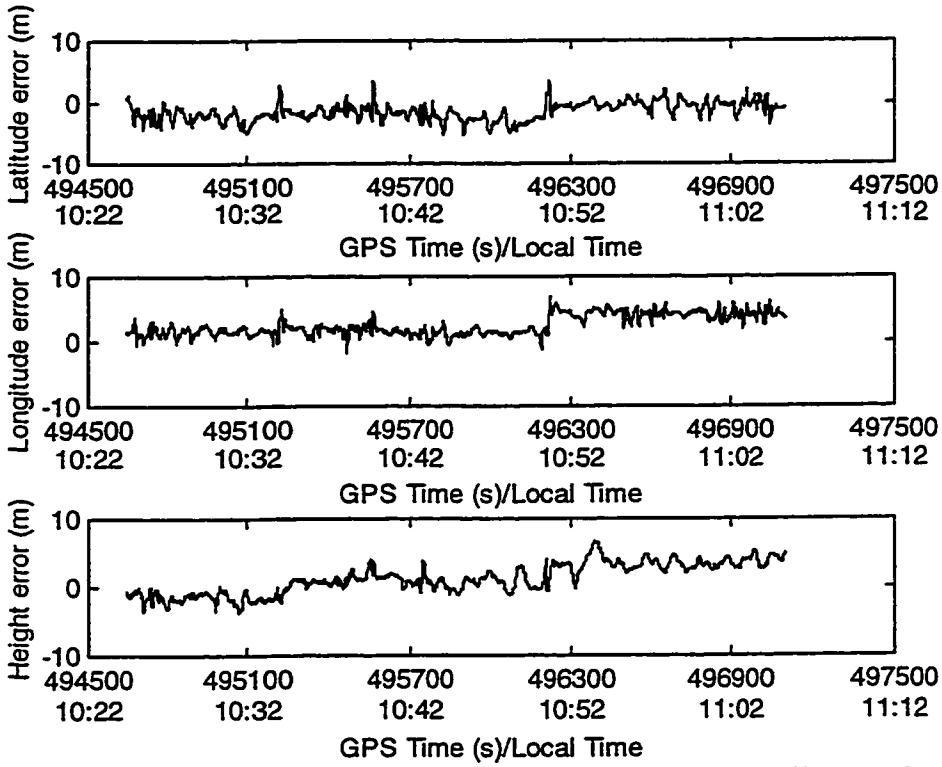

Figure 6-17 DGPS Position Errors From Post-Mission Processing

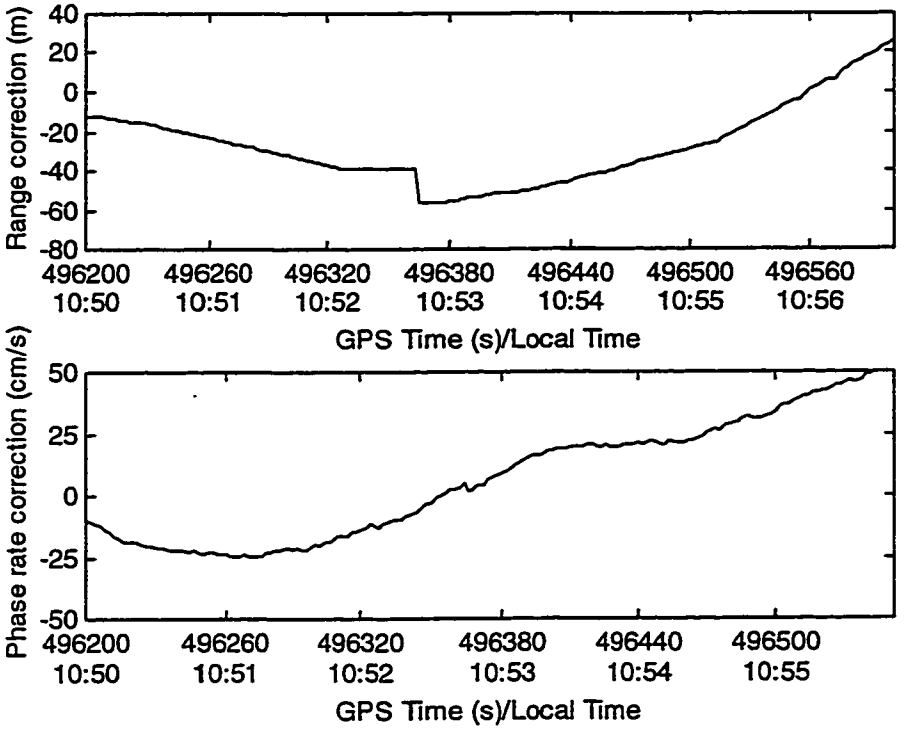

Figure 6-18 Differential Corrections For PRN 22

Table 6-4 DGPS and DGPS/INS Position Errors of Kinematic Test #1

	Mean (m)		RMS (m)	
	DGPS	DGPS/INS	DGPS	DGPS/INS
Latitude error	-1.60	-1.47	2.07	2.01
Longitude error	2.02	1.83	2.66	2.60
Height error	1.65	1.49	2.99	2.64

Table 6-5 DGPS and DGPS/INS Velocity Errors of Kinematic Test #1

	Mean (cm/s)		RMS (cm/s)	
	DGPS	DGPS/INS	DGPS	DGPS/INS
East velocity error	-0.0	-0.0	0.6	3.0
North velocity error	-0.1	0.0	1.3	4.1
Vertical velocity error	-0.3	-0.4	5.7	5.3

Table 6-6 DGPS/INS Attitude Errors of Kinematic Test #1

	Roll error	Pitch error	Azimuth error
Mean (arcsec)	1.74	-0.92	-250
RMS (arcsec)	5.0	5.7	277

6.4.2 Results of Kinematic Test #2

A second kinematic test was conducted to evaluate the system performance under a different GPS geometry. The two tests were about 9 hours apart. The car started at S, the parking lot of a shopping mall, then followed A, B, C, D, E, F, G, A, B, C D, E, F, G. Because the transmission capacity of the radio is limited, the car was driven basically along the same route as in the first test. The trajectory is shown in Figure 6-19. When the car went under the 20 m long overpass on B for the second time, two satellites dropped. In other cases, only one or no satellite dropped. The IMU velocity and attitude are given

in Figures A-3 and A-4 in the appendix, respectively. Ambiguities were fixed when computing the reference solution in post-mission processing.

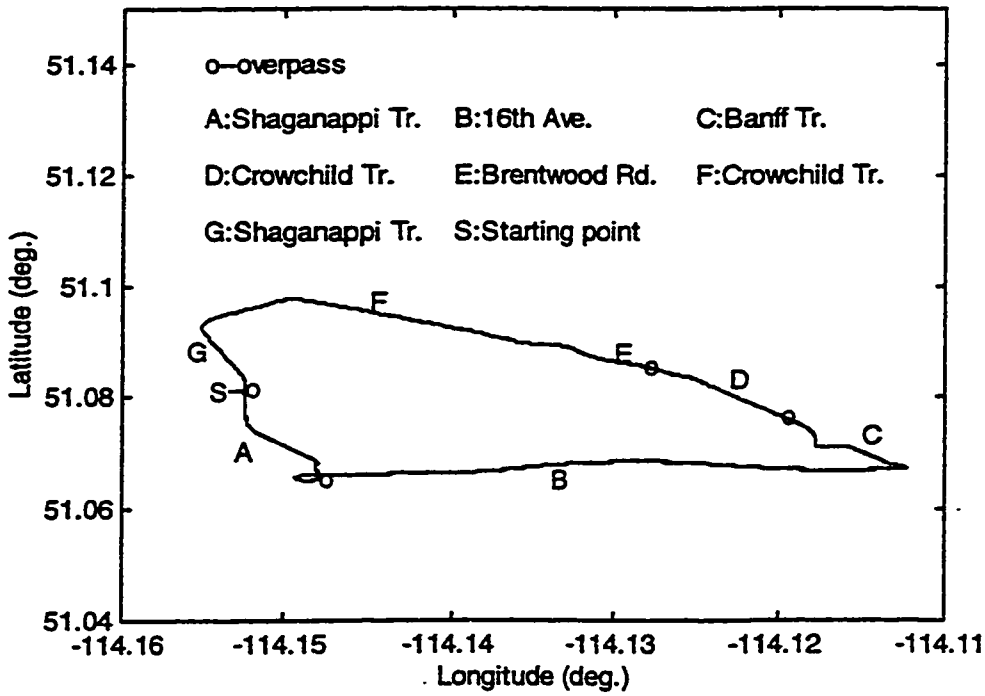

Figure 6-19 Trajectory of Kinematic Test #2

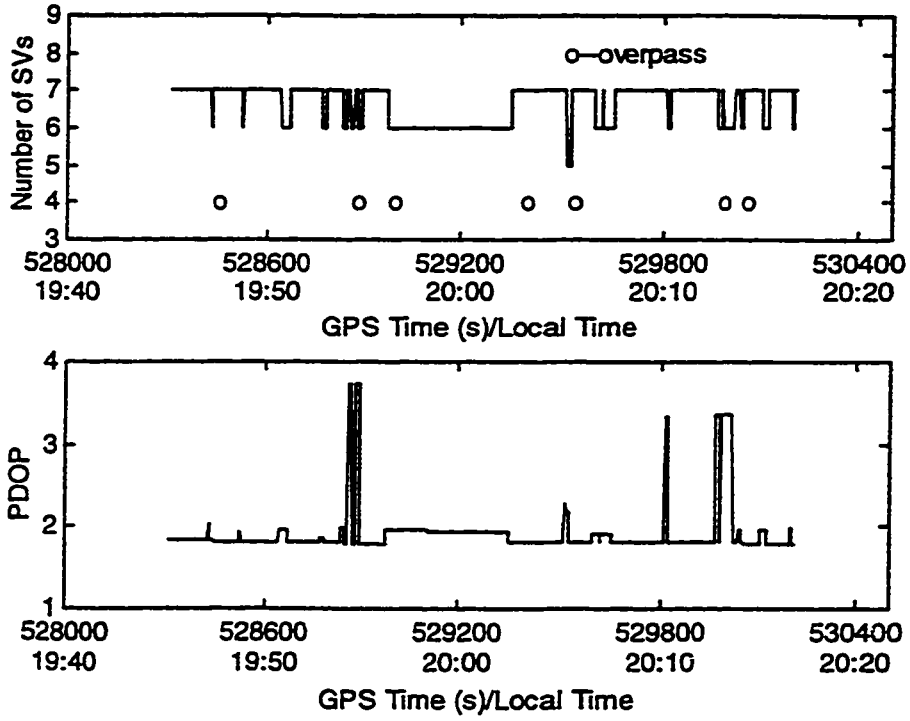

Figure 6-20 Number of Satellites Observed and PDOP During Kinematic Test #2

During the test, 5 to 7 satellites were observed and the PDOP value was between 1.79 and 3.74 as shown in Figure 6-20. The DGPS and DGPS/INS position and velocity errors are given in Figures 6-21a to 6-22c, respectively; the DGPS/INS attitude errors are given in Figure 6-23. Statistical values of these errors are listed in Tables 6-7 to 6-9. Compared with the first test, the PDOP values vary over a larger range, which causes larger spikes in the DGPS position and velocity errors. Both DGPS position and velocity accuracies are poorer than those of the first test. The DGPS/INS position accuracy (RMS) is better than that of DGPS improving the RMS by about 40% to 45%. The DGPS/INS horizontal velocity accuracy is worse than that of DGPS; the DGPS/INS vertical velocity accuracy is better than that of DGPS. Spikes in DGPS/INS velocity errors are due to spikes in either DGPS velocity errors or DGPS position errors. Attitude errors are bigger than those of the first test due to the poorer DGPS velocity accuracy used in the updates. Spikes in

the DGPS/INS velocity errors at GPS time 529515 s cause a jump in the azimuth error which contributes much to the large azimuth error.

During the test, the highest PDOP value is 3.74, the corresponding 3-D positioning error is about 21 m which indicates that the user equivalent range error (UERE) is 5.6 m. But the post-mission processing result which is given in Figure 24 indicates that the UERE is less than 2 m. The highest 3-D velocity error is about 1.5 m/s which does not match the combination of the PDOP value and the raw Doppler accuracy which is about 1 cm/s. This problem needs further investigation.

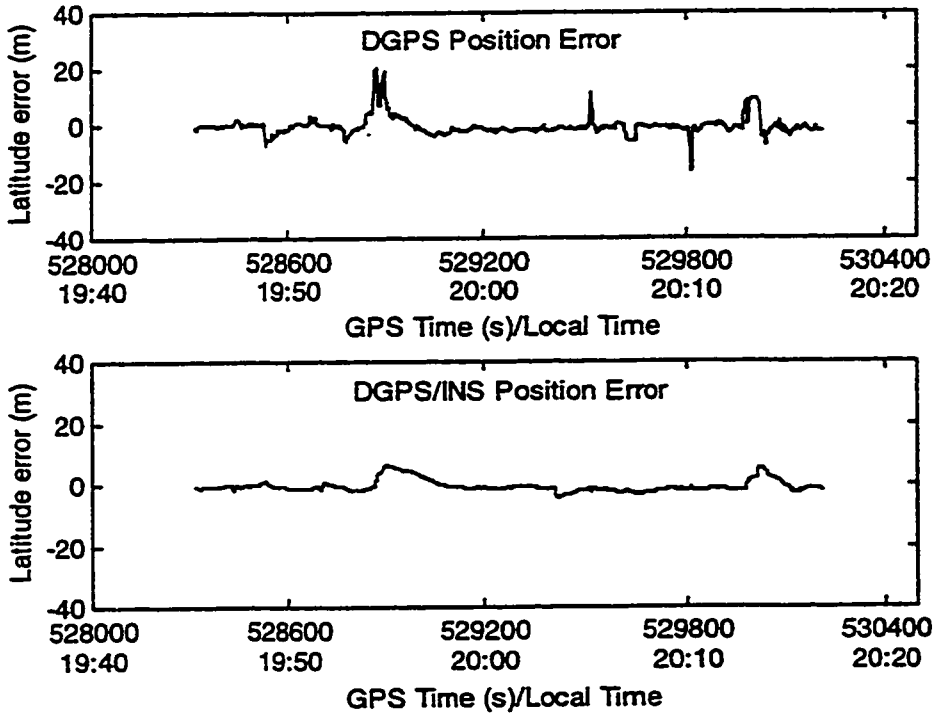

Figure 6-21a DGPS and DGPS/INS Latitude Errors of Kinematic Test #2

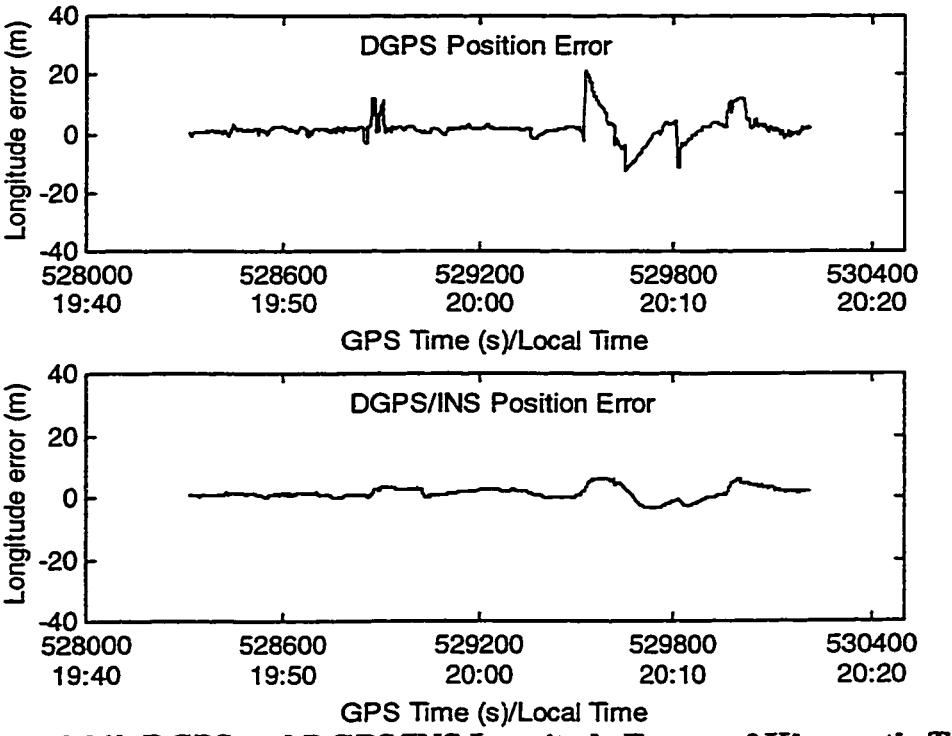

Figure 6-21b DGPS and DGPS/INS Longitude Errors of Kinematic Test #2

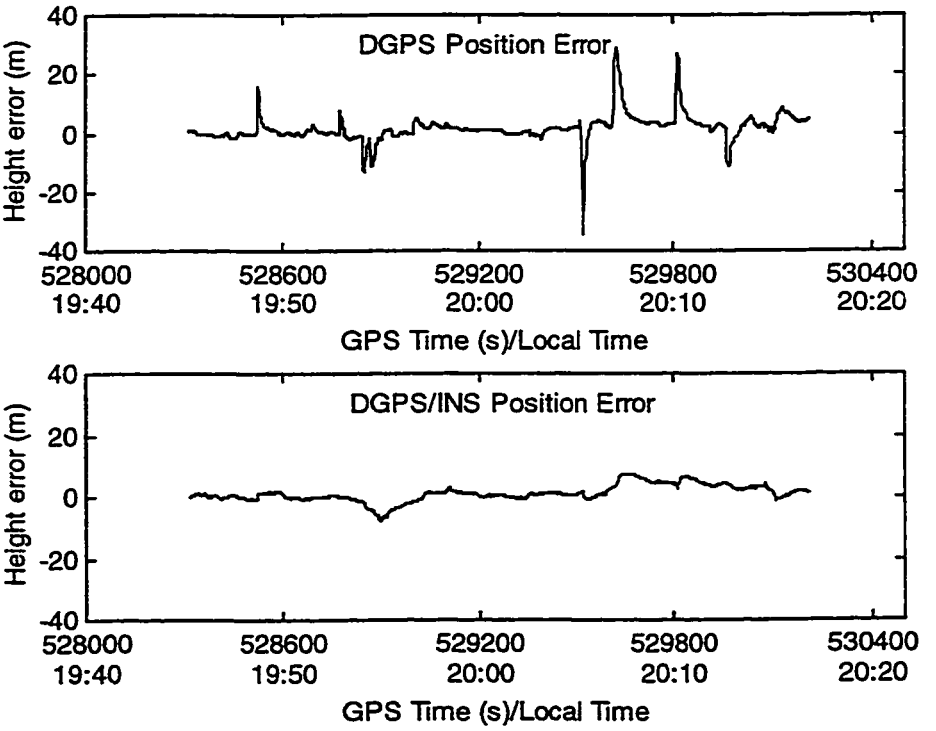

Figure 6-21c DGPS and DGPS/INS Height Errors of Kinematic Test #2

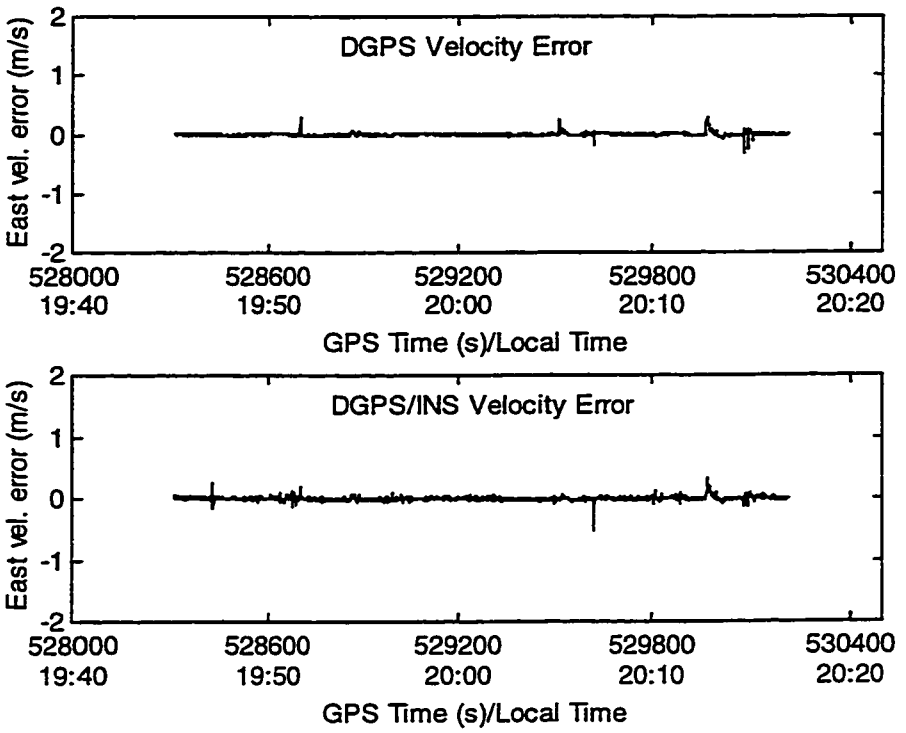

Figure 6-22a DGPS and DGPS/INS East Velocity Errors of Kinematic Test #2

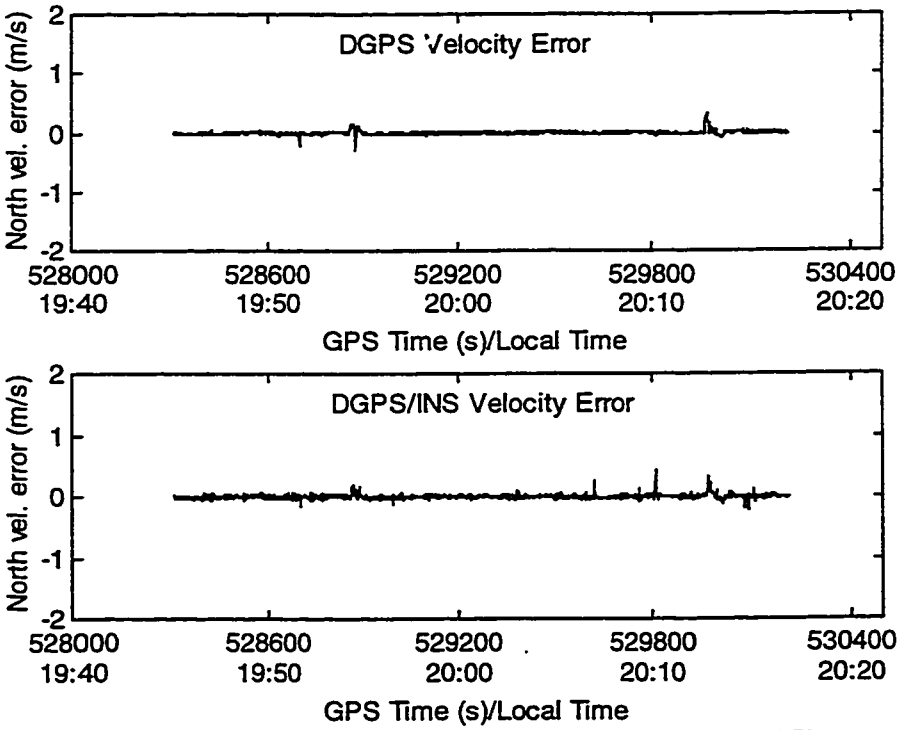

Figure 6-22b DGPS and DGPS/INS North Velocity Errors of Kinematic Test #2

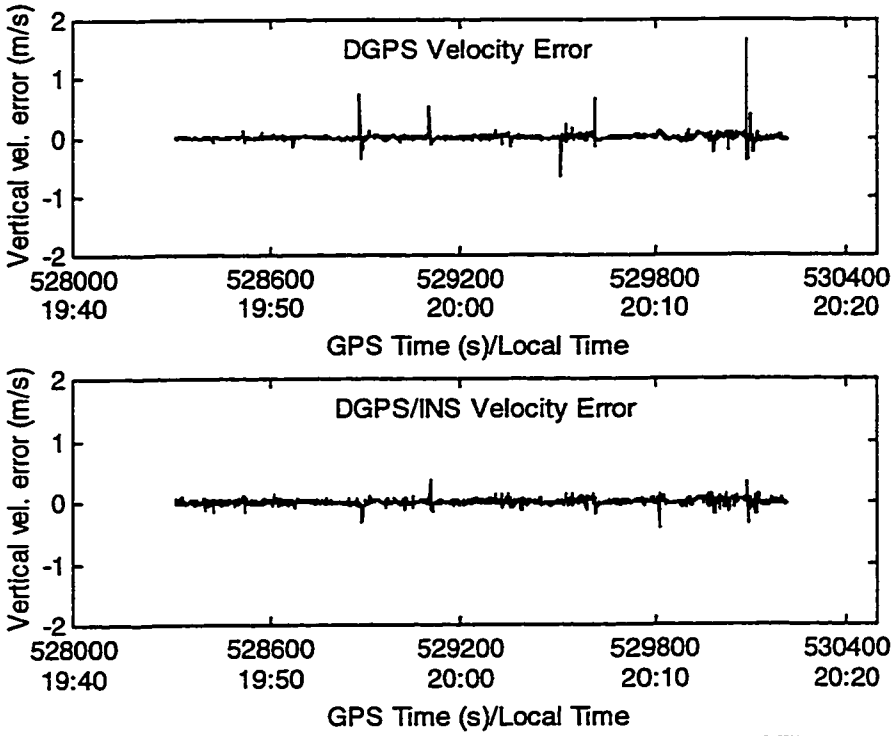

Figure 6-22c DGPS and DGPS/INS Vertical Velocity Errors of Kinematic Test #2

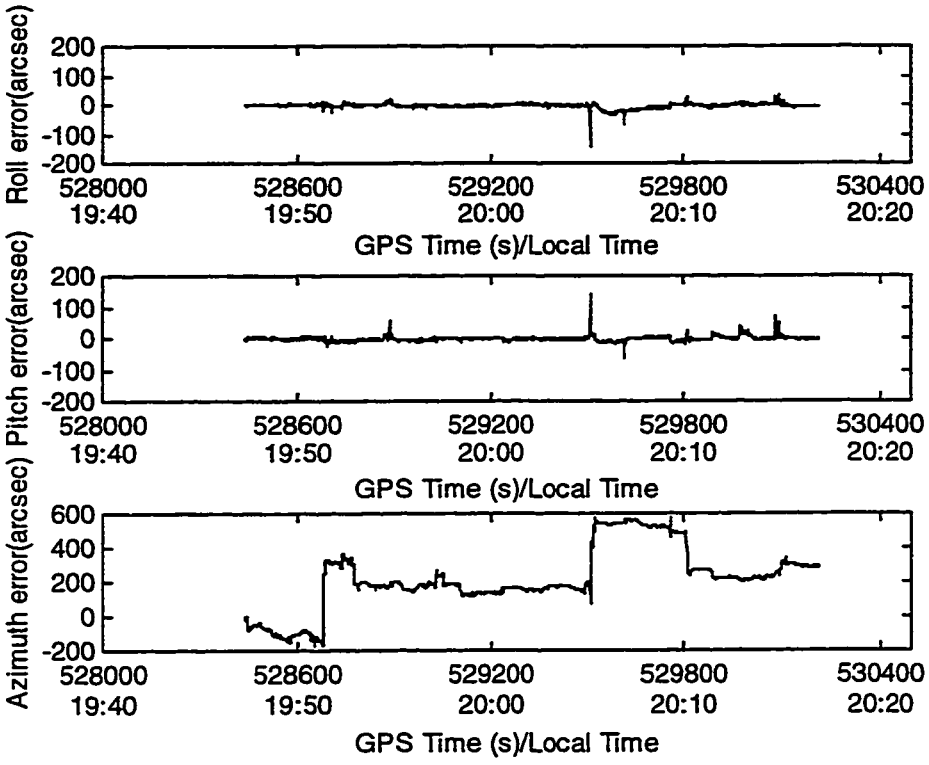

Figure 6-23 DGPS/INS Attitude Errors of Kinematic Test #2

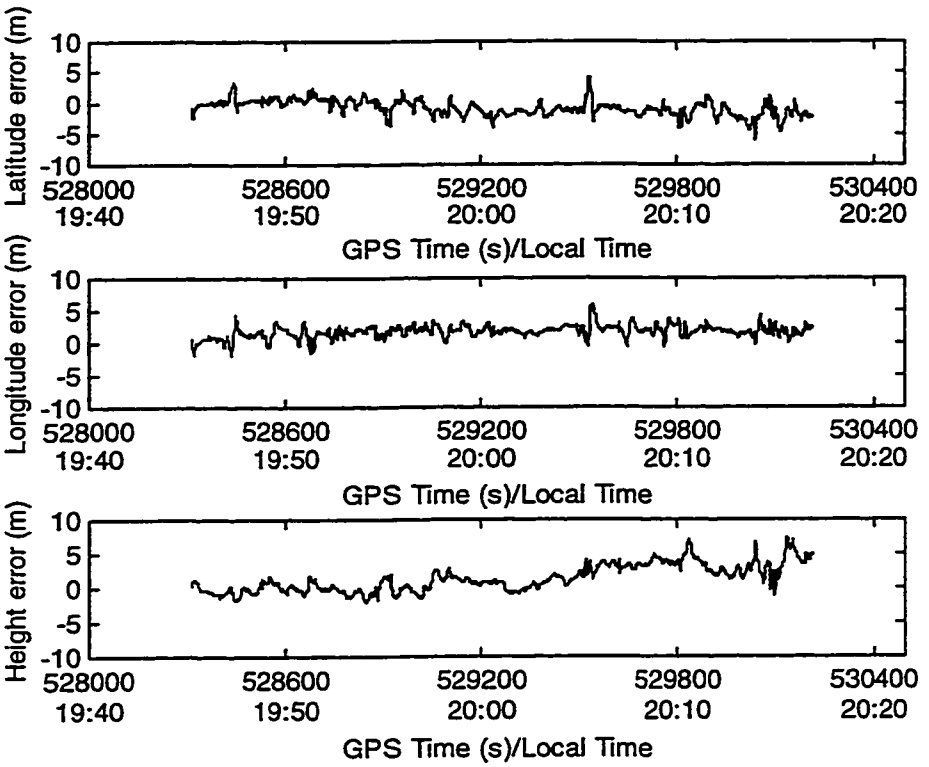

Figure 6-24 DGPS Position Errors From Post-Mission Processing

Table 6-7 DGPS and DGPS/INS Position Errors of Kinematic Test #2

	Mean (m)		RMS (m)	
	DGPS	DGPS/INS	DGPS	DGPS/INS
Latitude error	-0.47	-0.57	3.40	2.15
Longitude error	1.69	1.36	4.33	2.41
Height error	1.65	1.28	5.04	2.95

Table 6-8 DGPS and DGPS/INS Velocity Errors of Kinematic Test #2

	Mean (cm/s)		RMS (cm/s)	
	DGPS	DGPS/INS	DGPS	DGPS/INS
East velocity error	0.1	-0.3	2.9	3.7
North velocity error	0.1	-0.1	2.8	3.9
Vertical velocity error	0.1	-0.3	8.2	5.2

Table 6-9 DGPS/INS Attitude Errors of Kinematic Test #2

	Roll error	Pitch error	Azimuth error
Mean (arcsec)	-3.9	-2.0	217
RMS (arcsec)	9.9	9.2	281

6.5 Discussion

The results of the tests show that the INS systematic errors are eliminated by DGPS position and velocity updates. The DGPS/INS is less affected by GPS measurement noise. But multipath shows up in DGPS/INS. The attitude accuracy mainly depends on the DGPS velocity accuracy and the dynamics of the vehicle. DGPS velocity is not reliable when a satellite drop occurs. When this happens, it is suggested that no updates be carried out. Over a few seconds, the INS will still give reliable navigation results.

The choices of the thresholds for velocity and position misclosures between GPS and INS for the integration are important. Larger thresholds will allow more spikes in DGPS position and velocity to affect the DGPS/INS solution, and its performance will deteriorate. But if the thresholds are too small, there will be fewer updates, and the DGPS/INS performance will also be affected. In the worst case, if there are no updates for a certain period of time, the misclosures will become larger and larger and eventually the INS will not accept GPS updates anymore.

The two kinematic tests indicate that the PDOP affects DGPS positioning accuracy. During kinematic test #1, spikes in PDOP cause spikes in both position and velocity errors. The generally higher and increasing PDOP after GPS time 496366 s causes larger biases in the errors of DGPS longitude and height which result in a large mean in DGPS positioning compared with test #2. During test #2, the PDOP shows higher spikes and a pulse-like pattern. This results in larger standard deviations in the DGPS position and velocity errors which contribute to a poorer attitude accuracy.

The accuracy achieved in these tests is with respect to the results from post-mission GPS/INS processing using carrier phase data. Even though code range positioning and transmission latency cause a deterioration of accuracy of a few metres in position, a few cm/s in velocity, 10 arcseconds in pitch and roll and 0.08 degree in azimuth, such a system is more reliable than one using carrier phase data. Ambiguity resolution is the major problem of carrier phase data positioning. Generally speaking, a wide-laning technique gives more reliable results than a single frequency technique. Wide-laning will add cost to the system hardware because dual-frequency receivers are needed. The

decision whether to use a code range or carrier phase in the integration will therefore depend on the accuracy and reliability required for a specific application.

CHAPTER 7

CONCLUSIONS AND RECOMMENDATIONS

The objective of this research was the development of a prototype real-time DGPS/INS integrated system based on the available hardware and some software resources. The LTN-90-100 IMU has been used as the strapdown inertial navigation component. A radio data link system has been used to transmit GPS differential corrections. Decentralized Kalman filters have been designed to perform DGPS positioning calculations and to integrate GPS-derived position and velocity with the INS. Lab and field tests have been conducted to validate the system design and assess the system performances. Based on the test results, the following conclusions and subsequent recommendations can be made.

7.1 Conclusions

(1) DGPS position and velocity updates eliminate time dependent INS system errors through decentralized Kalman filters effectively.

(2) The position and velocity accuracy of the integrated system is limited by the DGPS positioning accuracy and the synchronization error. The attitude accuracy is mainly determined by the quality of the inertial sensors, DGPS velocity accuracy, synchronization error and the vehicle dynamics.

(3) The achievable accuracies are better than 5 m in position, cm/s level in velocity, 10 arcseconds in pitch and roll and 0.08 degree in azimuth with respect to post-mission GPS/INS using carrier phase data.

(4) The attitude accuracies are relative to the reference which did not have independent angular velocity sensors. The absolute attitude accuracy of the system is therefore lower.

7.2 Recommendations

(1) The problem of spikes in DGPS positioning errors caused by satellite drops needs further investigation. It affects the overall system accuracy in a major way and is not acceptable in many applications.

(2) More tests are needed to evaluate the system performance when GPS signals are blocked.

(3) Whether the jumps in differential corrections are caused by hardware or software problem needs further investigation.

(4) For long baseline (over 10 km) applications, the current radio data link system has to be replaced by available commercial differential GPS broadcast system.

(5) The optimal position and velocity update rate should be studied in order to reduce the computational burden and to reduce the remaining noise to a minimum.

(6) Parallel processors should be used to reduce the host computer burden. Up to now, collection of the rover GPS raw data and corrections from master station, GPS and INS navigation computations are all done by the host computer. This results in larger synchronization error due to the frequent interrupts.

REFERENCES

Britting, K.R. (1971), **Inertial Navigation Systems Analysis**, Wiley-Interscience, New York, USA.

Cannon, M.E. and Huangqi Sun (1994), **Assessment of a Non-Dedicated GPS Receiver System for Precise Airborne Attitude Determination**, Proceedings of ION GPS-94, Salt Lake City, Utah, September 20-23, pp. 645-654.

Cannon, M.E. (1996), **GPS Theory and Application**, ENGO 625 lecture notes, Department of Geomatics Engineering, The University of Calgary, Calgary, Canada.

Cannon, M.E., Gerard Lachapelle and Michael C. Szarmes (1997), **DGPS Kinematic Carrier Phase Signal Simulation Analysis for Precise Velocity and Position Determination**, NAVIGATION, The Institute of Navigation, Alexandria, VA, 44, 2, 231-245.

Chen, D. (1993), **Fast Ambiguity Search Filter (FASF): A Novel Concept for GPS Ambiguity Resolution**, Proceedings of ION GPS-93, Salt Lake City, Utah, September 22-24, pp. 781-787.

Chen, D. and G. Lachapelle (1994): **A Comparison of the FASF and Least-Squares Search Algorithms for Ambiguity Resolution On-The-Fly**, Proceedings of International Symposium on Kinematic Systems in Geodesy, Geomatics and Navigation, Banff, Canada, pp. 241-253.

Cohen, C.E. and B.W. Parkinson (1992), **Aircraft Applications of GPS-Based Attitude Determination**, Proceedings of ION GPS-92, Albuquerque, September 16-18, pp. 775-782.

Cox, D.B. (1978), **Integration of GPS with Inertial Navigation System**, NAVIGATION, Journal of the Institute of Navigation, Vol. 25, No. 2, pp. 236-245.

Crane, Carl D., David G. Armstrong and Arturo Rankin (1995), **Autonomous Navigation of Heavy Construction Equipment**, Computers in Civil Engineering, Vol. 10 , pp. 357-370.

El-Mowafy, Ahmed (1994), **Kinematic Attitude Determination From GPS**, UCGE Report No. 20074, Department of Geomatics Engineering, The University of Calgary, Calgary, Canada.

El-Sheimy, Naser (1996), **The Development of VISAT- A Mobile Survey System for GIS Application**, UCGE Report No. 20101, Department of Geomatics Engineering, The University of Calgary, Calgary, Canada.

Euler, H. (1992), **Fast GPS Ambiguity Resolution On-The-Fly For Real-Time Applications**, Proceedings of the 6th International Geodetic Symposium on Satellite Positioning, Columbus, Ohio,Vol. 2, pp. 650-659.

Euler, Hans-Jurgen (1994), **Achieving High-Accuracy Relative Positioning in Real-Time: System Design, Performance and Real-Time Results**, Proceedings of IEEE Position Location and Navigation Symposium, Las Vegas, pp. 540-546.

Gao, Y., E.J. Krakiwsky, M.A. Abousalem and J.F. McLellan (1993), **Comparison and Analysis of Centralized, Decentralized, and Federated Filters**, NAVIGATION, Journal of the Institute of Navigation, Vol. 40, No. 1, pp. 69-86.

Gao, Y., Z. Li and J. F. McLellan (1997), **Carrier phase Based Regional Area Differential GPS for Decimeter-Level Positioning and Navigation,** Proceedings of ION GPS-97, Kansas City, Missouri, pp. 1305-1313.

Gelb, A.(ed.) (1974), **Applied Optimal Estimation**, The M.I.T. Press, Cambridge, Massachusetts.

Greenspan, Richard L. (1995), **Inertial Navigation Technology from 1970-1995,** NAVIGATION, Journal of the Institute of Navigation, Vol. 42, No. 1, pp. 165-185.

Hartman, R.G. (1988), **An Integrated GPS/INS Design Approach,** NAVIGATION, Journal of the Institute of Navigation, Vol. 35, No. 1, pp. 121-134.

Hashemipour, H. R., S. Roy and A.J. Laub (1988), **Decentralized Structures for Parallel Kalman Filtering,** IEEE Trans. Automatic Control, Vol. AC-33, pp. 88-94.

Hatch, R. (1991), **Instantaneous Ambiguity Resolution**, Proceedings of International Association of Geodesy Symposia 107 on Kinematic Systems in Geodesy, Surveying and Remote Sensing, Springer Verlag, New York, pp. 299-308.

Hatch, R. and H. Euler (1994), **Comparison of Several AROF Kinematic Techniques,** Proceedings of ION GPS-94, Salt Lake City, Utah, September 20-23, pp. 363-370.

Hein, G and Werner, W. (1995), **Comparison of Different On-The-Fly Ambiguity Resolution Techniques**, Proceedings of ION GPS-95, Palm Springs, California, September 12-15, pp. 1137-1144.

Henriksen, J., G. Lachapelle, J. Raquet and J. Stephen (1996), **Analysis of Stand-Alone GPS Positioning Using Post-Mission Information**, Proceedings of ION GPS-96, Kansas City, Missouri, September 17-20, pp. 251-259.

Hofmann-Wellenhof, B., H. Lichtenegger and J. Collins (1994), **GPS Theory and Practice**, Springer-Verlag, New York.

Howell, G. and W. Tang (1994), **A Universal GPS/INS Kalman Filter Design,** Proceedings of ION GPS-94, Salt Lake City, Utah, September 20-23, pp. 443-451.

Karatsinides, S.P. (1994), **Enhancing Filter Robustness in Cascade GPS-INS Integration,** IEEE Transactions on Aerospace and Electronic Systems, AES 30, 4, pp. 1001-1007.

Kee, Changdon and Bradford W. Parkinson (1991), **Wide Area Differential GPS**, NAVIGATION, Journal of the Institute of Navigation, Vol. 38, No. 2, pp. 123-145.

Knight, D.T., A.W. Osborne, R.W. Snow and D.G. Kim (1993), **Demonstration of A New Tightly-Coupled GPS/INS**, Proceedings of ION GPS-93, Salt Lake City, Utah, September 22-24, pp. 205-214.

Kwan, William, William R. Lee, Lawrence O. Lupash and John A. McLean (1993), **The Design and Implementation of the AC-130U GPS/INS Integrated Filter**, Proceedings of the ION GPS-93, Salt Lake City, Utah, Vol.1, pp. 225-234.

Lachapelle, G., C. Liu, G. Lu, B. Townsend, M.E. Cannon and R. Hare (1993), **Precise Marine DGPS Positioning Using P Code and High Performance C/A Code Technologies**, Proceedings of National Technical Meeting, The Institute of Navigation, Alexandria, VA, pp. 241-250.

Lachapelle, G., R. Klukas, D. Roberts, W. Qiu, and C. McMillan (1995), **One-Meter Level Kinematic Point Positioning Using Precise Orbit and Timing Information**, Geomatica, Canadian Institute of Geomatics, Ottawa, Vol. 49, No. 2, pp. 193-203.

Lan, Hubiao (1996), **Development of A Real-Time Kinematic GPS System: Design, Performance and Results**, UCGE Report No. 20107, Department of Geomatics Engineering, The University of Calgary, Calgary, Canada.

Lapucha, D. (1990), **Precise GPS/INS Positioning for a Highway Inventory System**, UCGE Report No. 20038, Department of Surveying Engineering, The University of Calgary, Calgary, Canada.

Lipman, J.S. (1992), **Trade-offs in the Implementation of Integrated GPS Inertial Systems**, Proceedings of ION GPS-92, Albuquerque, New Mexico, September 16-18, pp. 1125-1133.

Liu, Ziwen (1992), **Comparison of Statistical Methods for the Alignment of Strapdown Inertial Systems**, UCGE Report No. 20047, Department of Geomatics Engineering, The University of Calgary, Calgary, Canada.

Litton (1984), **Technical Description of LTN-90-100 Inertial Reference System**, Document # 500406, published by Aero Product Division, Litton Systems California, Canoga Park, California, U.S.A.

Lu, Gang (1995), **Development of a GPS Multi-Antenna System for Attitude Determination**, UCGE Report No. 20073, Department of Geomatics Engineering, The University of Calgary, Calgary, Canada.

McLellan, James, Mohamed Abousalem, Ed Whatley and Paul Galyean (1994), **ACC-Q-POINT FM Subcarrier WADGPS**, Proceedings of ION GPS-94, Salt Lake City, Utah, September 20-23, pp. 1017-1024.

Nelthropp, D., J. Campanile and L. Federici (1992), **Integration of Embedded GPS/INS on the T-45A Aircraft**, Proceedings of ION GPS-92, Albuquerque, New Mexico, September 16-18, pp. 215-223.

Owen, T.E. and R. Wardlaw (1992), **Evaluating the Velocity Accuracy of an Integrated GPS/INS System: Flight Test Results**, Proceedings of the ION National Technical Meeting, San Diego, January 27-29, pp. 13-22.

Parkinson, B.W. and J.J. Spilker (1996), **Global Positioning System: Theory and Applications**, Progress in Astronautics and Aeronautics, Vol. 163, American Institute of Aeronautics and Astronautics, Inc., Washington, D.C.

Schwarz, K.P., G.S. Fraser and P.C. Gustafson (1984), **Aerotriangulation Without Ground Control**, International Archives of Photogrammetry and Remote Sensing, 25, Part A1, Rio de Janeiro, June 16-29.

Schwarz, K.P., A. EI-Mowafy and M. Wei (1992), **Testing a GPS Attitute System in Kinematic Mode**, Proceedings of ION GPS-92, Albuquerque, September 16-18, pp. 801-809.

Schwarz, K.P., M.A. Chapman, M.E. Cannon and P. Gong (1993), **An Integrated INS/GPS Approach to the Georeferencing of Remotely Sensed Data**, Photogrammetric Engineering and Remote Sensing, Vol. 59, 11, pp. 1667-1674.

Schwarz, K.P., M.A. Chapman, M.E. Cannon, P. Gong, and D. Cosandier (1994a), **A Precise Positioning/Attitude System in Support of Airborne Remote Sensing**, Proceedings of the GIS/ISPRS Conference, Ottawa, Canada.

Schwarz, K.P. and G.S. Zhang (1994b), **Development and Testing of a Low Cost Integrated GPS/INS**, Proceedings of ION GPS-94, Salt Lake City, Utah, September 20-23, pp. 1137-1144.

Schwarz, K.P. and M. Wei (1994c), **Aided Versus Embedded- A Comparison of Two Approaches to GPS/INS Integration**, Proceedings of IEEE Position Location and Navigation Symposium, Las Vegas, pp. 314-322.

Schwarz, K.P. and M. Wei (1997), **INS/GPS Integration for Geodetic Applications**, partial lectures for ENGO623, Department of Geomatics Engineering, The University of Calgary, Calgary, Canada.

Skaloud, Jan, M. Cramer and K.P. Schwarz (1996), **EXTERIOR ORIENTATION BY DIRECT MEASUREMENT OF CAMERA POSITION AND ATTITUDE,** Proceedings of ISPRS'96, Commission III, WG 1, Vienna, Austria, July 9-19.

Sun, Huangqi (1994), **GPS/INS Integration for Airborne Applications**, UCGE Report No. 20069, Department of Geomatics Engineering, The University of Calgary, Calgary, Canada.

Talbot, Nicholas C. (1991), **High-Precise Real-Time GPS Positioning Concepts: Modeling and Results**, NAVIGATION, Journal of the Institute of Navigation, Vol. 38, No. 2, pp. 147-161.

Tang, Chuanya (1996), **Accuracy and Reliability of Various DGPS Approaches**, UCGE Report No. 20095, Department of Geomatics Engineering, The University of Calgary, Calgary, Canada.

Tang, Wang and Gene Howell (1993), **Integrated GPS/INS Kalman Filter Implementation Issues**, Proceedings of the ION GPS-93, September 22-24, pp. 217-224.

Teunissen, P.J.G. and C.C.J.M. Tiberius (1994): **Integer Least-Squares Estimation Of the GPS Phase Ambiguities**, Proceedings of International Symposium on Kinematic Systems in Geodesy, Geomatics and Navigation, Banff, Canada, pp. 221-231.

Upadhyay, T.N., et al. (1982), **Benefits of Integrating GPS and Inertial Navigation System**, Proceedings of the ION 38th Annual Meeting, Washington, D.C., pp. 120-132.

Wei, M. and K.P. Schwarz (1990a), **A Strapdown Inertial Algorithm Using an Earth-Fixed Cartesian Frame**, NAVIGATION, Journal of the Institute of Navigation, Vol. 37, N0. 2, pp. 153-167.

Wei, M. and K.P. Schwarz (1990b), **Testing a Decentralized Filter for GPS/INS Integration**, Proceedings of IEEE Position Location and Navigation Symposium, Las Vegas, pp. 429-435.

Wong, R.V.C. (1988), **Development of a RLG Strapdown Inertial Survey System**, UCGE Report No. 20027, Department of Surveying Engineering, The University of Calgary, Calgary, Canada.

Zhang, Gengsheng (1995a), **A Low-Cost Integrated INS/GPS System**, UCGE Report No. 20078, Department of Geomatics Engineering, The University of Calgary, Calgary, Canada.

Zhang, Qiyue John (1995b), **Development of a GPS-Aided Inertial Platform for an Airborne Scalar Gravity System**, UCGE Report No. 20080, Department of Geomatics Engineering, The University of Calgary, Calgary, Canada.

APPENDIX

NAVIGATION RESULTS OF THE KINEMATIC TESTS

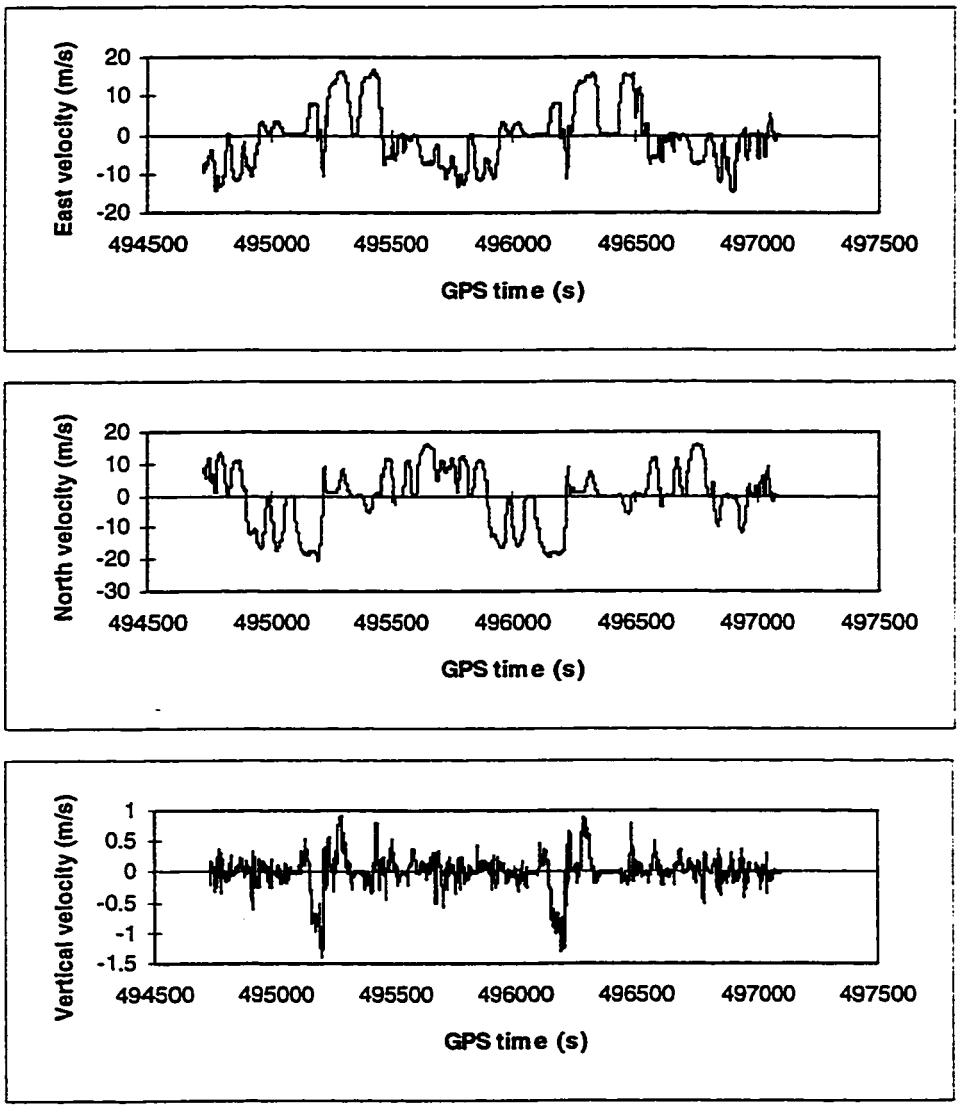

Figure A-1 IMU Velocity During Kinematic Test #1

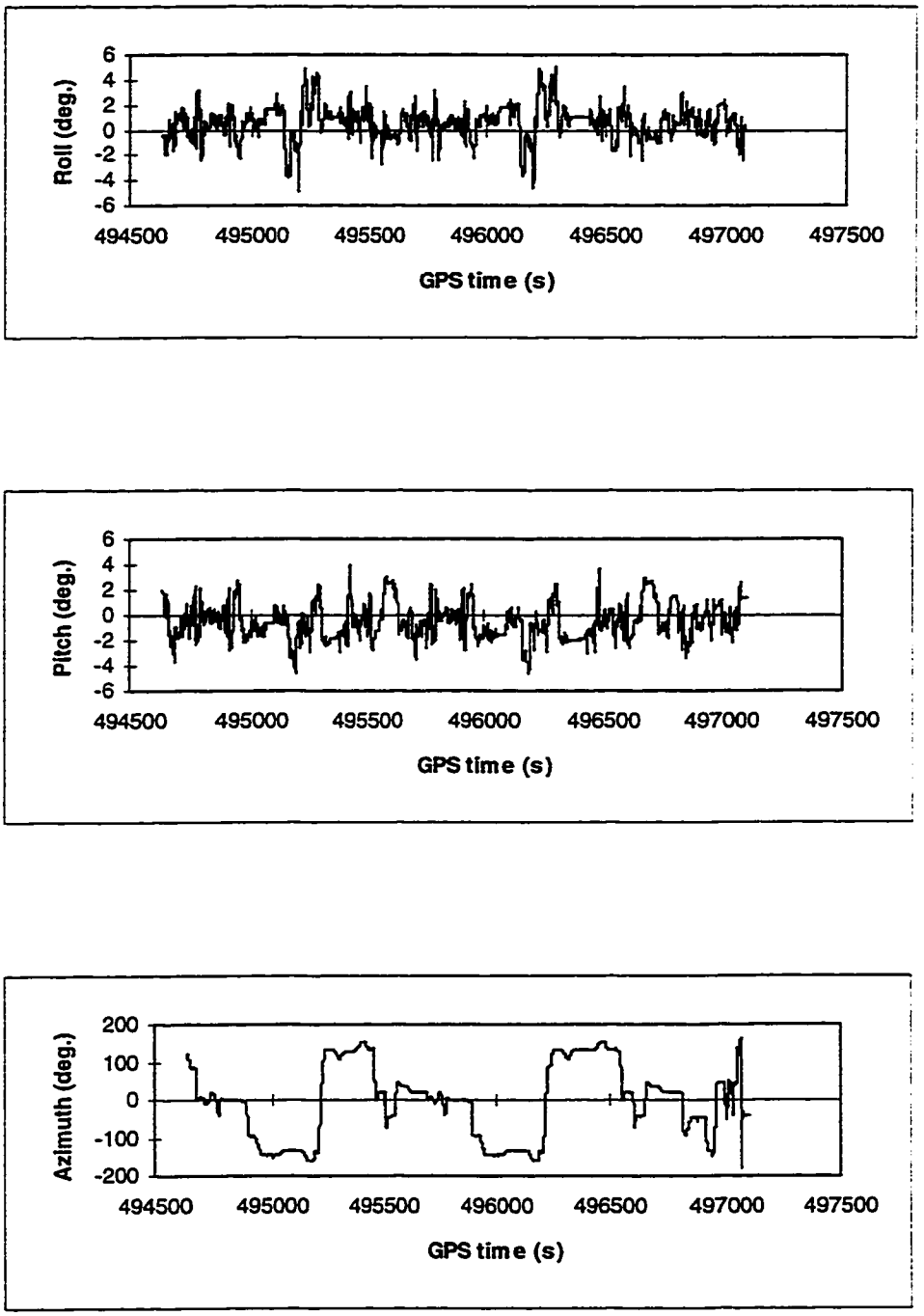

Figure A-2 IMU Attitude During Kinematic Test #1

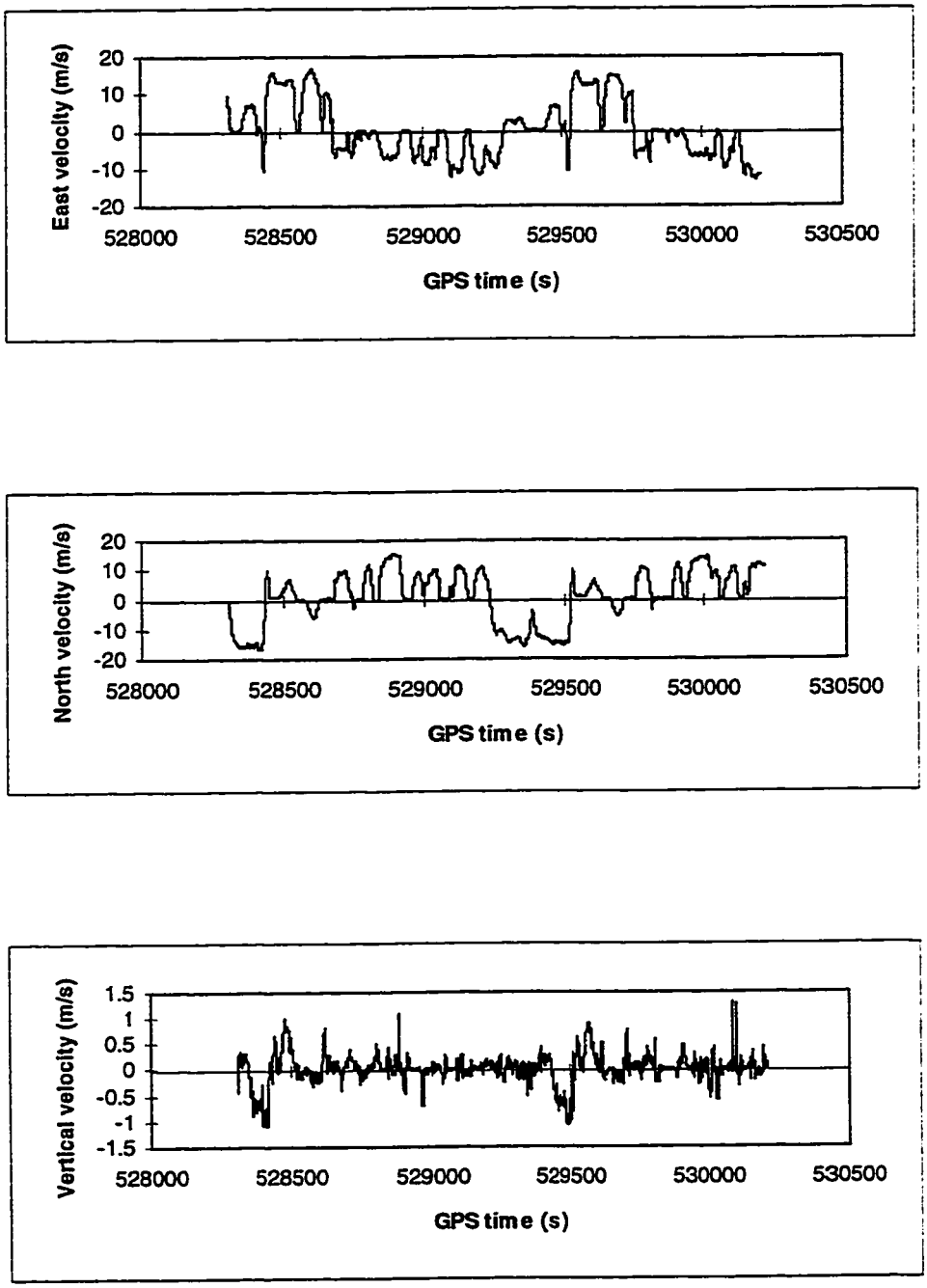

Figure A-3 IMU Velocity During Kinematic Test #2

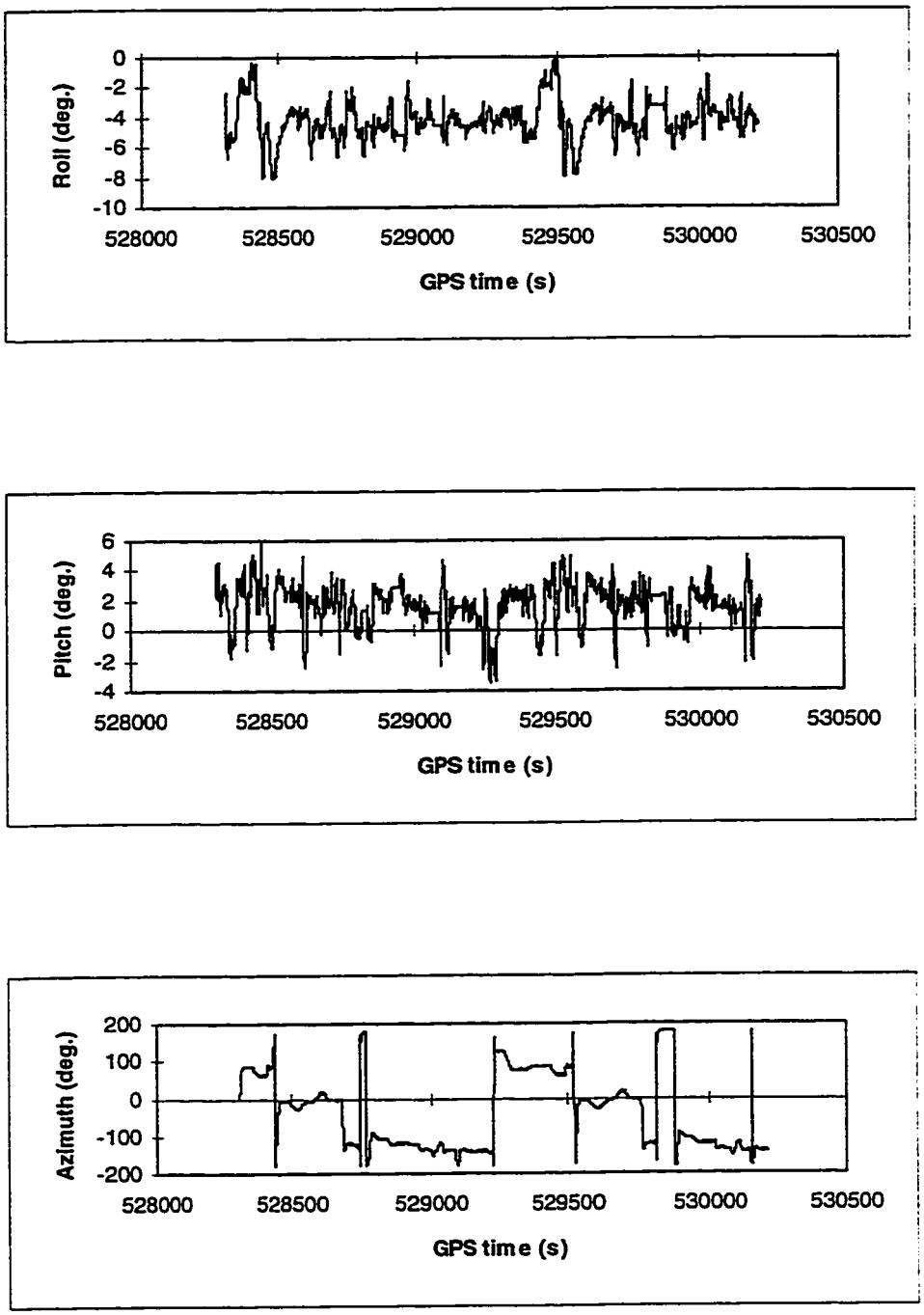

Figure A-4 IMU Attitude During Kinematic Test #2

IMAGE EVALUATION
TEST TARGET (QA-3)

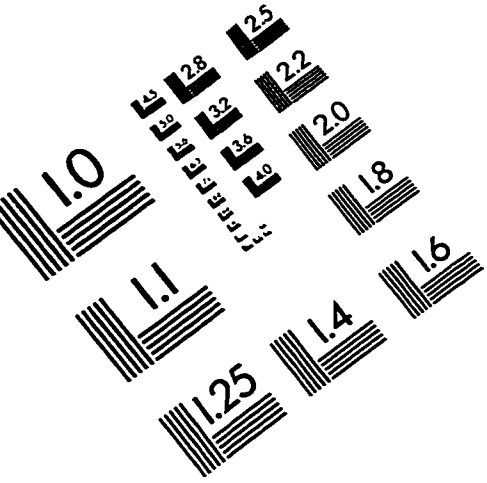

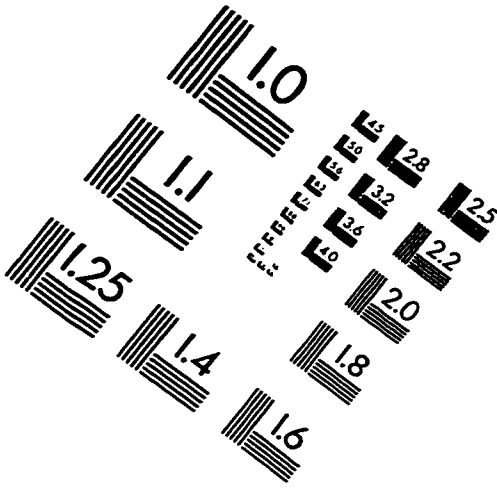

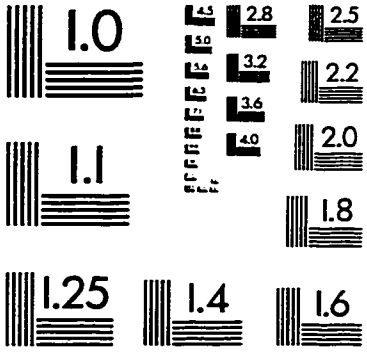

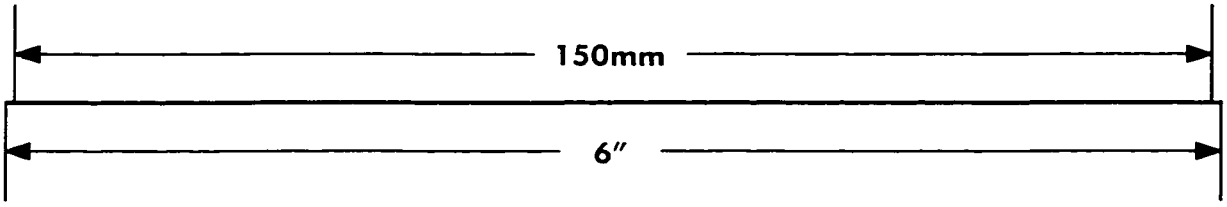

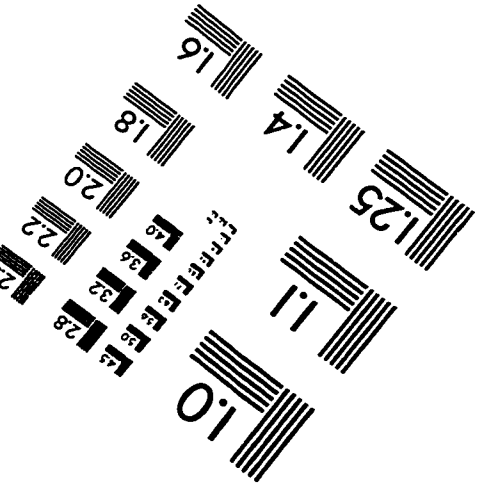

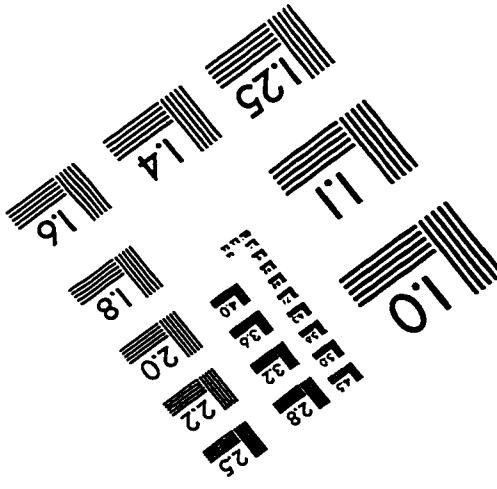

APPLIED IMAGE, Inc
1653 East Main Street
Rochester, NY 14609 USA
Phone: 716/482-0300
Fax: 716/288-5989